THE ROLE OF FORCE GENERATION IN METASTATIC CANCER PROGRESSION

A Dissertation

Presented to the Faculty of the Graduate School

of Cornell University

In Partial Fulfillment of the Requirements for the Degree of

Doctor of Philosophy

by

Casey Marie Kraning-Rush

August 2013

THE ROLE OF FORCE GENERATION IN METASTATIC CANCER PROGRESSION

Casey Marie Kraning-Rush, Ph.D.

Cornell University 2013

Metastasis, or the process by which cancer cells escape a primary tumor and travel through the body to form secondary tumors, is believed to be responsible for over 90% of the 7.9 million annual cancer-related fatalities reported worldwide. To migrate from the original tumor, cancer cells must navigate an extremely dense and heterogeneous stromal environment to arrive at a blood or lymph vessel, which they can then penetrate to enter the circulatory or lymphatic system. Each of these steps requires cells to pull on its matrix using contractile, or traction, forces. However, the precise relationship of force generation to metastatic cell structure and function remains largely unknown.

Herein, I demonstrate that metastatic cells exert increased contractile forces which facilitate the invasion of the extracellular microenvironment (ECM). Using traction force microscopy, I show that human metastatic breast, prostate, and lung cancer cell lines exhibit increased traction stresses compared to non-metastatic counterparts on physiologically-relevant substrates. Additionally, I find that the increased collagen density and matrix stiffness previously shown to be a hallmark of the tumor microenvironment promote increased traction forces through cell spread area-dependent and independent mechanisms. Finally, I develop a novel 3D model for one mode of metastatic migration in which secondary cancer cells follow microtracks that are formed by leading tumor cells secreting proteases and cleaving ECM fibers.

By using physiologically relevant 3D collagen channels to study cancer cell migration, I specifically assessed the role of force in protease-independent migration, and, surprisingly, found that contractile force was dispensable for this form of protease-independent migration. Instead, my results point to focal adhesion, actin filaments, and microtubules being key mediators of protease-independent migration within patterned collagen microtracks. Ultimately, these studies help to define the role that cellular force generation plays in metastatic invasion, and also yield insight into the biophysical mechanisms that tumor cells use to migrate. These insights could potentially lead to a targeted therapeutic approach to combating those mechanisms to delay or prevent metastasis and its subsequent fatal damage.

BIOGRAPHICAL SKETCH

Casey Marie Kraning-Rush was born in Fort Wayne, Indiana on April 16, 1986 to Mark and Karen Kraning. She graduated from R. Nelson Snider High School as salutatorian in 2004. Casey attended Butler University in Indianapolis, IN with a full tuition Lilly Endowment Scholarship. She graduated summa cum laude with a B.S. in Chemistry and highest honors in May 2008. In August 2008, Casey entered the Ph.D. program in Biomedical Engineering at Cornell University, having been awarded both a prestigious Presidential Life Sciences Fellowship and a Sage Fellowship. She joined the lab of Cynthia A. Reinhart-King and began her research by studying the role of matrix mechanics and the tumor microenvironment on cancer cell forces and migration behavior. She was awarded a National Science Foundation Graduate Research Fellowship in 2009 and received her M.S. in Biomedical Engineering in 2012. During her time at Cornell, Casey also won several additional awards, including a Young Investigator Trans-Network Project Award from the Physical Sciences and Oncology Center (National Institute of Health), a travel award from the Caroline Coffey Fund, a Graduate Student Extended Abstract Award from the Biomedical Engineering Society, and a Young Investigator Award from the Cornell University Center on the Microenvironment and Metastasis, as well as several poster awards. Casey completed her Ph.D. in the spring of 2013. Casey enjoys reading novels, trying new foods, playing board games with friends, and thinks it is awesome that you just read this. And she also gives you major props if you know who she stole that last bit from.

To my friends and family, past and present,

For your unwavering support.

ACKNOWLEDGMENTS

First and foremost, although I cannot express adequate thanks to my research advisor and mentor, Dr. Cynthia Reinhart-King, I will, as always, give it my best effort. I am sincerely grateful to Cindy for taking a chance on a student transitioning from a background in basic science to the (quite intimidating) world of engineering, and for giving me the tools, resources, and support I needed to thrive in it. Her determination and ambition have inspired me from the outset, and have pushed me to the absolute limits – allowing me to witness firsthand what I am capable of accomplishing once my mind is set. Ultimately, this has allowed me to gain confidence in myself both as an independent scientist and also on a more fundamental and personal level that I know will stay with me as I transition into a new career. Thank you, Cindy, for everything.

I would also like to thank my dissertation committee members, Drs. David Erickson, Tracy Stokol, and Paraskevi Giannakakou for their support and supervision of my research over the past few years. I would also like to particularly thank David and Evi for allowing me to spend time working in their labs and getting to know their students. I always felt welcome, and I greatly valued the experiences.

I am grateful to have worked on some excellent collaborations with colleagues and investigators both within and outside of the Reinhart-King lab: Brooke Mason, Shawn Carey, Michael Mak, Erica Pratt, Dr. Joe Califano, Dr. John Huynh, Dr. Francois Bordeleau, Dr. Chantal Chanel-Vos (Weill Cornell), Dr. Daniele Gilkes (Johns Hopkins), Dr. David Erickson, Dr. Brian Kirby, and Dr. Paraskevi Giannakakou (Weill Cornell). I would also like to thank Dr. Micah Dembo, Dr. Michael King and

Dr. Lawrence Bonassar for graciously providing tools necessary for the completion of this research.

I gratefully thank the funding sources that have supported my work as a graduate student, including a Sage Fellowship, a Presidential Life Sciences Fellowship, and a National Science Foundation Graduate Research Fellowship. I would like to specifically thank Susi Varvayanis, the Director of Applied Resources for the Center for Life Science Enterprise who oversaw the Presidential Life Sciences program, for being incredibly kind and helpful these past five years. I would also like to thank the Biomedical Engineering Society and the Caroline Coffey Fund for funding my travel to present at past conferences.

I would also like to thank the members of the Office of Physical Sciences-Oncology Center, specifically Dr. Nas Kuhn, Dr. Sean Hanlon, Dr. Nicole Moore, Dr. Jerry Lee, and Dr. Larry Nagahara, for creating an open and free environment in which to discuss science, and for giving me numerous opportunities to present and develop my research. Additionally, I am thankful for the opportunity to have met and developed connections with colleagues throughout the network, specifically Rory Staunton, Dr. David Liao, Dr. Stephanie Fraley, Dr. Shannon Mumenthaler, and Dr. Parag Mallick.

Many thanks go to Dr. Michael Shuler, Dr. Peter Doerschuk, and the wonderful administrative staff who run the department, particularly Belinda Floyd. I'd also like to thank the Weill Hall building staff for their hard work keeping everything up and running on a daily basis, even when the ceiling quite literally caves in.

I would be remiss not to thank the undergraduate students and masters students who I have had the opportunity to work with during my time at Cornell: Leah Roldan, Olivia Torre, Sahana Somasegar, Viral Oza, Jonathan Charest, Brittany Cable, Alina Starchenko, and Na Young Kim. I have great faith that each will find great success on their paths through life.

I would particularly like to thank the professors from Butler University who supported my decision to go rogue and become an engineer. Dr. Geoffrey Hoops, my research and academic advisor, has remained a continual source of support for me over the last 5 years, and I am indebted to him for teaching me how to become a scientist. Dr. Todd Hopkins and Dr. Meng-Chih Su were also both instrumental in my early success.

Special thanks to the female scientists in my life who I have had the good fortune to meet and be inspired by – some from a very young age: Sharon Orr, Dr. Jackie Litzgus, Dr. Shelly Etnier, Dr. Anne Wilson, Dr. Kristy Ainslie, Dr. Kayte Fischer, Dr. Tejal Desai, Dr. Julie Goddard, and, of course, Dr. Cindy Reinhart-King. Through their mentoring, these women have taught me how to be a strong female role model, and how to best attempt that whole work-life balance thing. I'm sure I'll master it in the end.

Thanks to friends from my past who pop in now and again to catch up on life, and who are always there to support me when I need a friend: Beth Avila, Josh Daring, Eric Sundstrom, Josh Kaminski, Claire Nicholson, and Kiara and Bri'anne Smith.

I am absolutely grateful for the friends I have made in Ithaca, and particularly in the Reinhart-King (a.k.a. CRK) lab. Brooke Mason, John Huynh, Joe Califano, and

Shawn Carey – you were an amazing family to be a part of, and I am proud to call you my friends. I will always remember the inside jokes and excellent adventures we shared. Drs. Saumendra Bajpai and Francois Bordeleau – I am so thankful to have been able to get to know you and learn from your expertise. Marsha Lampi, Alex MacGregor, Turi Alcoser, and Julie Kohn – you all have a lot to live up to, but from the short time we've shared, I know that you are each a fantastic addition to the CRK lab, and that you will shape it into a new family of your own. I have no doubts about your future successes, and I look forward to hearing about them.

I must express my heartfelt gratitude towards my parents, Mark and Karen, and the rest of my family, for their infinite love and support over the past 27 years. Their encouragement has meant so much.

Finally, I must thank the one person in my life that I could not have made it through the past five years without – my husband, Jason Kraning-Rush. He has been my rock through seemingly endless days in lab, hours at the microscope, literal *months* staring at cells moving around on a computer screen. He has been responsible for my health and sanity, and it has not been an easy journey for either one of us. Jason has supported me at every single turn, and I cannot express how deep my love and appreciation run. Now – on to the next chapter of our life, together.

TABLE OF CONTENTS

LIST OF FIGURES

Chapter 1: Introduction

Chapter 2: Cellular Traction Stresses Increase with Increasing Metastatic Potential

Chapter 3: Microfabricated Collagen Tracks Facilitate Single Cell Metastatic Invasion in 3D

Chapter 4: Actin Cytoskeleton and Focal Adhesions Regulate MMP-Independent Cancer Cell Migration in 3D Microtracks

Chapter 5: Additional Data

LIST OF TABLES

LIST OF ABBREVIATIONS

A549	Metastatic lung cancer cell line
ADAM	A disintegrin and metalloproteinase
AFM	Atomic force microscopy
ANOVA	Analysis of variance
BEAS2B	Non-metastatic lung epithelial cell line
BSA	Bovine serum albumin
CAFs	Carcinoma-associated fibroblasts
CD	Cytochalasin D
cDNA	Complementary DNA
CO_2	Carbon dioxide gas
CTCs	Circulating tumor cells
Ctrl	Control
DAPI	4’,6-diamidino-2-phenylindole
ECM	Extracellular matrix
EGF	Epithelial growth factor
EGTA	Ethylene glycol tetraacetic acid
FACS	Fluorescence-activated cell sorting
FAK	Focal adhesion kinase
FITC	Fluorescein isothiocyanate
GAPs	GTPase-activating proteins
GEFs	Guanine nucleotide exchange factors
GFP	Green fluorescent protein
HEPES	4-(2-hydroxyethyl)-1-piperazineethanesulfonic acid
HIF1	Hypoxia-inducible factor 1

HRP	Horseradish peroxidase
IVM	Intravital microscopy
KD	Knock down
LA	Latrunculin A
MCF10A	Nonmetastatic mammary epithelial cell line
MCF10AT	Family of transformed cell lines derived from MCF10A cells
MCF10AT1	Tumorigenic but non-metastatic mammary cell line
MCF10CA1a	Highly metastatic mammary cell line
MDAMB231	Highly metastatic breast carcinoma cell line
MLC	Myosin light chain
MLCK	Myosin light chain kinase
MMPs	Matrix metalloproteinases
mRNA	Messenger RNA
mPADs	microfabricated post array detection systems
MT1-MMP/MMP14	Membrane-bound type 1 matrix metalloproteinase
N6	N-6-((acryloyl)amino) hexanoic acid, succinimidyl ester
NaCl	Sodium chloride
NaOH	Sodium hydroxide
NC	Nocodazole
NC-GM6001	GM6001 negative control
O_2	Oxygen gas
PA	Poly(acrylamide)
PBS	Phosphate-buffered saline
PC3	Highly metastatic prostate cancer cell line
PDMS	Polydimethylsiloxane
PKC	Protein kinase C

PMMA	Poly(methylmethacrylate)
PIC	Protease inhibitor cocktail
PrEC	Primary prostate epithelial cells
PS-OC	Physical Sciences – Oncology Center
qRT-PCR	Quantitative real time polymerase chain reaction
Reox	Reoxygenation
ROCK	Rho-associated coiled-coil containing protein kinase
RT	Room temperature
SD	Standard deviation
SDS	Sodium dodecyl sulfate
SDS-PAGE	Sodium dodecyl sulfate – polyacrylamide gel electrophoresis
SEM	Standard error of the mean OR scanning electron microscopy
siRNA	small interfering RNA
TBS	Tris-buffered saline
TFM	Traction force microscopy
TIMP2	Tissue inhibitor of metalloproteinases 2
TPA	12-O-Tetradecanoylphorbol 13-acetate
Tris-HCl	Tris(hydroxymethyl)aminomethane-hydrochloric acid
Triton	Octyl phenol ethoxylate
Tween	Polyoxyethylene 20 sorbitan monolaurate
TX	Paclitaxel

LIST OF SYMBOLS

Symbol	Description	Units
^{o}C	Degree Celsius	Degree
$<d^2>$	Mean Square Displacement	μm^2
E	Young's Modulus	$Pa = N/m^2$
F	Traction Force	N
ν	Poisson's Ratio	---
P	Persistence	minutes
S	Migration Speed	$\mu m/min$

CHAPTER 1

INTRODUCTION

Portions of this chapter were published as a book chapter titled "Quantifying Traction Stresses in Adherent Cells" in *Methods in Cell Biology* (Kraning-Rush et al., 2012b) and also as a review titled "Controlling Matrix Stiffness and Topography for the Study of Tumor Cell Migration" in *Cell Adhesion & Migration* (Kraning-Rush and Reinhart-King, 2012).

1.1 Introduction to Cancer Cell Migration: A Biophysical Approach

Of the 7.9 million cancer-related fatalities reported every year worldwide, over 90% are believed to be the result of metastatic disease (Christofori, 2006), in which a subset of cells from the original tumor spread throughout the body. Although advances have been made in the treatment of primary tumors through surgery, chemotherapy and radiation treatment, methods for effectively diagnosing the likelihood of metastasis or treating the disease after it has reached this stage remain elusive (Steeg, 2006). Despite its link to poor prognosis, there are no direct clinical tests available to definitively diagnose the metastatic potential for a given tumor (Steeg, 2006). While advances in genetic profiling have led to the generation of several multi-gene expression signatures for predicting clinical prognosis of specific cancers (Ramaswamy et al., 2003; Sotiriou et al., 2003), these signatures have not yet shown broad applicability to a wide range of patients, whose tumors display great heterogeneity both across patient populations and within a single patient (Gerlinger et al., 2012). Additionally, while these signatures may statistically correlate with poor clinical prognosis, they do not provide information on the physical attributes of the tumor cells which may contribute to metastatic invasion. However, though a single gene expression signature may not

function across a broad pool of patients, different alterations in gene expression patterns may result in similar phenotypic changes at the cellular level which result in invasive behavior. As such, the biophysical characteristics of tumor cells may be an excellent target both for determining patient prognosis and also for designing targeted therapies.

To understand how the biophysical properties of tumor cells can affect invasion, it is important to fully characterize the physical mechanisms employed by metastatic cancer cells to invade. During metastasis, cells from the primary tumor acquire characteristics that enable them to escape and migrate through a heterogeneous stromal environment to establish secondary tumors. By no means a static system, as a tumor develops, the cancer cells within experience a wide range of effects, including increased matrix stiffness as the extracellular matrix (ECM) becomes highly cross-linked and irregular (Lopez et al., 2011; Paszek et al., 2005), increased ligand density as tumor cells begin to secrete greater amounts of matrix proteins such as collagen or fibronectin (Ioachim et al., 2002; Levental et al., 2009), decreased or erratic exposure to oxygen caused by an irregular and leaky vasculature (Harris, 2002), and elevated interstitial pressure caused by increased proliferation within a confined environment (Tse et al., 2011). These often harsh conditions can have a profound phenotypic and epigenetic effect on these cancer cells, often leading to the generation of a highly invasive subpopulation capable of metastasizing. Moreover, to successfully navigate this dynamic microenvironment, metastasizing tumor cells must reorganize the basement membrane, invade into surrounding stroma (Rosel et al., 2008; Wolf et al., 2007), migrate along ECM fibers (Provenzano et al., 2008b; Wyckoff et al., 2006) and transmigrate through the endothelial cell barrier (Mierke et al., 2008b) to enter the circulatory or lymphatic system. In addition to enzymatically degrading the ECM with

matrix metallo-proteinases (MMPs), metastatic cells use contractile forces to mechanically rearrange their ECM to clear an open path for subsequent migration (Wolf et al., 2007). Because force generation plays a central role in several of these key behaviors, I focus on it here as a potential phenotypic marker of metastatic potential and further elucidate the specific role it plays during metastasis.

In this chapter, I will first examine the use of cellular force in non-pathological cell behaviors and detail different methods for quantifying contractile force generation, while emphasizing the role that matrix stiffness plays in mediating these forces. Next, I will discuss previous research regarding cellular forces during disease progression, particularly in relation to cancer. Finally, I will illustrate the importance of translating these findings into a more physiological context by describing work done to mimic the native 3D architecture of the tumor and analyzing the role which force generation plays in different invasion mechanisms within this complex 3D microenvironment, with specific reference to the formation and migration within proteolytic microtracks.

1.2 Cellular Force Generation in Cell Migration

Cellular traction forces have been shown to drive cell adhesion (Reinhart-King et al., 2003), spreading (Reinhart-King et al., 2005), migration (Dembo and Wang, 1999; Pelham and Wang, 1997), and extracellular matrix (ECM) deposition and remodeling (Lemmon et al., 2009). To migrate, a cell must undergo changes in cellular force production to modify both its shape and its internal tension to interact with the surrounding ECM, which provides both a substrate for the cell to adhere to as it moves forward, but also a barrier through which the cell must advance (Ehrbar et al., 2011). In most adherent cells, forward movement is initiated by actin polymerization, causing a pseudopod to extend from the leading edge of the cell. Cell extensions interact with

the surrounding ECM and initiate binding through transmembrane integrin receptors, forming focal complexes and focal adhesions (Hynes, 2002).

Cell-matrix adhesions vary greatly in size, shape, and complexity, with over 100 proteins estimated to play a role in their formation and dissociation (Fraley et al., 2010; Parsons et al., 2010). One of the most important classes of adhesion proteins are integrins. Integrins are heterodimeric transmembrane proteins which exist in 24 different configurations and bind to specific extracellular matrix proteins. Upon binding the extracellular matrix, integrins experience a conformational change in their intracellular tail domain which facilitates binding to the actin cytoskeleton through various linker proteins, including talin and vinculin (Wozniak et al., 2004). As integrins become connected to the actin cytoskeleton, other focal adhesion proteins are recruited to the complex, including scaffolding proteins such as paxillin and zyxin, and adaptor proteins, such as focal adhesion kinase (FAK) and p130Cas, which can further associate with additional signaling molecules and activate various pathways. In particular, the Rho/ROCK signaling pathway can be activated in this manner. This complex pathway consists of the Rho-family small guanosine triphosphatases (GTPases), including Rac, Rho, and Cdc42, which are regulated by the dynamic behavior of guanine nucleotide exchange factors (GEFs), which activate the Rho-family GTPases by associating them with GTP, and GTPase-activating proteins (GAPs), which inactivate the GTPases by hydrolyzing GTP to GDP (Amano et al., 2010). These GTPases subsequently regulate adhesion assembly and disassembly, thus controlling actomyosin contractility and cellular migration. For example, Rho will associate with its effector protein, Rho-associated kinase (ROCK) to control the activity of myosin via two distinct mechanisms. First, it will inactivate myosin light chain (MLC) phosphatase, thus inhibiting the dephosphorylation of MLC and

resulting in increased levels of phosphorylated MLC and thus increased contractility. Second, it can also phosphorylate MLC directly to enhance actomyosin contractility (Amano et al., 2010). Contractile force caused by actomyosin contraction generates both intracellular tension and extracellular tension transmitted to the substrate, ultimately causing the cell's posterior focal adhesions to release and allowing the cell to move forward (Lauffenburger and Horwitz, 1996). While the signaling mechanisms and adhesion complexes present during 2D migration are well-characterized, their role in cell migration within 3D matrices is less clear. Recent studies indicate that classical focal adhesions are less prominent in 3D, and the proteins involved in their assembly and disassembly in 2D play different roles and have differing degrees of importance in regulating 3D cell migration (Fraley et al., 2012; Fraley et al., 2010).

During migration, changes in the cytoskeleton alter cell-matrix dynamics and cellular force generation. Indeed, contractile force generation is intimately connected to the stiffness of the extracellular matrix either beneath the cell (i.e. on 2D substrates) or surrounding the cell (i.e. incorporated within 3D matrices). Stiffness within the human body varies greatly, ranging from very soft environments, such as those found in the brain (Young's Modulus, E = ~250-500 Pa) (Miller et al., 2000) or in adipose tissue (E = ~20 Pa) (Wellman et al., 1999), to significantly more rigid environments, such as articular cartilage (E = ~950 kPa) (Freed et al., 1997) or rigid bone (E = ~GPa) (Zysset et al., 1999). Cells are able to detect and respond to changes in mechanical properties through the network of focal adhesion proteins discussed above, which act as mechanotransducers by linking the actin cytoskeleton to the ECM (Geiger et al., 2009). Increased 2D matrix stiffness is associated with an increase in focal adhesion size and number (Engler et al., 2004), increased Rho activation (Huynh et al., 2011), and the formation of well-defined actin stress fibers (Yeung et al., 2005), which can all

contribute to increased migration. Because migration is fundamental to many essential biological processes including development, immune response, inflammation, and wound healing, and because cells must exert force to migrate, many groups have described methods to characterize force generation of adherent cells (Dembo and Wang, 1999; du Roure et al., 2005; Galbraith and Sheetz, 1997; Harris et al., 1980; Tan et al., 2003), and several of these will be discussed in the next section.

1.3 Techniques for Quantifying Cellular Force Generation

The earliest technique used to describe the traction forces exerted by cells was developed by Harris and colleagues in the 1980s. In this landmark paper, cells were seeded on top of an elastomeric silicone rubber substrate (Harris et al., 1980). As the cells adhere and migrate, they generate wrinkles within the substrate during contraction. While both the cells and the wrinkles they produced were easily visualized, it was difficult to extract out quantitative information regarding the cellular forces as the wrinkles were typically nonlinear and irregularly shaped. Therefore, although informative as a probe of cellular forces, this technique yielded only semi-quantitative data in the form of number and length of wrinkles (Harris et al., 1981). In later work using wrinkling substrates, cellular force data was extracted by using flexible microneedles to exert a known force onto the substrate, reversing the wrinkle caused by the cell (Burton and Taylor, 1997).

Building upon the work pioneered by Harris et al., in the early 1990s the idea of observing and measuring bead displacement in an elastic substratum, rather than wrinkles, was introduced. A thin layer of latex beads was airbrushed over a non-wrinkling elastic film created by crosslinking silicone oil to the sides of a rigid vessel. This created a tightly stretched film upon which cellular forces transmitted to the

surface could be more directly detected through bead displacements (Lee et al., 1994; Oliver et al., 1995). This technique had the advantage of being more sensitive than the silicone rubber wrinkling technique, in that relatively small forces (~20 nN) could be detected based on bead movements. Additionally, the silicone oil could be cross-linked to varying degrees to produce a range of substrate moduli. However, this approach did suffer from some limitations. For instance, more compliant silicone substrates were unable to completely recover from cellular deformation (Lee et al., 1994). Moreover, these substrates were non-porous and poorly adhesive, and their mechanical properties could not be sufficiently tuned to match the strength of the majority of mammalian cell types (Dembo and Wang, 1999).

These limitations were overcome in the late 1990s with the advent of polyacrylamide (PA) hydrogels as a substrate on which to plate cells (Brandley et al., 1987; Wang and Pelham, 1998). The mechanical and chemical properties of PA gels are ideal for the study of cellular forces. First, similar to the earlier generation of silicone films, PA gels are optically transparent, allowing cells cultured on them to be easily imaged, and they can also have fluorescent markers embedded into them, allowing the user to measure deformations caused by cell migration using standard fluorescent microscopy. More importantly, PA gels are elastic and will deform in direct proportion to a broad range of applied force. Once this force is removed, PA gels immediately and reproducibly recover to an unstressed conformation. PA gels have also been utilized to study the effects of stiffness on a wide variety of cell behaviors, including, but not limited to, proliferation (Brown et al., 2010; Klein et al., 2009), adhesion (Jannat et al., 2010; Willcox et al., 2005), migration (Isenberg et al., 2009; Lo et al., 2000; Peyton and Putnam, 2005), differentiation (Engler et al., 2006; Trappmann et al., 2012), matrix degradation (Alexander et al., 2008), network

formation (Califano and Reinhart-King, 2008), cell-cell and cell-matrix interactions (Califano and Reinhart-King, 2008; Califano and Reinhart-King, 2010b). PA gels are ideal for these studies because stiffness can be precisely tuned simply by varying the ratio of monomer (acrylamide) to cross-linker (bis-acrylamide) to achieve a Young's modulus (E) in the range of tens of pascals to hundreds of kilopascals (Kraning-Rush et al., 2012b; Yeung et al., 2005). Additionally, PA gels can be functionalized using any protein or amino acid fragment of interest, and the concentration of this protein can be held constant, independent of the gel stiffness. PA gels are also nontoxic and create a more physiologic environment than glass or PDMS for short term culture of a wide variety of adherent mammalian cell types (Wang and Pelham, 1998).

The polyacrylamide system was rapidly adapted for use in quantifying the traction forces of adherent cells by Dembo and co-workers, giving rise to the technique of traction force microscopy (TFM), which is the primary technique used by our lab to quantify cellular force (Dembo and Wang, 1999).

Traction Force Microscopy

Traction force microscopy (TFM) is a technique that allows for the precise quantification of traction stresses generated by cells adherent to an underlying two-dimensional substrate, most often a PA gel, as described above (Dembo et al., 1996). As cells adhere to and migrate over sufficiently compliant substrates, traction forces generated by the cell create deformations. These deformations are detected by the inclusion of markers (usually sub-micron diameter fluorescent beads) within the PA gel that relax back to their original position when the cell is either released chemically from the substrate (e.g. with trypsin) (Fig 1.1A-B), or when it migrates away from the field of interest during a time-course study. Because this technique relies on the cell's

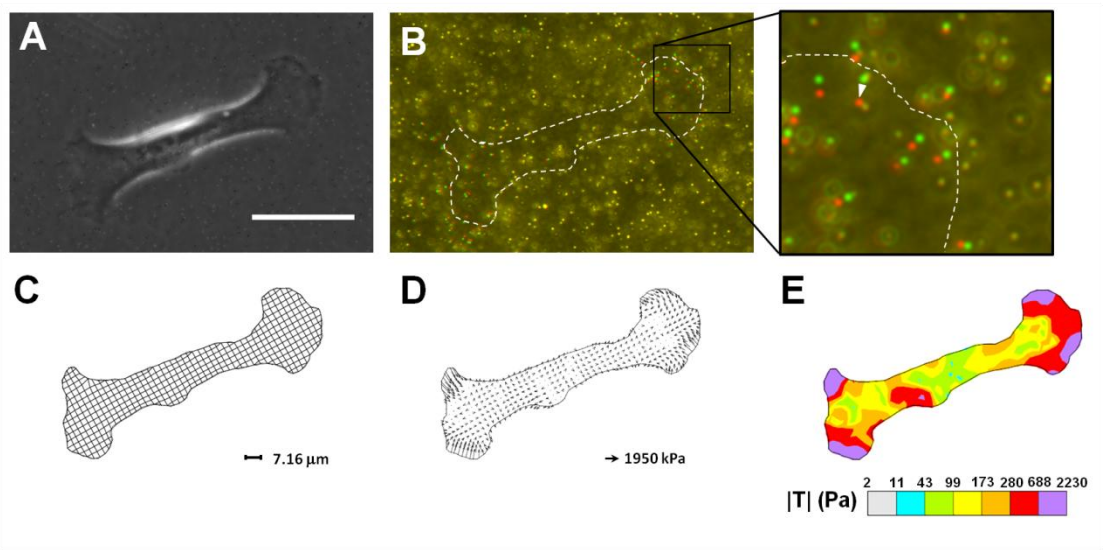

Figure 1.1. Traction force microscopy is used to quantify traction forces in 2D. MDA-MB-231 cells were seeded onto a polyacrylamide substrate (A). To quantify traction forces, fluorescent images are acquired of the bead field beneath the cell during force generation (B, red) and after the cell has been released with trypsin (B, green). An overlay of these two images indicates the regions of greatest bead displacement (inset, white arrow). To calculate the most likely traction field causing the observed bead displacement, the cells is first discretized into a mesh (C). Individual tractions are then calculated for each node of the mesh (D). From these tractions, a color contour plot can be generated indicating regions of highest and lowest traction forces (E). Scale bar = 50 µm.

ability to deform its substrate by a detectable amount, the range of substrate stiffness testable using TFM is inherently limited. While there is considerable variation between the strength of different cell types, TFM may have an upper limit of $E \sim$ 10-30 kPa. Above this range, the displacement of fiduciary markers is typically negligible.

Experimentally, calculation of the substrate strain field requires images of the bead field in both its stressed state (with the cell present) and relaxed state (without the cell). The image of the beads in their relaxed state is typically captured after the cell is removed and the beads in the field of view have returned to their "unstressed" position due to the elastic nature of the PA gel substrate. The displacements caused by the cells are computed by comparing the stressed and relaxed images of the bead field. The calculation of traction forces is based on the Boussinesq equations, which describe the relationship between the deformation of a material due to forces applied to its free surface (Landau et al., 1986). In this regard, the elastic PA gel substrate is assumed to be a uniform and isotropic elastic material, and it is assumed that the inclusion of marker beads in the substrate does not perturb this elastic behavior. Additionally, the external loads acting on the substrate surface are assumed to be solely tangential, thus satisfying a condition of plane stress (this assumes that the normal and shear stress components in the z-direction are negligible or zero). Therefore, because compliant substrates may not adequately support the weight of adherent cells and will allow significant bead displacement in the z direction, violating the plane stress approximation, TFM has a lower limit of ~1 kPa.

Substrate deformations are calculated based on the movements of beads embedded within the PA gel substrate. While it is possible, in theory, to map individual bead

movements by hand, this would be cumbersome. To automate this process, Marganski et al developed an algorithm based on correlation-based optical flow, which has been refined since it original description (Marganski et al., 2003). This algorithm takes two images (the stressed and relaxed bead field images described above) as the input. Bead tracking is done by systematically scanning all pixels in the null image to find the pixel coordinates of the fluorescent beads (identified as strict pixel intensity maxima after image intensity normalization). For each bead that is tracked, a box of pixels centered on the local maximum intensity pixel is defined and the relative pixel intensities in that box serve as a 'fingerprint' for the tracked bead. This search box is used to determine the coordinates of the corresponding 'fingerprint' in the stressed image. This process is iterated for every pixel in the image and is able to determine the bead displacements with sub-micron resolution.

Once the substrate deformations have been properly mapped, the calculation of traction stresses is solved as an inverse problem, meaning that the measurements of substrate deformation are used to statistically compute the most likely traction stress field that will give rise to the observed deformations (Fig 1.1C-D). TFM solves the problem using the formulas original described by Boussinesq for a point force acting on an elastic half-space (Landau et al., 1986). Specifically, the displacement *d* of the *p*th bead marker is related to the traction field (T) by Eq. (1.1),

$$d_{p\alpha} = \iint g_{\beta\alpha}(\mathbf{m}_p - \mathbf{r}) T_\beta(\mathbf{r}) dr_1 dr_2 \qquad (1.1)$$

where $g_{\beta\alpha}(\mathbf{m}_p - \mathbf{r})$ represent the coefficients of a Green's tensor that give the substrate displacement in the α direction at location **m** induced by a force in the β direction acting at location **r** (Dembo and Wang, 1999). The functions for the coefficients of the Green's tensor incorporate both the Poisson's ratio and Young's

modulus (*E*) of the polyacrylamide substrate (Dembo and Wang, 1999). Importantly, the *E* is a parameter which can be determined experimentally (Lo et al., 2000).

To ensure the existence of such an integral relationship, it is sufficient that the traction field satisfy a constraint of global force balance. The traction field is thus derived from numerical integrals computed over the mesh to determine the maximum likelihood tractions based on the displacement field. These tractions are tied to chi-square and Bayesian statistics that iterate until convergence. Once solved, the magnitude and direction of traction forces, and other parameters including the bead displacement vector field and strain energy density field may be examined (Fig 1.1D-E). For many cells types, the magnitude of traction forces is on the order of ~0.05-2 μN (Califano and Reinhart-King, 2010a; Gaudet et al., 2003; Paszek et al., 2005; Reinhart-King et al., 2003). Others have used a similar experimental system (PA gels embedded with fluorescent beads), but have solved the inverse problem using Fourier's method to solve the general equations of equilibrium relating displacements to tractions (Butler et al., 2002).

TFM has been widely utilized to study the specific mechanisms by which cells use force to migrate. Performing TFM on cells while manipulating the actomyosin cytoskeleton has revealed that actin stress fibers are critical for the transmission of forces to the substrate (Kraning-Rush et al., 2011; Pelham and Wang, 1999). In a study by Kumar et al, a single actin stress fiber within a living cell was ablated using multiphoton laser nanoscissors, resulting in large scale cytoskeletal rearrangement, particularly on compliant substrates (Kumar et al., 2006). This study and others lend support to the tensegrity model of cellular architecture, wherein a network of

cytoskeletal elements maintains a prestress within the cell which drives its adhesion and migration behavior (Wang et al., 1993; Wang et al., 2001).

Studies in fibroblasts have also revealed that traction forces tend to be spatially concentrated at the periphery of the cell, with little to no force being exerted beneath the nucleus of the cell. Force generation is also generally greater at the leading edge, or anterior of the cell, with weaker, more passive forces located in the posterior of the cell (Dembo and Wang, 1999; Munevar et al., 2001; Pelham and Wang, 1999). Interestingly, this trend is reversed in neutrophil migration, when forces are concentrated in the uropod of the cell during migration (Smith et al., 2007). Additionally, in fibroblast (Gaudet et al., 2003) and endothelial cell (Califano and Reinhart-King, 2010a; Reinhart-King et al., 2003) models, increasing the density of ECM protein conjugated to the surface of PA gels has been shown to increase both the spread area of cells and the magnitude of the force generated by these cells, although whether this phenomenon is driven by stronger cells spreading more or by larger cells inherently exerting greater forces remains an area of debate. Moreover, in this fibroblast model, the increase in force and area was also directly correlated to an increase in migration speed with increasing collagen density, suggesting that stronger traction forces drive increased cell motility (Gaudet et al., 2003).

In addition to the widespread use in the study of mammalian cells described here, 2D TFM has also been used to study the forces generated by several other unique cell types, for example, during the unique single cell and multicellular stages in the life of the amoeba *Dictyostelium discoideum* (Delanoe-Ayari et al., 2008; Lombardi et al., 2007), during migration of the malarial parasite *Plasmodium berghei* in the stage after

it is injected into the host's skin during a mosquito bite (Munter et al., 2009), and during the migration of fish keratocytes on compliant substrates (Lee, 2007).

Alternative 2D Methods

In addition to traction force microscopy, several other techniques have been developed to quantify traction forces during cell migration. In the late 1990's, Galbraith and Sheetz developed a micro-machined device consisting of an array of lithographically patterned silicon cantilever pads coated with ECM protein (Galbraith and Sheetz, 1997). This method allows for the quantification of isolated subcellular tractions, and as a result is quite sensitive, measuring forces on the order of single $nN/\mu m^2$. However, an individual cell can only depress a limited number of cantilevers at a time, limiting the spatial resolution of forces. Additionally, because the cantilevers can move in only one direction, they can only be used to quantify traction forces in that direction. For cells that do not cross the cantilever beam at a 90^o angle, forces are calculated based on the assumption that traction stresses are directed along only the long axis of the cell, which is not necessarily always valid (Califano and Reinhart-King, 2010a; Dembo and Wang, 1999). Moreover, production of the device requires an elaborate fabrication procedure that requires specialized technology that may not be readily accessible for many labs.

The most commonly used alternative to traction force microscopy is the use of microfabricated post array detection systems (mPADs) (du Roure et al., 2005; Tan et al., 2003). In this method, cylindrical microposts are fabricated out of polydimethylsiloxane (PDMS), and extracellular matrix protein is conjugated to the top of the posts to enable cell adhesion. Traction forces are based on the extent of deflection of the posts from their original position. Post deflection can then be linearly

correlated to the local traction forces exerted by the cell using classical beam bending theory. In this system, the height of the micropost can be varied to adjust the rigidity of the posts, and thus to adjust the stiffness of the substrate sensed by the cell. Each post acts as an individual vertical cantilever, sensing force at a discrete location beneath the cell. Moreover, unlike the silicon cantilevers described above, mPADs are able to detect forces generated in all directions of the x-y plane. A more detailed description of the fabrication process and supporting theory and computation can be found elsewhere (Fu et al., 2010; Sniadecki and Chen, 2007; Yang et al., 2011).

While elastomeric microposts offer several advantages over the original silicon cantilever system, there are several disadvantages that are important to note, especially when comparing this technique to PA gel-based traction force microscopy. First, there is considerable controversy over the appropriateness of culturing cells on a topographical landscape which is very distinct from the native environment of mammalian cells. mPADs restrict adhesions to distinct circular patches, imposing arbitrary constrictions on the size, shape, and location of focal adhesions, thus controlling where and how the cell transmits force (Yang et al., 2007). While this system has been used to elegantly determine the amount of force that individual focal adhesions can exert (Fu et al., 2010), it remains unclear how these calculations relate to the forces actually transmitted in the native physiological environment. Additionally, while the elastomeric posts may be more easily fabricated than the silicon cantilevers, and protocols have been published describing this process in great detail (Yang et al., 2011), an advanced microfabrication facility is still required to reproducibly fabricate the posts. PA gels, on the other hand, are easily produced using standard laboratory chemicals and equipment.

Another significant limitation of mPAD technology is the lower limit of E that can be produced. Posts have been successfully fabricated with a lower limit of $E \sim 1.5$ kPa (Fu et al., 2010), which is considerably higher than that of PA gels ($E \sim 0.1$ kPa), although it should be fairly noted that performing traction force microscopy on PA gels of $E < 1$ kPa has its own limitations. PA gels can also be used to examine the effect of mechanical communication of multiple cells through the underlying substrate (Califano and Reinhart-King, 2010a; Reinhart-King et al., 2008), a technique that could not be done using microposts, which effectively isolate cells from one another. On the other hand, the ability to mechanically isolate cells can be advantageous. For example, microposts were recently used to determine specific point forces at cell-cell junctions (Liu et al., 2010). In summary, elastomeric microposts and PA gels each have their own distinct advantages and disadvantages which must be considered when determining the appropriate system to use for quantifying traction forces in a given experiment.

3D Force Generation

While traction forces have been well characterized in 2D, very few cells exist physiologically in a strictly 2D environment. Rather, most cells reside in a fully 3D environment, surrounded by a fibrous and spatially complex extracellular matrix. However, the nature of processes known to be governed by traction forces, such as adhesion, migration, ECM deposition and remodeling, has been shown to be drastically altered in 3D compared to 2D. For example, when cells are embedded within a 3D collagen matrix, focal adhesions become smaller, often below the detection limit of conventional microscopy (Fraley et al., 2010). However, despite the apparent absence of classical focal adhesions, focal adhesion proteins still govern adhesion and motility in 3D by controlling protrusive behavior and matrix

deformation (Fraley et al., 2012; Fraley et al., 2010), two behaviors unimportant in controlling 2D migration. Additionally, the composition and regulation of these adhesions are significantly altered in 3D.

As in 2D, cell migration in 3D is partially governed by cellular force generation and matrix stiffness, although the connection and regulation of these aspects is much more complex and difficult to clearly elucidate (Dikovsky et al., 2008; Fraley et al., 2010; Mierke et al., 2008a; Zaman et al., 2006). Unlike 2D migration, cell migration in 3D is considerably restricted, controlled in large part by the pore size of the surrounding matrix (Carey et al., 2012; Wolf et al., 2003). While it is unclear what the precise role of force generation is in governing 3D cell motility, it is known that cells are able to exert force and contract a 3D matrix. There are a variety of techniques that have been developed to quantify single cell traction stresses within *in vitro* 3D microenvironments, typically relying on tracking either beads, as in a 3D analog of 2D traction force microscopy (Fraley et al., 2010; Shih and Yamada, 2010), or on tracking structural components of the matrix (Friedl et al., 1997; Kim et al., 2006) as the cell migrates in 3D.

The most common technique for mapping 3D traction forces is to track the displacement of fluorescent beads which have been embedded in a 3D matrix. There are two primary challenges this to this technique. First is the difficulty inherent in tracking bead displacement in three dimensions. This cannot be done reliably using traditional phase or epifluorescent microscopy, but rather requires rapid scanning confocal microscopy to precisely localize the beads in relation to the cell boundary with spatial accuracy in three dimensions. Second is the challenge of the matrix itself. Traditional 2D techniques require that the mechanics of the matrix be well-

characterized and isotropic. However, the native physiological environment in which cells normally reside is anything but isotropic. Rather, it is known to be extremely heterogeneous in terms of both chemical and mechanical composition. Synthetic hydrogels can be created which are mechanically isotropic, but which lack the fibrous nature of the native environment. For example, Legant et al. have developed an isotropic PEG hydrogel which they have used to calculate traction stresses of individual cells in 3D, finding that fibroblasts can exert forces up to 5 kPa, with forces primarily localized at polarized cell protrusions (Legant et al., 2010). This study represents one of the most thorough quantitative descriptions of traction forces in 3D to date, and is an excellent starting point for future work. However, the fibrous nature of the ECM cannot be ignored, as it imparts complex mechanical and chemical properties to the ECM, and is a critical determinant of cell behavior both *in vivo* and *in vitro*. An isotropic matrix which lacks fibrous architecture may not induce analogous force behavior in cells

To this end, other studies have translated changes in the native dynamic architecture of a fibrous ECM into quantifications of cellular forces. The use of a fibrous ECM permits native cell behaviors including ECM deposition, ECM remodeling and crosslinking, proteolytic path making and following. Additionally, because of the difference in refractive index between fibers and the surrounding media, the ECM fibers can be imaged using confocal reflectance microscopy. Therefore, interactions between individual cells and individual matrix fibers can be tracked in real time, allowing ECM reorganization to be used to describe cellular force generation in 3D environments both qualitatively and quantitatively.

1.4 Matrix Stiffening and Force Generation in Disease States

Matrix stiffness is altered during the progression of multiple diseases, including cancer (Levental et al., 2009; Paszek et al., 2005) and cardiovascular disease (Huynh et al., 2011), which together account for over 50% of fatalities in people over the age of 65. For example, during both aging and atherosclerosis, blood vessels stiffen dramatically, a phenomenon which has been shown by Huynh et al. to destabilize endothelial cell-cell contacts (Califano and Reinhart-King, 2008) and increase vascular permeability, further promoting atherogenesis (Huynh et al., 2011; Krishnan et al., 2011). While this study focused on the mechanisms of atherosclerotic progression, one could speculate from their results that the observed increase in permeability of blood vessels on stiff substrates could also have profound implications for tumor vasculature. It is well established that tumor vasculature is generally highly disorganized and leaky, which causes difficulties in effectively delivering chemotherapeutics to the tumor site (Pink et al., 2012). One possible cause of this deviance from normal vasculature could be the increased stiffness of the tumor microenvironment, which could drive an increase in endothelial cell branching and permeability, in a manner parallel to that previously observed in atherogenesis (Huynh et al., 2011). Further studies will be required to determine if this is indeed the case. Additionally, changes in matrix stiffness have been linked to many other disorders such as diabetes (Airaksinen et al., 1993), liver fibrosis and cirrhosis (Wells, 2008), emphysema (Kononov et al., 2001), and scleroderma (Enomoto et al., 1996).

During neoplastic progression, increased ECM deposition and crosslinking lead to a significant increase in tumor stiffness (Baker et al., 2012; Paszek et al., 2005). For example, in breast cancer, while a healthy mammary gland is highly compliant (E = ~200 Pa), the average tumor is over an order of magnitude stiffer (E = ~4000 Pa)

(Paszek et al., 2005). Additionally, both the stroma surrounding the tumor and the tumor vasculature exhibit increased stiffness (E = ~800-1000 Pa and ~450 Pa, respectively) compared to healthy mammary tissue and vasculature (E = ~200 Pa) (Lopez et al., 2011; Paszek et al., 2005). Interestingly, recent work by Lopez et al. has also shown that the tumor epithelium is significantly stiffer than isolated tumor epithelial cells (Lopez et al., 2011), suggesting that the stromal microenvironment plays a critical role in maintaining the stiff mechanical phenotype of the tumor. This increase in matrix stiffness has been shown to cluster integrins, upregulate focal adhesions, increase invasion, alter cell growth and morphology, and increase cell contractility (Baker et al., 2012; Kraning-Rush et al., 2012a; Levental et al., 2009; Paszek et al., 2005). Several of these effects have recently been shown to be mediated by increased phosphorylation of the focal adhesion kinase (FAK)/Src-signaling pathway resulting from enhanced enzymatic crosslinking of the tumor's extracellular matrix (Baker et al., 2012).

Given the intimate role that matrix stiffness plays in controlling traction forces, it is logical that cell contractility will likewise be affected by disease-induced matrix stiffening, or perhaps even a factor driving this stiffening. In the seminal work on tensional homeostasis during tumor progression, Paszek et al. found that increasing the stiffness of the 3D microenvironment surrounding mammary epithelial cells drives malignant progression by clustering integrins, increasing focal adhesion formation, disrupting adherens junctions, and increasing cell proliferation (Paszek et al., 2005). Likewise, Tang et al. found that increasing 2D stiffness promotes a metastasis-like phenotype in colon carcinoma cells (Tang et al., 2010), suggesting that increased mechanical stiffness may be an important driving factor in a wide range of cancer models. Additionally, Paszek et al. examined the relationship between malignancy and

contractile force generation. Using the human isogenic nonmalignant S-1 mammary epithelial cells and malignant T4-2 cell lines, they found that tractions forces were significantly elevated in the malignant cancer cells, and that these forces were RhoA-dependent (Paszek et al., 2005). Likewise, Rosel et al. found that in a rat sarcoma model of protease-independent amoeboid migration, highly metastatic A3 cells generated traction forces that were five times greater than the spontaneously transformed, non-metastatic K2 cells, with traction forces at the leading edge found to be even higher (Rosel et al., 2008). Moreover, using a Deformation Quantification and Analysis (DQA) algorithm to quantify collagen fiber deformation, Wyckoff et al. found that during non-proteolytic amoeboid migration, metastatic MTLn3E murine mammary tumor cells generated increased force, and were thus able to push through collagen fibers and invade into the ECM in 3D, while their non-metastatic parental cells were unable to invade (Wyckoff et al., 2006). However, more recent research has called into question the existence of protease-independent migration in native collagen environments, and this remains an area of great controversy in three dimensional tumor migration research (Sabeh et al., 2009), which will be discussed in more detail in the following section.

Surprisingly, in contrast to these four studies, Indra et al. recently found that in yet a different set of murine mammary tumor cells, traction forces actually decreased as the metastatic potential of the subpopulations increased (Indra et al., 2011). Similarly, using patterned PA gels and inducing tumoral transformation, Tseng et al. found that increased contractility appeared to be dependent on the method of transformation, with TGFβ-treated mammary epithelial cells generating increased force, while ErbB2 receptor-activated cells and CK2b-knockdown cells exerted weaker forces (Tseng et al., 2011). Given these conflicting results, the precise role of force generation in

cancer progression, and particularly in relation to proteolytic activity, remains somewhat unclear. It may be that the effect of malignant transformation on force generation is specific to the type of cancer and the underlying genetic mutations. Additionally, one significant challenge that remains in the study of the effects of matrix stiffening on tumor progression and force generation is difficulty in decoupling the effects of chemical and structural changes (e.g. ECM fiber crosslinking, reorganization, and bundling) from the effects of the intrinsic changes in stiffness that have been shown to accompany these changes.

1.5 ECM Architecture Affects Cancer Cell Behavior in 3D

Cells in the body experience a rich 3D topographical environment resulting from the various structural proteins of the ECM, which has proven difficult to effectively replicate *in vitro*. Collagen is the dominant structural protein in the human body, and as such gels consisting of polymerized collagen fibers have become one of the most popular *in vitro* systems for studying cellular response to physiological topographical cues (Carey et al., 2012; Kraning-Rush et al., 2012b; Kraning-Rush et al., 2011; Paszek et al., 2005; Provenzano et al., 2008b). Notably, increased stromal collagen deposition and crosslinking have been linked to poor prognosis in cancer patients (Ioachim et al., 2002; Levental et al., 2009; Provenzano et al., 2008a; Ramaswamy et al., 2003). While these factors contribute to the increased matrix stiffness of the tumor microenvironment, as discussed above, they also significantly alter the architecture of the ECM, which has been shown to directly mediate tumor cell migration. Metastatic cancer cells have been shown to disseminate from the primary tumor using a variety of techniques, migrating either as individual cell using amoeboid or mesenchymal-type movement, or collectively as cell sheets, strands, or clusters (Friedl 2003 Nat Rev). Moreover, recent work has shown that cancer cells can actively remodel the ECM

fibers surrounding a tumor, using contractile force to align the fibers perpendicularly to the tumor (Provenzano et al., 2006; Provenzano et al., 2008b). Cancer cells have been shown to then persistently migrate along these aligned fibers in a largely one-dimensional fashion both *in vitro* and *in vivo* (Conklin et al., 2011; Provenzano et al., 2008b). Indeed, Conklin et al. recently linked the presence of bundled and aligned collagen fibers to poor long-term survival in breast cancer patients (Conklin et al., 2011).

Microtrack Formation in Cancer Invasion

Cancer cell migration on the single cell level has been traditionally defined in two main categories: protease-dependent and protease-independent (Friedl and Wolf, 2003; Sabeh et al., 2009; Wolf et al., 2003; Wyckoff et al., 2006). Protease-dependent migration relies on the ability of cells to produce matrix metalloproteinases (MMPs) which can cleave ECM fibers and clear a pathway for the cell body (Sabeh et al., 2004; Sabeh et al., 2009). Protease-independent migration relies on mechanical forces exerted by the cell to displace the ECM fibers, and allows cells to move through the resulting space by adopting an amoeboid-like morphology (Sahai and Marshall, 2003; Wyckoff et al., 2006). Extensive work has been done in the last decade to show that when one of these pathways is inhibited, cancer cells are able switch their behavior and continue the invasion process (Friedl and Wolf, 2010; Wolf et al., 2003). However, these results have recently been called into question (Sabeh et al., 2009). New evidence suggests that many of these experiments utilized collagen which had been extracted with pepsin (Sahai and Marshall, 2003; Wolf et al., 2003), a process which removes the nonhelical telopeptides at the ends of the collagen molecules and prevents the fibrils from forming the covalent cross-links which are found *in vivo* (Sabeh et al., 2009). This lack of covalent cross-links has been shown to allow

protease-independent cancer cell migration that is not recapitulated in the more physiologically relevant, non-pepsinized collagen which retains robust cross-links (Sabeh et al., 2009). These data would suggest that all cancer cells rely on MMP activity to invade and metastasize, and perhaps have a lesser requirement for force generation. However, work has also been done on tumor cells *in vivo* showing that ROCK-mediated force generation, *not* MMP activity, is required for cancer cell motility (Wyckoff et al., 2006). Additionally, MMP-inhibitors to date have largely failed in clinical trials (Hua et al., 2011), suggesting that more studies need to be performed to validate this hypothesis. Moreover, extensive research on cancer cells in a broad variety of contexts has shown that, when presented with an obstacle or challenge, cancer cells will dramatically alter their metabolism, signaling, and behavior to adapt and survive (Hanahan and Weinberg, 2000; Hanahan and Weinberg, 2011). Additionally, it is known that some cancer cells can use proteolysis to form tube-like "microtracks" (Friedl and Wolf, 2008) which other cancer cells can then use to invade without using MMPs themselves.

Microtrack formation begins when individual cells disperse from the primary tumor using mesenchymal migration. Cells will generate protrusions along the leading edge which will attach to the ECM through integrin binding and activation (Friedl and Wolf, 2003). As the pseudopod elongates, the cell will generate traction forces to pull itself through the matrix. When the cell encounters a zone of physical resistance, where it is restricted by the surrounding ECM fibers, it will activate pericellular proteolysis to cleave these fibers and free the cell body to continue migrating forward (Friedl and Wolf, 2008). As the cell pushes forwards, it will mechanically reorient and align the surrounding collagen fibers along the direction of migration. Finally, the anterior of the cell will release its matrix adhesions to allow itself to glide forward.

Thus, in its wake the cell will leave a proteolytic microtrack, approximately the width of a single cell. As subsequent cells move into this space, they no longer encounter a zone of physical resistance, and therefore have no impetus to degrade the ECM further. As multiple cells enter the microtrack, the microtrack can be widened further, both with and without further degradation, eventually forming a 'macrotrack' and enabling collective cell invasion, in the form of strands or sheets, through the ECM (Ilina et al., 2011; Wolf et al., 2007). This mode of migration in the secondary cancer cells may be one example of true protease-independent migration which exists *in vivo*, and may also help to explain the failure of clinical MMP inhibitors, if they are administered after initial invasion has begun.

3D Microfabricated Structures for the Study of ECM Architecture on Cell Behavior

Given the importance of studying cells in environments which mimic their native environment, there has been a movement over the past few decades to recapitulate the topographical features encounter by normal and neoplastic cells *in vivo*. There has been a considerable amount of research using rigid micro- and nano-fabricated substrates such as polydimethylsiloxane (PDMS), poly(methylmethacrylate) (PMMA), silicon, and others to specifically assess the effects of tightly controlled topographical features on cell adhesion (Biela et al., 2009), morphology (Biela et al., 2009; Curtis and Wilkinson, 1999; Kulangara and Leong, 2009), migration behavior (Bettinger et al., 2009; Curtis and Wilkinson, 1999; Teixeira et al., 2003), and other cell functions. Cell behavior has been extensively analyzed on substrates containing features such as grooves, ridges, posts, and wells that are fabricated at the sub-cellular, cellular, and super-cellular scales (for detailed reviews, see (Curtis and Wilkinson, 1999), (Kulangara and Leong, 2009) and (Bettinger et al., 2009)). Nanogratings or ridges in

particular have been used by many labs to induce cytoskeletal alignment and guided migration in different cell types, including smooth muscle cells, macrophages, corneal epithelial cells, fibroblasts, endothelial cells, and neurons, with optimal ridge width varying significantly with cell type (Biela et al., 2009; Corey and Feldman, 2003; Teixeira et al., 2003; Wojciak-Stothard et al., 1996). Interestingly, in a seminal study by Doyle et al., fibroblast migration on micropatterned 1D substrates was found to closely mimic 3D migration along ECM fibers (Doyle et al., 2009). They also found that the mechanisms of migration employed by the fibroblasts were similar between 1D and 3D environments, but were in distinct contrast to 2D migration mechanisms (Doyle et al., 2009), thus highlighting the ongoing need for improved 3D and 3D-like topographical model systems.

Additionally, several groups have used microfabricated structures to study cancer cell migration under conditions of mechanical confinement within narrow PDMS channels which mimic the dimensions of microtracks created by tumor cells *in vivo*, as discussed in the previous section (Irimia and Toner, 2009; Mak et al., 2011; Rolli et al., 2010; Scherber et al., 2012; Tong et al., 2012). When introduced to channels that are of average cell-width (approximately 3-10 μm), cancer cells have been shown to preferentially and persistently invade through these channels, with (Tong et al., 2012) or without (Irimia and Toner, 2009; Mak et al., 2011) the application of the chemical gradients often required to induce persistent cell migration on planar 2D substrates. Interestingly, this mechanism of migration appears to resemble the migration in 1D and 3D fibrillar environments by Doyle et al., discussed above (Doyle et al., 2009), particularly in its dependence on intact microtubule dynamics (Irimia and Toner, 2009). In another example of using rigid substrates to study cancer cell migration, Liu et al. have used microfabricated silicon posts with height of several hundred microns,

nicknamed Tepuis, to study metastatic prostate cancer invasion behavior (Liu et al., 2011). They found that highly metastatic PC-3 prostate cancer cells efficiently invade the Tepui tops and proceed to confluency, while less metastatic LNCaP cells are not able to achieve similar levels of invasion (Liu et al., 2011).

While these systems have been used to elegantly describe the effects of different micro- and nano-topographical features on several key cell functions, it remains difficult to interpret their physiological relevance, as no surface within the body (with the exception of bone) shares such a rigid stiffness. As discussed previously, matrix stiffness has been shown to have a dramatic effect on cell migration, adhesion, force generation, and multiple other behaviors. Therefore, to more accurately assess the effects of topographical features on cell behavior, there is a great need to adapt methods to create topography on softer, more physiologically-relevant substrates. Additionally, to specifically determine the mechanisms guiding cancer migration within cell-generated microtracks, a system must be generated which recapitulates as closely as possible the native microtrack environment.

1.6 Organization of the Dissertation

The objective of this work is to elucidate the role of force generation during metastatic invasion, particularly in relation to invasion through proteolytic microtracks. Herein, I present data describing how matrix composition, including mechanical stiffness, ligand availability, and three-dimensional architecture, affects cancer cell behavior in terms of both force generation and motility.

In Chapter 2, I demonstrate that force generation on 2D substrates is increased in metastatic breast, prostate, and lung cancer cells, compared to their non-metastatic

counterparts. Additionally, I show that traction forces are increased with increased matrix stiffness and collagen density. This work implicates traction forces as a potential contributor to metastatic invasion. These studies are the first to my knowledge to compare the traction stresses of paired metastatic and non-metastatic cells from several human cancer models. Moreover, these findings provide the first evidence that differential profiles of metastatic cancer cells may aid in determining metastatic ability, and could be useful as a mechanical biomarker of metastatic potential.

In Chapter 3, I present a novel method for creating 3D collagen microtracks which recapitulate the natural proteolytic tracks formed during metastatic invasion. Using this technique, I show that migration speed and invasion distance within these microtracks is increased in both tumor cells and non-invasive mammary epithelial cells. Finally, I demonstrate that this migration occurs entirely independently of MMP activity, revealing novel insight into the clinical challenges of treating patients with MMP inhibitors.

In Chapter 4, I examine in more detail the specific mechanisms guiding cancer cell migration within the collagen microtracks first described in Chapter 3. Surprisingly, I show that migration continues to occur when contractility is inhibited via the Rho/ROCK pathway. Instead, I find that migration is contingent upon having an intact and polarized actin and microtubule cytoskeleton and, additionally, is also dependent on focal adhesion formation. This work is the first to identify the governing principles of MMP-independent migration within the 3D microtrack environment.

In Chapter 5, additional data related to various side projects is discussed, including the effects of hypoxia on force generation. In Chapter 6, conclusions and future directions are presented. Experimental protocols are provided in the appendices.

CHAPTER 2

CELLULAR TRACTION STRESSES INCREASE WITH INCREASING METASTATIC POTENTIAL

This chapter was published in *PLoS One* (Kraning-Rush et al., 2012a).

2.1 Abstract

Cancer cells exist in a mechanically and chemically heterogeneous microenvironment which undergoes dynamic changes throughout neoplastic progression. During metastasis, cells from a primary tumor acquire characteristics that enable them to escape from the primary tumor and migrate through the heterogeneous stromal environment to establish secondary tumors. Despite being linked to poor prognosis, there are no direct clinical tests available to diagnose the likelihood of metastasis. Moreover, the physical mechanisms employed by metastatic cancer cells to migrate are poorly understood. Because metastasis of most solid tumors requires cells to exert force to reorganize and navigate through dense stroma, we investigated differences in cellular force generation between metastatic and non-metastatic cells. Using traction force microscopy, we found that in human metastatic breast, prostate and lung cancer cell lines, traction stresses were significantly increased compared to non-metastatic counterparts. This trend was recapitulated in the isogenic MCF10AT series of breast cancer cells. Our data also indicate that increased matrix stiffness and collagen density promote increased traction forces, and that metastatic cells generate higher forces than non-metastatic cells across all matrix properties studied. Additionally, we found that cell spreading for these cell lines has a direct relationship with collagen density, but a biphasic relationship with substrate stiffness, indicating that cell area

alone does not dictate the magnitude of traction stress generation. Together, these data suggest that cellular contractile force may play an important role in metastasis, and that the physical properties of the stromal environment may regulate cellular force generation. These findings are critical for understanding the physical mechanisms of metastasis and the role of the extracellular microenvironment in metastatic progression.

2.2 Introduction

While significant advances have been made in the treatment of primary tumors through surgery, chemotherapy and radiation treatment, a mechanism for effectively diagnosing the likelihood of metastasis remains elusive (Steeg, 2006). Metastasis is the leading cause of death among cancer patients, resulting in over 90% of cancer-related fatalities (Christofori, 2006). Moreover, there is currently no procedure or test that can definitively determine the metastatic potential of a specific tumor. Clinical oncologists routinely rely on pathology reports and historical statistics to determine patient prognosis and to design a course of palliative therapy (Ravdin et al., 2001).

Because metastasis has become the primary obstacle in cancer treatment, there is a substantial body of work attempting to discover a biological marker (or set of markers) for metastasis, but with marginal success (Sidransky, 2002). Previous studies have linked overexpression of VEGF-D (Stacker et al., 2001), urokinase plasminogen activator (Duffy, 1996), the growth factor receptor CXCR2 (Mierke et al., 2008b) and activator protein-1 (Ozanne et al., 2000) to increased metastatic breast cancer invasion in vitro and in vivo. Additionally, studies have shown that a combination of genes can affect organ-specific tropism (Kang et al., 2003). However, these discoveries have generally not been applicable to multiple cancer types, or even within subtypes of a

single cancer. Recently, advances in genetic profiling have led to the identification of a 17-gene expression signature for metastasis in primary adenocarcinomas (Ramaswamy et al., 2003), as well as a 70-gene expression signature for predicting the clinical prognosis of breast cancer (Sotiriou et al., 2003). While patients whose tumors contain these expression patterns will benefit from this kind of genetic analysis, it may not be applicable to a broad spectrum of patients with heterogeneous tumor populations. Additionally, while these signatures may show significant statistical correlation with poor prognosis, they are not descriptive of the physical behaviors of the tumor cells that lead to these clinical results.

Alterations in gene expression patterns result in phenotypic changes at the cellular level during cancer progression. As such, the biophysical characteristics of tumor cells may be a more appropriate and accessible clinical indicator than individual genetic alterations. During metastatic invasion, cancer cells encounter a complex and constantly evolving microenvironment (Kumar and Weaver, 2009) consisting of upregulated extracellular matrix proteins (Ioachim et al., 2002; Levental et al., 2009; Ramaswamy et al., 2003), different degrees of extracellular matrix (ECM) crosslinking (Levental et al., 2009), mechanical heterogeneity (Lopez et al., 2011; Paszek et al., 2005), varying oxygen levels (Harris, 2002), as well as exposure to shear stress and interstitial pressure (Kumar and Weaver, 2009). To successfully navigate this dynamic microenvironment, tumor cells must generate force to reorganize the basement membrane, invade into surrounding stroma (Rosel et al., 2008; Wolf et al., 2007), migrate along ECM fibers (Provenzano et al., 2008b; Wyckoff et al., 2006) and transmigrate through the endothelial cell barrier (Mierke et al., 2008b) to enter the circulatory or lympathic system. In addition to enzymatically degrading the ECM with matrix metalloproteinases, metastatic cells can use force to mechanically

rearrange their ECM to clear a path for migration (Wolf et al., 2007). There is evidence from in vivo imaging that cells use re-oriented fibers as "train-tracks" to guide their migration away from the primary tumor (Provenzano et al., 2008b). Traction forces have previously been shown to mediate normal cell migration (Lauffenburger and Horwitz, 1996), adhesion (Pelham and Wang, 1997; Reinhart-King, 2008), mechanotransduction (Discher et al., 2005), and ECM remodeling (Bloom et al., 2008; Lemmon et al., 2009; Provenzano et al., 2008b). Notably, these processes are also involved in cancer progression. Paszek et al. have shown a marked difference in the magnitude and organization of traction stresses between cancerous and untransformed mammary epithelial cells, suggesting inherent differences in cell force generation in the cancerous phenotype (Paszek et al., 2005). However, the effects of metastatic potential on force generation have not yet been thoroughly investigated.

Matrix stiffness has been shown to have a distinct effect on force-mediated cellular behaviors including migration (Baker et al., 2009; Gjorevski and Nelson, 2010; Ulrich et al., 2009; Zaman et al., 2006), adhesion (Discher et al., 2005; Huynh et al., 2011; Kim and Asthagiri, 2011), and ECM remodeling (Levental et al., 2009; Wolf et al., 2007). Because metastasizing cancer cells are exposed to both the increased stiffness of the stroma surrounding most solid tumors, as well as more compliant adipose tissue, it is important to understand the effects of a dynamic mechanical environment on cancer cell force generation. Similarly, ligand density has also been shown to have a significant effect on the force generation of non-cancerous cell types, such as endothelial cells and fibroblasts (Califano and Reinhart-King, 2010a; Gaudet et al., 2003; Willcox et al., 2005). During cancer progression, the chemical nature of the extracellular matrix experiences significant changes, affecting the number and nature

of binding sites available for tumor cell adhesion and migration. Collagen metabolism has been shown to be dysregulated, with elevated expression, increased deposition, and an increase in collagen crosslinking that contributes to the overall stiffening of the surrounding microenvironment (Levental et al., 2009). These factors lead to an increase in mammographic density, which has been specifically correlated to an increased risk for the development of breast cancer (Martin and Boyd, 2008). An increase in collagen expression has also been clinically linked to metastatic tumors by genetic analysis of tumor biopsies (Ramaswamy et al., 2003). Therefore, understanding the independent and interdependent relationships between substrate mechanics, collagen density, and force generation is critical for understanding the mechanism(s) driving metastatic progression.

In this study, we investigate traction force generation as a biophysical marker of metastatic potential. We quantify contractile forces of highly metastatic breast, prostate, and lung cancer cell lines compared to non-tumorigenic epithelial cell lines seeded on substrates of varying stiffness and collagen density using traction force microscopy. Here, we show that highly metastatic cancer cells exert significantly increased forces across all matrix properties studied. Moreover, our data show that increased matrix stiffness and collagen density both promote increased traction forces. These findings provide the first evidence to our knowledge that differential force profiles of metastatic cells may aid in determining metastatic potential.

2.3 Materials and Methods

Cell Culture

MCF10A mammary epithelial cells (American Type Culture Collection (ATCC), Rockville, MD) were maintained in Dulbecco's Modified Eagle's Media

supplemented with 5% horse serum, 20 ng/mL EGF (Invitrogen, Carlsbad, CA), 10 μg/mL insulin, 0.5 μg/mL hydrocortisone, 100 ng/mL cholera toxin (Sigma-Aldrich, St. Louis, MO), and 1% penicillin-streptomycin (Invitrogen)(Debnath et al., 2003). MDAMB231 highly metastatic breast adenocarcinoma cells (ATCC) were maintained in Minimum Essential Medium supplemented with 10% fetal bovine serum, and 1% penicillin-streptomycin (Invitrogen).

PC3 highly metastatic prostate adenocarcinoma cells (ATCC) were maintained in Kaighn's Modification of Ham's F-12 Medium (ATCC) supplemented with 10% fetal bovine serum and 1% penicillin-streptomycin (Invitrogen). PrEC primary human prostate epithelial cells (Lonza, Walkersville, MD) were maintained in PrEGM prostate epithelial cell growth medium (Lonza) supplemented with SingleQuots (Lonza) according to the manufacturer's recommended protocol.

BEAS2B bronchial epithelial cells (ATCC) were maintained in BEBM bronchial epithelial cell basal medium (Lonza) supplemented with SingleQuots (Lonza) according to ATCC recommended protocol, and 1% penicillin-streptomycin (Invitrogen). A549 metastatic lung carcinoma cells (ATCC, CCL-185) were kindly provided by Paraskevi Giannakakou (Weill Cornell Medical College) and were maintained in RPMI 1640 supplemented with 10% fetal bovine serum, 1% penicillin-streptomycin, and 1 μg/mL puromycin (Invitrogen).

MCF10AT1 transformed mammary epithelial cells and MCF10CA1a metastatic mammary epithelial cells were obtained from the Barbara Ann Karmanos Cancer Institute (Detroit, MI) and were maintained in 1:1 Dulbecco's Modified Eagle's Media / F12 supplemented with 5% horse serum, 20 ng/mL EGF (Invitrogen), 10 μg/mL

insulin, 0.5 μg/mL hydrocortisone, 100 ng/mL cholera toxin (Sigma-Aldrich), and 1% penicillin-streptomycin (Invitrogen)(Santner et al., 2001). All cells were cultured at 37^{o}C and 5% CO_2. Live cell imaging was performed in a custom temperature, humidity, and CO_2- controlled stage of a Zeiss Axio Observer Z1m inverted phase contrast microscope with a Hamamatsu ORCA-ER camera.

Substrate Synthesis and Traction Force Microscopy

Substrates of various Young's moduli (1 – 10 kPa) were synthesized with varying ratios of 3-7.5% acrylamide (40% w/v solution, Bio-Rad, Hercules, CA) and 0.1-0.35% N,N'-methylene-bis-acrylamide (2% w/v solution, Bio-Rad) as described previously (Kraning-Rush et al., 2012b; Reinhart-King, 2008). Substrate surfaces were functionalized using N-6-((acryloyl)amido)hexanoic acid, synthesized in our lab (Califano and Reinhart-King, 2010a), covalently bound to 0.0001-0.1 mg/mL type I rat-tail collagen (Becton Dickinson, Franklin Lakes, NJ). The Young's modulus (E) of the polyacrylamide substrates was verified as previously described (Califano and Reinhart-King, 2010a; Huynh et al., 2011; Kraning-Rush et al., 2012b). Traction force microscopy (TFM) was performed as previously described (Dembo and Wang, 1999; Kraning-Rush et al., 2012b; Kraning-Rush et al., 2011). Briefly, cells were seeded on polyacrylamide substrates (E = 1-10 kPa) embedded with 0.5-μm fluorescent beads and allowed to adhere overnight. Cells were then imaged in phase and bead distributions were imaged in fluorescence before and after removal of the cell with trypsin. Bead displacement within the substrate was tracked with correlation-based optical flow and converted into a strain field. These strain fields were converted into traction stresses using the LIBTRC analysis library developed by Professor Micah Dembo of Boston University, who invented the basic theory that underlies TFM (Dembo and Wang, 1999). Images were processed with LIBTRC

software to determine the cellular traction vectors, T, the total magnitude of the force, |F|, and the projected cell area. |F| is an integral of the traction field over the entire area of the cell,

$$|F| = \iint \left(T_x^2(x,y) + T_y^2(x,y)\right)^{1/2} dxdy \tag{2.1}$$

where $T(x,y) = \left[T_x(x,y), T_y(x,y)\right]$ is the continuous field of local traction vectors defined at local spatial coordinates (x,y) in the projected cell area (Reinhart-King et al., 2005). More than 40 cells were analyzed per condition.

Statistical Tests

Data were compared with analysis of variance and Tukey's Honestly Significantly Different test or Student's t test where appropriate in JMP software (v.8, SAS, Cary, NC). All data were logarithmically transformed prior to analysis to ensure normal distribution. All data are reported as mean ± standard error of the mean (SEM).

2.4 Results

Metastatic Cancer Cells Exert Stronger Traction Forces

To investigate the relationship between cellular traction force generation and metastatic potential, we examined the differences in traction force generation in three independent cancer models: breast, prostate, and lung cancer. These cancers comprise the three most fatal cancers in both men and women (Pickle et al., 2007), with metastatic disease being the ultimate cause of death in over 90% of these patients (Christofori, 2006). During metastatic progression, phenotypic changes in cancer cells result in altered adhesion and migration behavior, allowing cells to escape from the tumor mass into surrounding tissue (Kumar and Weaver, 2009). Because contractile force is known to mediate these behaviors in normal cells (Pelham and Wang, 1997; Reinhart-King, 2008), we hypothesized that cancer cells require increased force

generation to metastasize. For each type of cancer, we chose a cell line (breast, prostate, lung, respectively) that was previously characterized as highly invasive in vitro and metastatic in vivo (MDAMB231, PC3, and A549), as well as a non-tumorigenic, non-metastatic control cell population that is representative of healthy native epithelial tissue (MCF10A, PrEC, and BEAS-2B, respectively).

At a moderate stiffness mimicking tumorigenic conditions in breast tissue (Young's Modulus (E) = 5 kPa)(Paszek et al., 2005), measurements of cellular force using TFM indicate that MDAMB231 highly metastatic breast cancer cells exhibited stronger traction stresses compared to the non-metastatic MCF10A mammary epithelial cells (Fig. 2.1A). Likewise, both the PC-3 highly metastatic prostate cancer cells (Fig. 2.1B) and the A549 metastatic lung cancer cells (Fig. 2.1C) exhibited significantly greater traction stresses than the non-metastatic PrEC primary prostate epithelial cells and the BEAS-2B lung epithelial cells, respectively. These data suggest that increasing force generation in cells of high metastatic potential may be a biophysical characteristic of metastatic cells that could potentially act as a mechanical marker for metastasis.

Substrate Stiffness and Collagen Density Mediate Magnitude of Traction Force

Because cancer cells encounter heterogeneous environments exhibiting a range of stiffness during metastatic progression in vivo, such as stiff, matrix-dense regions near the tumor and compliant adipose tissue during stromal invasion (Paszek et al., 2005), we measured the traction forces exerted on substrates of varying stiffness (E = 1 – 10 kPa), with collagen density being held constant (0.1 mg/mL). We found that, in addition to exerting greater forces on substrates of tumorigenic stiffness (Fig. 2.1A), MDAMB231 cells also have a greater overall net traction force (|F|) than MCF10A

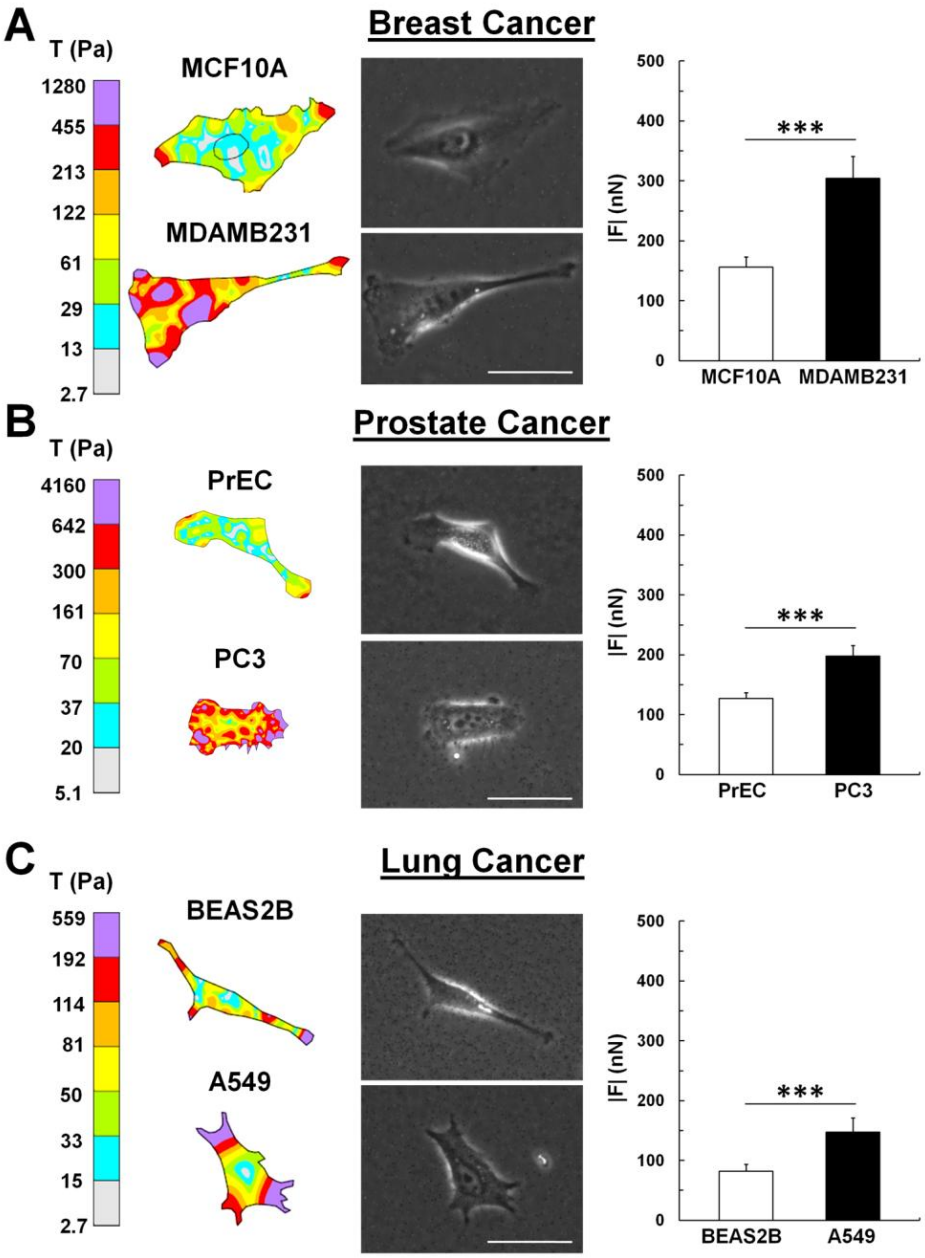

Figure 2.1. Metastatic cancer cells exert greater forces than non-metastatic cells. (A) Representative traction maps (left), corresponding phase images (middle), and overall net traction force (|F|, right) of non-metastatic mammary epithelial (MCF10A) and highly metastatic (MDAMB231) cancer cells. (B) Representative traction maps (left), corresponding phase images (middle), and |F| (right) of non-metastatic primary prostate epithelial cells (PrEC) and highly metastatic prostate cancer cells (PC3). (C) Representative traction maps (left), corresponding phase images (middle), and |F| (right) of non-metastatic bronchial epithelial cells (BEAS2B) and metastatic lung adenocarcinoma cells (A549). All cells are on polyacrylamide substrates with Young's Modulus (E) = 5 kPa and type I collagen concentration of 0.1 mg/mL. Scale bar = 50 μm. Mean + SEM; *** indicates $p < 0.001$.

trend was also recapitulated with the prostate and lung cancer models, in which the metastatic PC3 (Fig. 2.2B) and A549 (Fig. 2.2C) prostate and lung cancer cells exerted significantly greater forces than non-metastatic PrEC and BEAS2B cells on stiff substrates. On more compliant substrates (E = 1 kPa), the metastatic cells of each cancer type studied exert slightly higher forces than their non-metastatic counterparts. Additionally, we observed a significant increase in net traction force with increasing substrate stiffness within all 6 cell lines ($p < 0.01$), suggesting that the stiffness of the environment surrounding cancer cells can directly contribute to the amount of traction force exerted at a single cell level. These data indicate that the stiffness of the microenvironment significantly affects the magnitude of forces generated by metastatic and non-metastatic cells, and suggest that, in general, metastatic cells are able to exert greater net traction forces than non-metastatic cells.

Collagen content of the microenvironment also changes throughout neoplastic progression (Levental et al., 2009), with increased collagen expression particularly noted in clinical analyses of high grade tumors (Ramaswamy et al., 2003). As such, we examined the effect of collagen density on cancer cell traction forces. Using substrates of constant stiffness (E = 5 kPa) and varying collagen density (0.0001 – 0.1 mg/mL), we found that metastatic MDAMB231 breast cancer cells exert a greater net traction force ($|F|$) than non-metastatic MCF10A cells across the entire range of collagen densities tested (Fig. 2.3A). This trend is recapitulated with both the prostate and the lung cells, with metastatic PC3 (Fig. 2.3B) and A549 (Fig. 2.3C) prostate and lung cancer cells exerting greater forces than their non-metastatic counterparts, PrEC and BEAS2B cells, on substrates with varying collagen density. Similar to the previously observed trend of increasing force with increasing stiffness, all 6 cell lines also showed a significant increase ($p < 0.01$) in net traction force with increasing

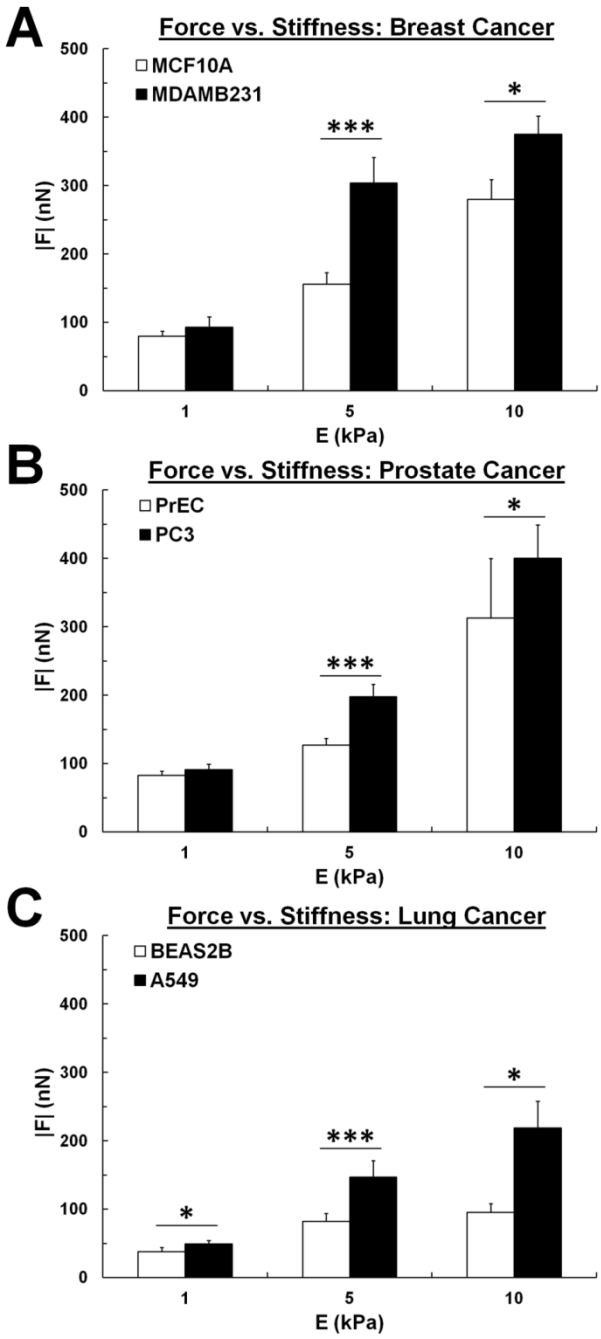

Figure 2.2. Increased matrix stiffness contributes to increased force generation. Net traction force (|F|) increases with increasing substrate stiffness (E = 1-10 kPa) for (A) MCF10A non-metastatic mammary epithelial cells and MDAMB231 metastatic cancer cells, (B) PrEC non-metastatic primary prostate epithelial cells and PC3 metastatic prostate cancer cells, and (C) BEAS2B non-metastatic bronchial epithelial cells and A549 metastatic lung cancer cells. Ligand density is maintained at 0.1 mg/mL collagen I. 5 kPa data is from Fig. 1. Note also that the metastatic cancer cells (black) exert greater forces than non-metastatic cells (white) at all matrix stiffness levels studied. Mean + SEM; * indicates $p < 0.05$; *** indicates $p < 0.001$.

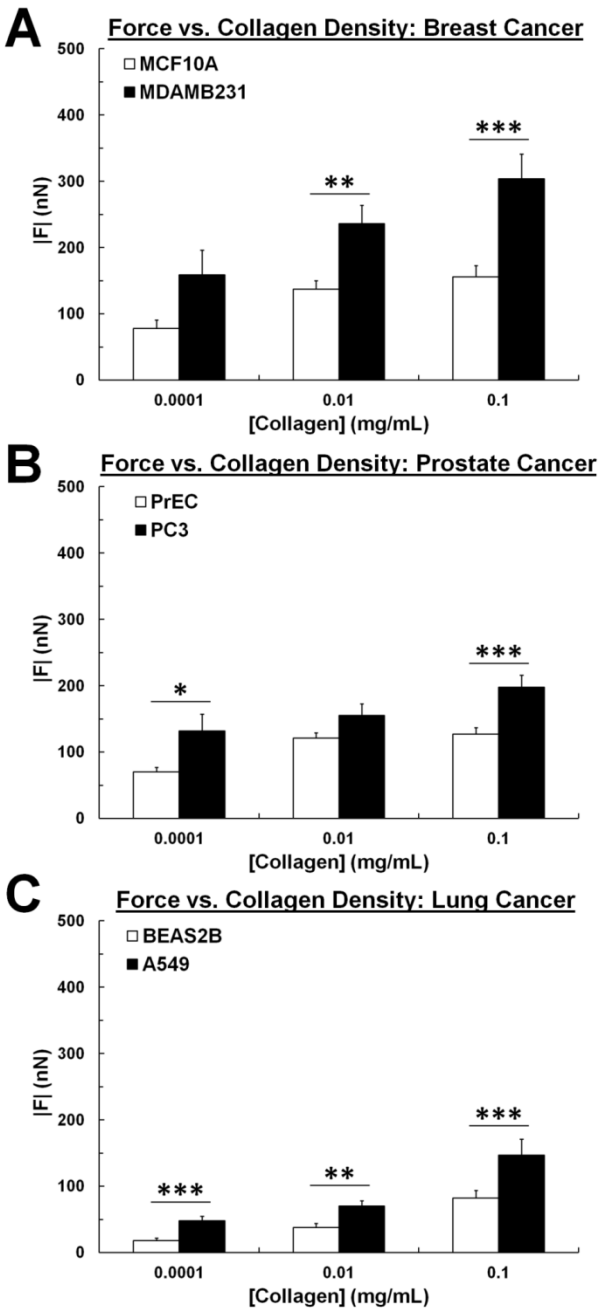

Figure 2.3. Increased collagen density contributes to increased force generation. Net traction force (|F|) increases with collagen density (0.0001-0.1 mg/mL collagen I) for (A) MCF10A non-metastatic mammary epithelial cells and MDAMB231 metastatic cancer cells, (B) PrEC non-metastatic primary prostate epithelial cells and PC3 metastatic prostate cancer cells, and (C) BEAS2B non-metastatic bronchial epithelial cells and A549 metastatic lung cancer cells. Stiffness is maintained at E = 5 kPa. 0.1 mg/mL collagen I data is from Fig. 1. Note also that the metastatic cancer cells (black) exert greater forces than non-metastatic cells (white) at all collagen densities studied. Mean + SEM; * indicates $p < 0.05$; ** indicates $p < 0.01$; *** indicates $p < 0.001$.

density, suggesting that increased collagen content within the tumor microenvironment can also drive force generation of cancer cells. Together these data indicate that metastatic and non-metastatic cells have differential force profiles that are significantly affected by mechanical and chemical matrix properties of the tumor microenvironment.

Differences in Force Generation are not Correlated to Differences in Cell Spreading

Because cellular force generation has been linked to cell spread area in previous studies (Califano and Reinhart-King, 2010a; Gaudet et al., 2003), we assessed whether increased cellular traction force in metastatic cells on both stiff matrices and those displaying high densities of collagen was simply caused by an increase in cell area (i.e. that larger cells exert higher forces). The area of isolated cells was measured during the TFM experiments previously described. We observed no significant or consistent trend when comparing the spreading area of metastatic breast, prostate, and lung cancer cells to their non-metastatic epithelial cell counterparts across substrates of constant collagen density and varying stiffness (Fig. 2.4A) or across substrates of constant stiffness and varying collagen density (Fig. 2.4B) ($p > 0.05$). These data indicate that the observed increases in traction force in metastatic versus non-metastatic cells are not linked to cell area. Interestingly, we noted that five of the six cell lines (excluding the non-metastatic PrEC prostate epithelial cells) exhibited a biphasic relationship with substrate stiffness, with the maximum cell spreading area occurring on polyacrylamide substrates of an intermediate stiffness (E = 5 kPa) (Fig. 2.4A). In contrast, we observed that these same five cell lines exhibited a direct relationship between spreading area and collagen density across the range of 0.0001 –

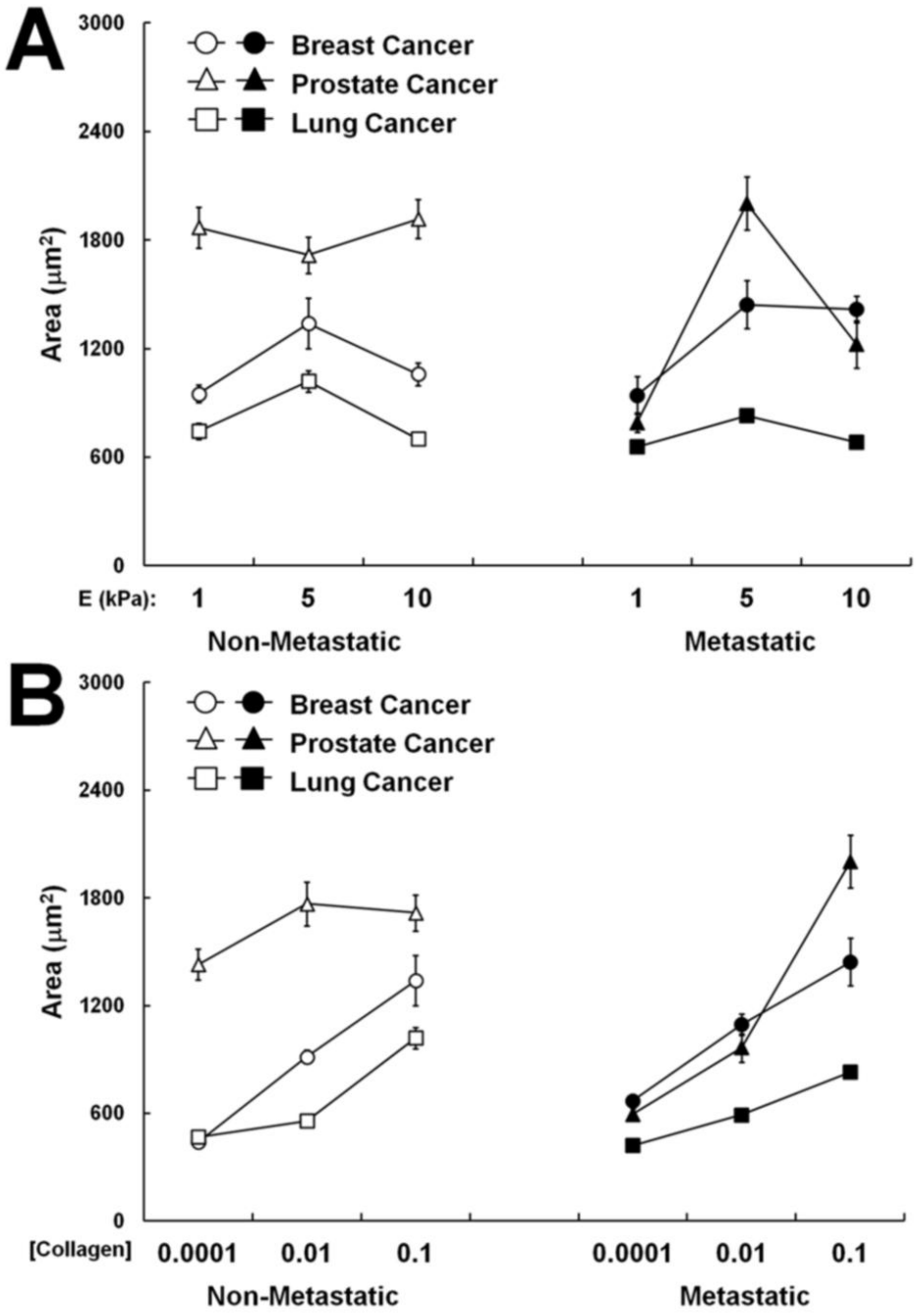

Figure 2.4. Cell area is differentially altered by matrix stiffness and collagen density. Projected cell area shows a biphasic relationship with substrate stiffness (A) and a direct relationship with collagen density (B) in the majority of the metastatic (black) and non-metastatic cells (white) studied. No consistent trend was observed when comparing the projected cell area of complementary metastatic and non-metastatic cells.

0.1 mg/mL, with increased area correlating with increased collagen density (Fig. 2.4B).

To further investigate the role of cell area in the generation of traction forces, we analyzed the net traction force (|F|) of each cell normalized by its projected area (|F|/A) as a measurement of average traction stress. When the traction forces of cells plated on substrates of variable stiffness were normalized by their respective areas, average traction stress increased with increasing stiffness ($p < 0.0001$, Fig. 2.5A). Therefore, the increased force on stiffer substrates is not due to increased cell spreading. However, the average traction stress of cells plated on substrates of variable collagen density revealed an overall equalization of forces across the collagen concentrations tested (Fig. 2.5B). These data suggest that increased collagen density may promote force generation by causing an increase in cell spreading.

Metastatic Cells Exert Increased Force in an Isogenic Model

Because the cell lines used in these experiments are of genetically distinct lineages, we further investigated our hypothesis that metastatic cells generated increased traction forces compared to non-metastatic cells using an isogenic cell model: the 10AT series of cell lines. The 10AT series consists of several cell lines which have been developed to represent the full spectrum of neoplastic progression (Santner et al., 2001). We focused on the MCF10AT1 and MCF10CA1a lines (Kim et al., 2009; Mehta et al., 2004; Santner et al., 2001), compared to their parental spontaneously immortalized MCF10A cells used previously in this work. MCF10AT1 cells were derived from MCF10A cells transfected with the constitutively active Ha-ras oncogene. These cells are considered ‘premalignant’ and will first form simple ducts

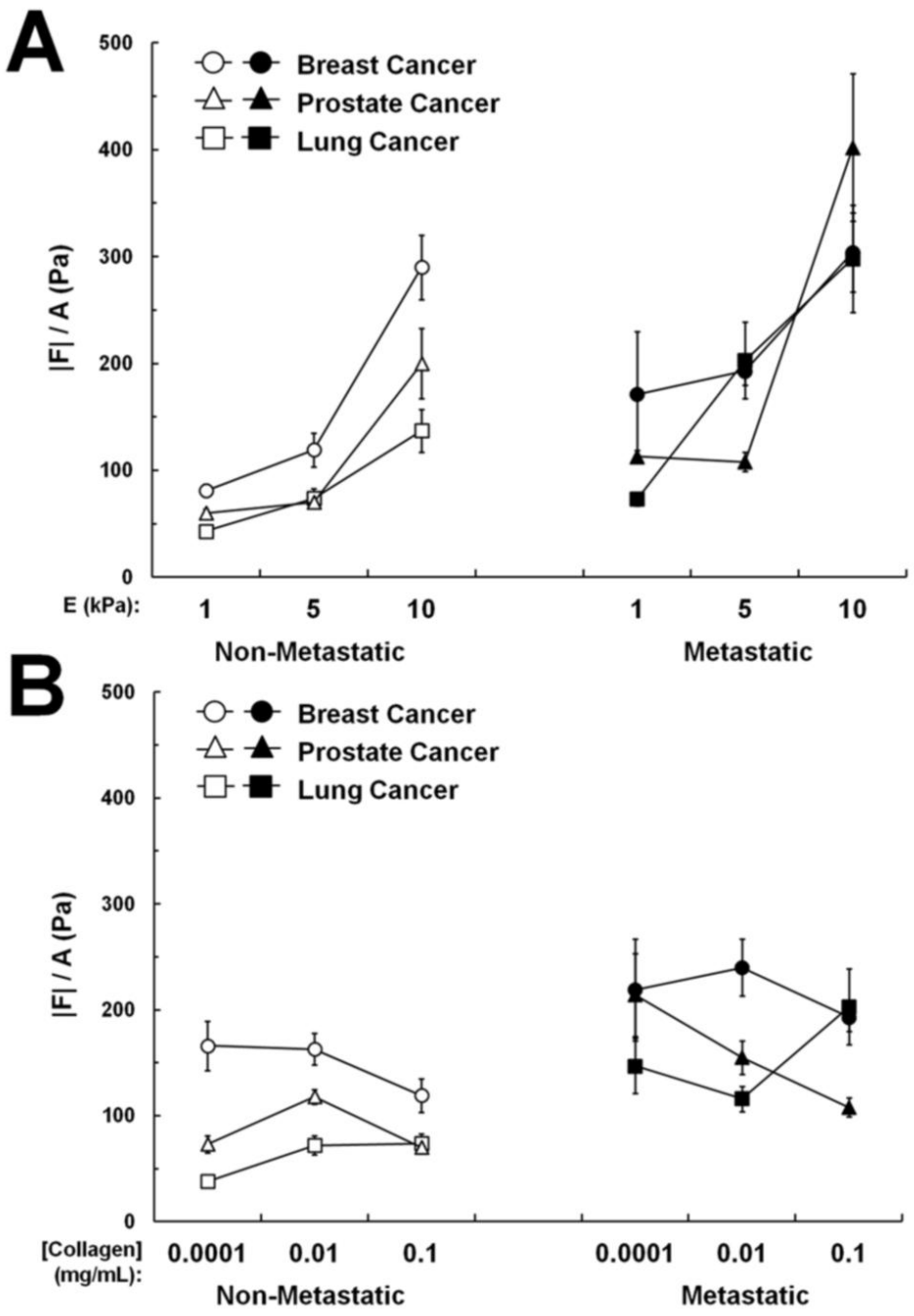

Figure 2.5. Average traction stress increases with stiffness, not collagen density. |F| of each cell is normalized by its projected area (|F|/A) as a measurement of average traction stress. Average traction stresses increase with increasing substrate stiffness (A) and become relatively uniform with increasing collagen density (B).

in nude mice xenografts, followed by benign lesions which occasionally progress to carcinomas (Mehta et al., 2004). MCF10CA1a cells were selectively derived from the MCF10AT1 carcinoma populations. These cells form undifferentiated carcinomas and rapidly growing metastases within the lungs Together, the MCF10A, MCF10AT1, and MCF10CA1a are isogenic human cell lines representative of different stages of metastatic potential: non-tumorigenic, premalignant, and highly metastatic (Fig. 2.6A) (Kim et al., 2009; Mehta et al., 2004; Santner et al., 2001). The highly metastatic MCF10CA1a derivative exerted significantly greater traction forces compared to the benign MCF10AT1 and non-tumorigenic parental MCF10A cells (Fig. 2.6B) on substrates mimicking the stiffness of tumorigenic breast tissue (E = 5 kPa)(Paszek et al., 2005). When the net traction force was normalized by projected area, there was a significant increasing trend in average traction stress ($p < 0.001$, Fig. 2.6D). Overall, these data from an isogenic cell model correlate well with the data from breast, prostate, and lung cells derived from different genetic backgrounds (Fig. 2.1).

2.5 Discussion

To date, there is no universal molecular marker of metastasis. Because of the known role of cellular force in cell migration, we explored traction force generation as a potential biophysical marker characteristic of cells with metastatic ability. The results presented here show that highly invasive breast, prostate, and lung cancer cells exert significantly greater traction forces than their non-invasive epithelial cell counterparts on 2D substrates of physiologically relevant stiffness and varying collagen density. These findings indicate that inherent force differences exist in cells of differing metastatic potential. Additionally, increased matrix stiffness and ligand density promote increased contractile force generation in contrasting ways: collagen density appears to lead to increased cellular force generation by directly mediating cell

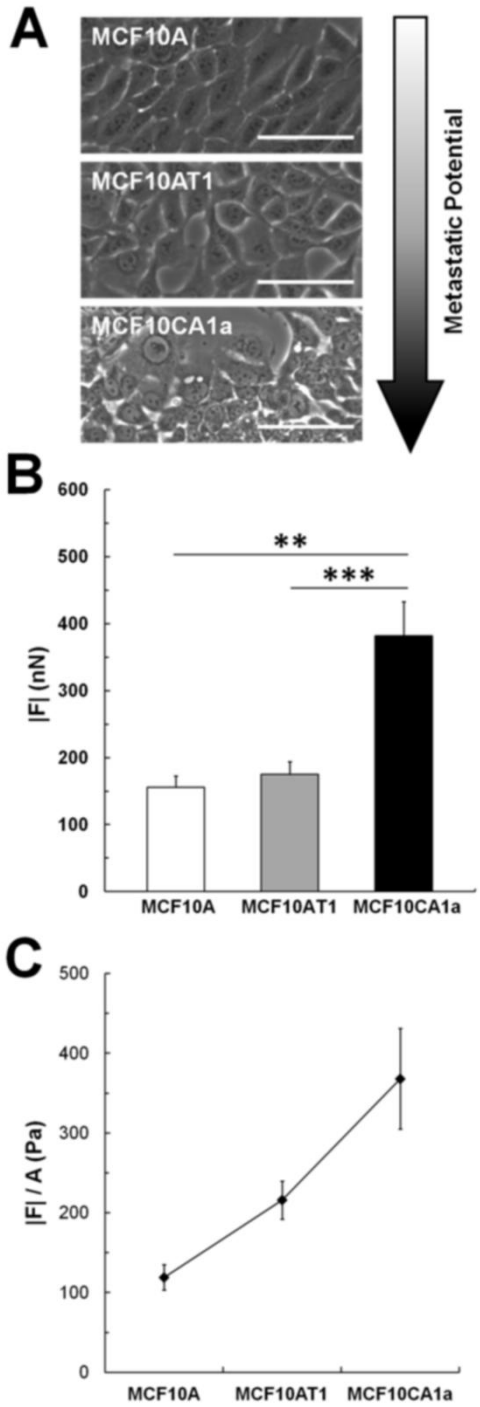

Figure 2.6. Metastatic derivative in a series of isogenic cell lines exerts greater forces. (A) Phase images of parental untransformed cells (MCF10A), transformed premalignant (MCF10AT1) and highly metastatic (MCF10CA1a) derivatives. (B) Net traction forces increase with increasing metastatic potential, with the highest forces exerted by the metastatic MCF10CA1a cells. (C) Average traction stress (|F|/A) increases with increasing metastatic potential. Mean ± SEM; ** indicates $p < 0.01$; *** indicates $p < 0.001$.

spreading, while matrix stiffness appears to increase cell forces independently of cell spreading.

Previous studies by others have also explored various biophysical traits as potential markers of metastasis. Atomic force microscopy (AFM) and optical stretching measurements have shown that metastatic cancer cells are more compliant than benign cells, both in established cell lines (Darling et al., 2007; Guck et al., 2005) and in primary tumor samples (Cross et al., 2007). These data allow speculation that a difference in the plasticity of cancer cells may contribute to their enhanced migration away from the primary tumor by allowing them to more easily maneuver through the ECM. These studies are the first indications that there are mechanical properties inherent in some cancer cells that may promote malignant and metastatic behavior. In our study, we explore another aspect of cell mechanics, cellular force generation, to show that metastatic cancer cells from a variety of cancer types exert greater traction stresses than their non-metastatic counterparts. We speculate that these higher forces could potentially drive cancer progression by promoting cellular behaviors such as cell migration, adhesion, and ECM remodeling during metastatic invasion.

Cellular mechanical properties can also be affected by the microenvironment. Using particle-tracking microrheology, Baker et al. showed that cells embedded in 3D matrices are stiffer than those plated on 2D substrates (Baker et al., 2009). They also show that 3D matrix stiffness and collagen density significantly affect the intracellular tension in tumor cells, although this relationship is dependent on both the type of cell and the cell's transformation state (Baker et al., 2009; Baker et al.). Increased matrix stiffness in turn has been shown to enhance cell motility in 2D and 3D (Ulrich et al., 2009; Zaman et al., 2006), while decreasing the stiffness of the tumor

microenvironment has been shown to inhibit malignant progression (Levental et al., 2009; Paszek et al., 2005). Increased ECM density has been identified as a risk factor for breast cancer (Martin and Boyd, 2008), and has also been shown to promote invasion by enhancing integrin clustering, upregulating Rho and PI3 kinase activity, and increasing focal adhesion formation (Levental et al., 2009; Paszek et al., 2005). Recently, Levental et. al. has shown that inhibiting collagen crosslinking increases tumor latency, reduces cell proliferation, and reduces tumor volume and incidence in a mouse model (Levental et al., 2009). In this work, we have shown that matrix stiffness and collagen density both mediate cellular force generation, with cells exerting greater force on substrates with either increased stiffness or increased collagen density.

Since both matrix stiffness and ligand density have been associated with increased cell spreading (Califano and Reinhart-King, 2010a; Engler et al., 2004; Gaudet et al., 2003; Willcox et al., 2005; Yeung et al., 2005), we examined their effects on cell spreading area here. We find that in the majority of the cell lines employed in this study, there existed a biphasic relationship between cell spreading and substrate stiffness (Fig. 2.4A), but a direct relationship between cell spreading and collagen density (Fig. 2.4B). While the relationship between area and collagen density is consistent with previous studies in numerous cell types (Califano and Reinhart-King, 2010a; Gaudet et al., 2003; Reinhart-King et al., 2005), the relationship between substrate stiffness and cell spreading contrasts with similar studies performed on several different non-cancerous cell types (Califano and Reinhart-King, 2010a; Engler et al., 2004; Yeung et al., 2005). However, there has been some evidence reported previously that the effect of matrix stiffness on cell spreading is highly variable and cell-type specific, particularly in cancer cells (Tilghman et al.).

Interestingly, we observe that cells on substrates of increasing stiffness exhibit increased average traction stresses, while cells on substrates of increasing collagen density exhibit no change in average traction stresses (Fig. 2.5). We speculate that matrix stiffness is able to promote force generation through a mechanosensing-mechanism which causes an upregulation of contractility-related proteins, while collagen density promotes force generation by controlling the number of available integrin binding sites available to the cell, therefore directly mediating the cell spreading area and allowing larger cells to exert greater forces. Importantly, metastatic cancer cells exert increased force compared to non-metastatic cells regardless of cell spreading area. This suggests increased force generation is inherently tied to the metastatic phenotype regardless of the microenvironment. It is also important to note that while this data is acquired in a 2D environment, previous work in our lab has shown that forces in 2D reflect the forces generated within a 3D environment (Kraning-Rush et al., 2011).

While we chose to focus on three of the most common metastatic cancers (breast, prostate, and lung), we cannot claim that contractile force will be a universal predictor of metastatic behavior without thoroughly characterizing every type of cancer. Indeed, recent work has shown that the method of transformation or exposure to different tumorigenic signals can significantly affect cellular mechanical properties in contrasting ways (Baker et al., 2010; Tseng et al.). Additionally, a recent study using a series of murine breast cancer cell lines of increasing metastatic potential observed the reverse trend to our data, showing that cells of increasing metastatic potential exert weaker contractile forces (Indra et al., 2011). While it is an elegant model of metastatic potential, the relevance of mouse-derived cancers to cancers which develop

within the human body continues to be disputed (Dennis, 2006). Based on the data shown in this study, particularly on the work done using the isogenic MCF10AT series of cell lines, we believe that pursuing traction force generation as a mechanical indicator of metastasis could potentially reveal mechanistic details that will lead to a better understanding of the initiation and progression of metastatic cancer. Additionally, examining proteins which are known to play key roles in mediating cell force, such as RhoA, ROCK, or myosin light chain phosphatase, may reveal a protein marker for traction stresses which could be more directly employed clinically to diagnose metastasis. Further studies will be needed on a broader range of cancer cells to determine the applicability of this kind of marker to a wide variety of cancers.

In conclusion, we have shown that metastatic cells exert significantly greater traction forces than non-metastatic cells in breast, prostate, and lung cancer models, and that these forces can be driven by the mechanical and chemical properties of the tumor microenvironment. These findings suggest that inherent force differences exist in cells of differing metastatic potential, and that these differences could be developed into a biophysical marker that could be used to determine the likelihood of metastasis. Additionally, our data suggest that identifying a mechanism to therapeutically target cellular force may be a promising avenue for inhibiting metastatic progression.

CHAPTER 3

MICROFABRICATED COLLAGEN TRACKS FACILITATE SINGLE CELL METASTATIC INVASION IN 3D

This chapter was published in *Integrative Biology* (Kraning-Rush et al., 2013).

3.1 Abstract

While the mechanisms employed by metastatic cancer cells to migrate remain poorly understood, it has been widely accepted that metastatic cancer cells can invade the tumor stroma by degrading the extracellular matrix (ECM) with matrix metalloproteinases (MMPs). Although MMP inhibitors showed early promise in preventing metastasis in animal models, they have largely failed clinically. Recently, studies have shown that some cancer cells can use proteolysis to mechanically rearrange their ECM to form tube-like "microtracks" which other cells can follow without using MMPs themselves. We speculate that this mode of migration in the secondary cells may be one example of migration which can occur without endogenous protease activity in the secondary cells. Here we present a technique to study this migration in a 3D, collagen-based environment which mimics the size and topography of the tracks produced by proteolytically active cancer cells. Using time-lapse phase-contrast microscopy, we find that these microtracks permit the rapid and persistent migration of noninvasive MCF10A mammary epithelial cells, which are unable to otherwise migrate in 3D collagen. Additionally, while highly metastatic MDAMB231 breast cancer cells are able to invade a 3D collagen matrix, seeding within the patterned microtracks induced significantly increased cell migration speed, which was not decreased by pharmacological MMP inhibition. Together, these data

suggest that microtracks within a 3D ECM may facilitate the migration of cells in an MMP-independent fashion, and may reveal novel insight into the clinical challenges facing MMP inhibitors.

3.2 Introduction

During metastatic invasion, cancer cells escape from the primary tumor site and migrate through the body to secondary locations, forming new tumors. Although this process is the cause of over 90% of cancer-related fatalities (Christofori, 2006), the precise nature of the mechanisms governing this behavior remains elusive. Additionally, tumor cell migration has been shown to be adaptable to both inherent and induced changes in their microenvironment (Friedl and Wolf, 2010; Sanz-Moreno et al., 2008), a phenomenon which remains difficult to accurately study in vivo or in vitro (Sabeh et al., 2009).

As tumors develop, they induce changes in the peritumoral microenvironment (Levental et al., 2009). Fibroblasts and other stromal cells deposit increased amounts of fibrillar collagen (Provenzano et al., 2008a), collagen crosslinking by lysyl oxidases and tissue transglutaminases is upregulated (Levental et al., 2009; Mehta et al., 2004), and increased tension generated on the extracellular matrix (ECM)(Samuel et al., 2011) leads to collagen fiber bundling and alignment perpendicular to the tumor front (Provenzano et al., 2006). This alignment has been shown to drive cancer cell invasion, as cells will migrate away from the tumor along these aligned fibers (Provenzano et al., 2008b; Wang et al., 2002). Moreover, 'leading' cancer cells have been shown to invade the ECM using proteolytic degradation (Gaggioli et al., 2007; Hotary et al., 2003; Sabeh et al., 2004; Wolf et al., 2007). These cells cleave collagen fibers using matrix metalloproteinases (MMPs) and reorganize them into parallel

bundles, creating a tube-like ‘microtrack’ (Friedl and Wolf, 2008; Wolf et al., 2007). Other ‘following’ cancer cells can in turn migrate through these open environments, either individually (Gaggioli et al., 2007; Wolf et al., 2007) or as collective strands (Alcaraz et al., 2011; Ilina et al., 2011), which can eventually widen the microtrack further. While proteases are required to form these channels initially, cells that subsequently follow these cleared microtracks do not need to further degrade the matrix. Therefore this mode of migration in the secondary cancer cells may be one example of true protease-independent migration which exists in vivo, and we speculate that it may also help to explain the general ineffectiveness of clinical MMP inhibitors (Coussens et al., 2002), if they are administered after initial invasion has begun and microtracks have already been formed.

While this type of migration behavior has been noted in several different cancer subtypes, including carcinomas and fibrosarcomas (Friedl and Wolf, 2003; Gaggioli et al., 2007; Wolf et al., 2007), it remains difficult to mimic the process in vitro. Microfabrication techniques have recently become popular for studying microtrack motility, analyzing tumor cell behavior within the confines of rigid PDMS or silicon channels (Balzer et al., 2012; Irimia and Toner, 2009; Mak et al., 2011; Pathak and Kumar, 2012; Rolli et al., 2010). These studies have shown that cancer cells will readily deform their cytoskeleton to squeeze through highly restrictive channels, to a greater extent than non-cancerous cell types (Mak et al., 2011). Additionally, several studies have demonstrated that cell migration speed is dramatically affected by channel width; once the channel width is significantly wider than the cell body width, to the point that the cell does not sense confinement, the cells will revert to a less persistent motile state, similar to that observed on unconstrained 2D environments (Balzer et al., 2012; Irimia and Toner, 2009). While these studies have yielded useful

insight into tumor cell behavior within physically confined spaces, the relevance of these findings to physiological conditions is uncertain. Specifically, PDMS substrates generally have a Young's modulus of ~1000 kPa (Ochsner et al., 2007), while the native microenvironment in which these cancer cells are found tends to be < 1 kPa (Lopez et al., 2011; Paszek et al., 2005). Stiffness has been found to have a profound effect on tumor cell physiology, directly mediating cell spreading, adhesion, migration, and force generation (Kraning-Rush et al., 2012a; Levental et al., 2009; Paszek et al., 2005). Therefore, the stiff nature of the PDMS channels may induce changes in the cells' cytoskeletal organization and function that are not necessarily recapitulated *in vivo*.

Recently, a study by Pathak & Kumar has partially overcome this limitation by patterning microchannels using polyacrylamide, a soft, viscoelastic hydrogel whose mechanical properties can be precisely tuned (Pathak and Kumar, 2012). Using a stiffness range of 400 Pa to 120 kPa, they find that migration speed is increased with increasing stiffness under mechanical confinement in 10 μm wide channels. Additionally, they attribute this behavior to an increased induction of polarity in actin stress fibers and traction forces in cells seeded in these narrow channels (Pathak and Kumar, 2012). While this technique allows for the separation of the individual effects caused by physiologically-relevant matrix stiffness and physical confinement, it does not recapitulate the subcellular fibrillar architecture of the ECM that can be sensed by tumor cells (Provenzano et al., 2006). Moreover, polyacrylamide cannot be degraded or remodeled by the cell. Alternatively, Ilina et al. have recently used two-photon laser microsurgery to create defined microtracks within dense 3D collagen matrices to study collective cell migration in tumor spheroids (Ilina et al., 2011). By utilizing a collagen matrix, this technique allows the cancer cells to proteolytically degrade and reorganize

the collagen fibers. However, the effects of laser ablation on the collagen fiber structure are unclear.

In this study we present a technique in which cancer cell motility can be studied in a physiologically relevant, 3D environment which mimics the complex architecture of the native peritumoral ECM. Using micromolding technologies (Nelson et al., 2008), microtracks can be accurately and reproducibly patterned across a range of collagen densities, and can mimic the structure of native tracks produced by proteolytically active cancer cells. Our data indicate that these microtracks permit the rapid and persistent migration of epithelial cells which cannot invade a 3D collagen matrix. Additionally, highly metastatic breast carcinoma cells, which can significantly invade a 3D matrix, have enhanced motility within the collagen microtracks. Interestingly, this migration is not slowed upon MMP inhibition, suggesting that migration within previously established microtracks can continue to occur in the absence of MMP's. This result may partially explain the lack of success of MMP inhibitors in clinical trials (Coussens et al., 2002).

3.3 Materials and Methods

Cell Culture and Reagents

MDAMB231 highly metastatic breast adenocarcinoma cells (American Type Culture Collection (ATCC), Rockville, MD) were maintained in Minimum Essential Medium supplemented with 10% fetal bovine serum and 1% penicillin-streptomycin (Invitrogen). GFP-expressing MDAMB231 cells (Cell BioLabs, San Diego, CA) were maintained in Dulbecco's Modified Eagle Medium supplemented with 2 mM L-glutamine, 10% fetal bovine serum, 0.1 mM MEM non-essential amino acids, and 1% penicillin-streptomycin (Invitrogen). MCF10A mammary epithelial cells (ATCC)

were maintained in Dulbecco's Modified Eagle Media supplemented with 5% horse serum, 20 ng/mL EGF (Invitrogen), 10 μg/mL insulin, 0.5 μg/mL hydrocortisone, 100 ng/mL cholera toxin (Sigma-Aldrich, St. Louis, MO), and 1% penicillin-streptomycin (Invitrogen)(Debnath et al., 2003). All cells were cultured at 37°C and 5% CO_2. For migration studies, GM6001 and the functionally inactive structural analog to GM6001 (N-t-butoxycarbonyl-L-leucyl-L-tryptophan methylamide, labelled here NC-GM6001) (Millipore, Billerica, MA) were applied to cells at a concentration of 20 μM. BB2516 (Sigma-Aldrich) was applied to cells at a concentration of 200 μM (Wolf et al., 2003). A commercial protease inhibitor cocktail (Cytoskeleton, Denver, CO) was applied containing working concentrations of 1 μM pepstatin A, 1.5 μM leupeptin, and 1 mM benzamidine, and 0.4 mM na-p-tosyl-L-arginine methyl ester (TAME).

RNA Interference and qRT-PCR

MDAMB231 cells at 70% confluency on tissue culture plastic were transfected with 2 nM non-targeting (control) siRNA or siRNA targeting MMP14 (MT1-MMP) using Lipofectamine 2000 (2 μg/mL, Invitrogen). The non-targeting sequence was 5'-UUC CUCUCCACGCGCAGUACAUUUA-3'. The sequence targeting MMP14 was 5'-CCUACGAGAGGAAGGAUGGCAAAUU-3'. Both the control siRNA and the siRNA targeting MMP14 (accession number NM_004995.2) were synthesized by Invitrogen. siRNA knockdown was confirmed with qRT-PCR.

Total RNA was isolated three days post-transfection using RNeasy® Plus Mini Kit (Qiagen, Valencia, CA) and was converted to cDNA by first combining 1 μg total RNA, 4 μM random primers (Invitrogen), and 0.5 mM dNTP mix (New England BioLabs, Ipswich, MA), and incubating for 5 minutes at 70°C. 1X reverse transcription buffer, 2U RNase inhibitor, and 10 U M-MuLV reverse transcriptase

(New England BioLabs) were added and the mixture was incubated at 42°C for 1 hour and 90°C for 10 minutes in a iCycler Thermal Cycler (Bio-Rad, Hercules, CA). 2U RNase H (New England BioLabs) was added to the mixture and incubated for 20 minutes at room temperature prior to storage at -20°C. qRT-PCR was performed with 1 μg of cDNA and 0.4 μM of specific primers against MMP14 (Forward: 5'-TGTGACGGGAACTTTGACACCG-3'; Reverse: 5'-ACGCTGCCCTTGAAACTGTGGC-3', Integrated DNA Technologies, Coralville, IA) and glyceraldehyde-3-phosphate dehydrogenase (GAPDH; Forward: 5'-CATGAGAAGTATGACAACAGCCT-3'; Reverse: 5'-AGTCCTTCCACGATACCAAAGT-3') using 1X iQ SYBR Green Supermix (Bio-Rad) on a MyiQ Single-Color Real-Time PCR Detection System (Bio-Rad).

Microscopy

Phase contrast imaging was performed in a custom temperature, humidity, and CO_2-controlled stage of a Zeiss Axio Observer Z1m inverted phase contrast microscope equipped with a Hamamatsu ORCA-ER camera and operated by AxioVision software (v. 4.8.1.0). Confocal fluorescence and reflectance imaging was performed with a Zeiss LSM700 confocal microscope on a Zeiss AxioObserver Z1 inverted stand equipped with a long working distance water-immersion C-Apochromat 40x/1.1 NA Zeiss objective and operated by Zen software (v. 2010, Carl Zeiss MicroImaging GmbH, Jena, Germany). Confocal reflectance images were obtained as previously described (Carey et al., 2012; Kraning-Rush et al., 2011).

Microtrack Fabrication

Silicon Master Fabrication and Imaging

Standard 100 mm-diameter silicon wafers containing wells measuring 10 x 300 and 10

x 1100 μm^2, spaced 500 μm apart were coated with photoresist (SPR 220-3.0 series) and etched to a depth of 20 and 30 μm as previously described (Charest et al., 2012). Wafers were imaged using a Leica 440 scanning electron microscope to confirm feature dimensions. These molds were used to cast poly(dimethylsiloxane) (PDMS, Ellsworth Adhesives, Germantown, WI) stamps using a standard 1:10 ratio of crosslinking agent to monomer.

Preparation of Collagen Microtracks

All collagen matrices were prepared using collagen extracted from rat tail tendons (Pel-Freez Biologicals, Rogers, AR) without pepsin as previously described (Carey et al., 2012). A 10 mg/mL stock solution was diluted to the desired collagen concentration (1.5 – 5 mg/mL) with ice-cold culture media and neutralized to pH 7.0 with 1N NaOH. PDMS stamps were rendered non-adhesive by coating with a 1% solution of bovine serum albumin (BSA, Sigma-Aldrich) in PBS at room temperature for 30 minutes. Modified stamps were inverted on a drop of diluted neutralized rat tail type I collagen between two thin PDMS spacers (~1.25 mm thick) and allowed to polymerize for 90 minutes at 37°C in a method similar to that described by Nelson et al. (Nelson et al., 2008). To facilitate confocal fluorescence or reflectance imaging, microtracks were prepared on 43 x 50 mm glass coverslips, with 22 x 22 mm coverslips adhered with vacuum grease for spacers. Small glass coverslips were removed after polymerization and microtracks were mounted onto custom made chambers to create a 35 mm diameter well surrounding the patterned microtracks. For cellular experiments, after stamps were removed, a dilute suspension of cells was applied (~80,000 cells/mL) and allowed to settle within the collagen tracks for 2-3 minutes at 37°C. Excess cells were carefully removed by rinsing with ice cold culture medium. A second thin layer of collagen, polymerized onto an 18 mm^2 diameter round

glass coverslip, was inverted onto the tracks to serve as a lid. Microtracks were incubated with collagen lids for 5 minutes at 37°C before being immersed in culture medium.

Microtrack Dimension Analysis

Patterned Microtracks

The dimensions of the patterned tracks were quantified from confocal reflectance images. 1 μm z-stacks were acquired of each track, and analyzed using ImageJ software (v. 1.44p, National Institute of Health, Bethesda, MD). The center z slice was determined and a grid of horizontal and vertical lines spaced 10 μm apart was overlaid onto the image. The line drawing function was used to measure the length across the track every 4 μm (2 measurements per track) and the width every 20 μm (15 measurements per track). To measure the depth of the track, the orthogonal view function in the Zen software was used to visualize the track in the x-z plane. This image was exported and analyzed in ImageJ using a similar grid, with measurements taken every 20 μm (15 measurements per track). Dimensions were quantified for n > 45 tracks per collagen concentration and are reported as Mean ± SD.

Naturally Formed Microtracks in 3D Collagen Matrices

A 10 mg/mL type I collagen stock solution was diluted to a 1.5 mg/mL solution with ice-cold culture media and neutralized to pH 7.0 with 1N NaOH. GFP-MDAMB231 cells were seeded into the collagen matrices in a glass bottom 24-well plate (MatTek, Ashland, MA) at low density (50,000 cells/mL) to minimize cell-cell interactions. 0.5 mL solution volume was added to a 24 well plate and incubated for 1 hr at 37°C for collagen polymerization. Gels were overlaid with 0.5 mL pre-warmed culture media and incubated for 48 hours. Gels were fixed with 3.7% (v/v) formaldehyde (JT Baker,

Phillipsburg, NJ) in phosphate buffered saline (PBS) and imaged with confocal fluorescence and reflectance.

The dimensions of the natural tracks formed by the cells were quantified from confocal reflectance z-stacks with 1 μm slices using ImageJ software. Z stacks were rotated such that the track was primarily horizontal and a grid of 10 x 10 μm squares was overlaid onto the image. The width of the track was measured every 10 μm. Widths were quantified for n > 25 tracks.

Cellular Studies

Fluorescent Staining

Cells seeded in collagen microtracks or 3D collagen matrices were allowed to spread overnight and were fixed with 3.7% (v/v) formaldehyde in PBS and permeabilized with 1% (v/v) Triton (JT Baker) in PBS. Samples were blocked with PBS/0.02% (v/v) Tween (JT Baker) with 3% (w/v) BSA and incubated with a diluted 1:100 Alexa Fluor 594-conjugated phalloidin (Invitrogen) in PBS to localize filamentous actin. Nuclei were stained with a 1:100 dilution of 4',6-diamidino-2-phenylindole (DAPI, Sigma-Aldrich) in purified deionized water.

Cell Migration Studies and Morphology Analysis

Cells were either seeded into 1.5 mg/mL type I collagen gels or into 3 mg/mL collagen microtracks at low density as described above. Gels and microtracks were incubated for 10 hours prior to phase contrast time-lapse imaging. Cells were imaged every 10 minutes for 8 hours. Dividing cells and cells that did not move from their original location after 4 hours were excluded from analysis. Detailed information about these cells can be found in Table 3.1. ImageJ software was used to determine the area,

perimeter, aspect ratio (length of long axis / length of short axis), and circularity, defined as (4πArea/Perimeter^2), where a circle has a value of 1, and a straight line has a value of 0 (Cornhill et al., 1980; Kraning-Rush et al., 2011). Cell centroid position based on cell outlines and was used to calculate the mean-square displacement ($<d^2>$)(Stokes et al., 1991). For both the 3D migration within the collagen gels and 2D migration studies on tissue culture plastic, cell migration speed (S) was determined by fitting the $<d^2>$ and the time interval (t) to the persistent random walk equation:

$$\left\langle d^2 \right\rangle = 2S^2P\left[t - P\left(1 - e^{-\left(t/P\right)}\right)\right] \qquad (3.1)$$

where P is the persistence time, using nonlinear least squares regression analysis as previously described (Reinhart-King et al., 2008). Because cells traveling in collagen microtracks do not travel in a random walk, but can only migrate in two directions, speed was calculated by dividing the final displacement by time, for cells migrating in one direction for a length of 100 minutes. Maximum invasion distance was quantified for all cells in both the 3D gels and the collagen microtracks by determining the displacement of the cell from its initial position at each time point up to 100 minutes. The maximum value calculated was considered the maximum invasion distance. 100 minutes was selected as the cutoff point to minimize the number of cells which migrated out of the field of view in the microtracks.

Statistical Analysis

Data were compared using analysis of variance with a post-hoc Tukey's Honestly Significant Difference (HSD) test or Student's t test where appropriate using JMP software (v.9, SAS, Car, NC). Statistical significance was considered with $p < 0.05$.

3.4 Results

Patterning of collagen microtracks

It has been shown previously that some subsets of cancer cells are capable of proteolytically degrading and reorganizing ECM fibers in such a way that a stable cleared pathway through a 3D matrix is generated (Fig. 3.1A) (Friedl and Wolf, 2008; Wolf et al., 2007). Our goal was to re-create these pathways in vitro in a defined and controllable manner to create a system that could then be used to explicitly study this unique method of cancer cell migration (Fig. 3.1B). To accomplish this, we adapted a method pioneered by Nelson et al. (Nelson et al., 2008) that uses a PDMS stamp cast from a silicon master to micromold a neutralized collagen solution into wells with defined dimensions (Fig. 3.1C).

To determine the relevant dimensions to use for patterning microfabricated tracks for our in vitro system, natural tracks formed by GFP-labeled MDAMB231 metastatic breast cancer cells embedded within collagen matrices were analyzed. After 48 hours of migration, the cells were fixed and natural tracks were imaged using confocal microscopy (Fig. 3.2A). The widths of the natural tracks were analyzed (Fig. 3.2B) and found to have an average width of 13.7 μm (Fig. 3.2B, red dotted line). These tracks were widely heterogeneous, both within a single track (average SD = 2.74 μm) and across tracks created by different cells (SD = 4.3 μm). Standard photolithographic techniques were used to etch wells into a silicon wafer with a width of 10 μm (Fig. 3.3A), a width calculated in over 50% of the tracks analyzed. PDMS stamps cast from this wafer were then used to imprint wells into a collagen gel, creating an array of thin, shallow wells that could be readily imaged using conventional phase contrast microscopy for time lapse studies (Fig. 3.3B). Additionally, because of the inherent differences in the refractive index of the collagen fibers and the spaces between them,

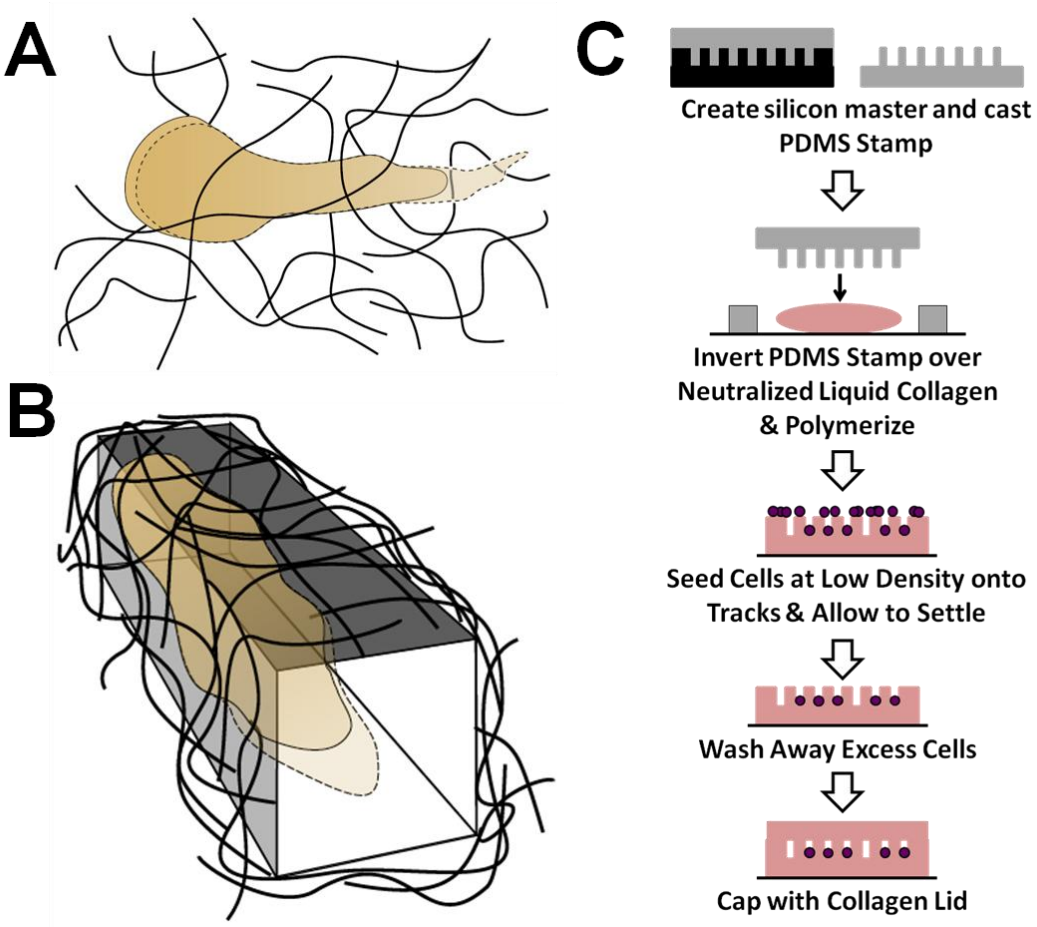

Figure 3.1. Schematic of method for patterning collagen microtracks. (A) A cancer cell migrating in a 3D matrix cleaves extracellular matrix fibers using proteases, creating an open pathway at the rear of the cell body. (B) Within a patterned 3D track, cancer cells can migrate through the matrix without the need for proteolytic activity. (C) Microtracks are created in a collagen gel using a PDMS stamp to micromold a neutralized collagen solution.

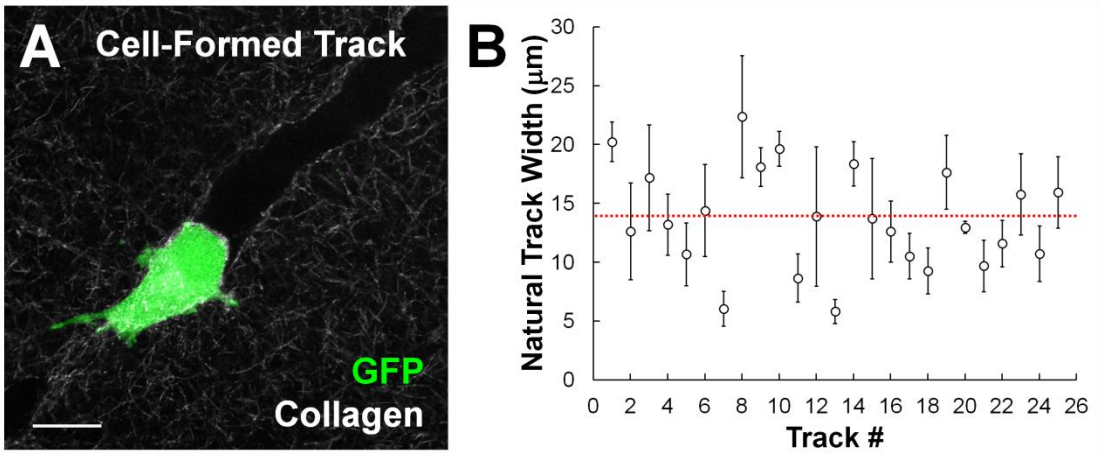

Figure 3.2. Metastatic cancer cells create heterogeneous tracks within 3D collagen matrices. (A) GFP-labeled MDAMB231 metastatic breast carcinoma cell creates a proteolytic track within a type I collagen matrix. Scale bar = 20 μm. (B) Plot of track widths in naturally formed tracks indicate a wide range of widths observed across different tracks, as well as significant deviation within a single microtrack. Each point represents one track (Mean ± SD). Red dashed line indicates overall mean across all tracks analyzed.

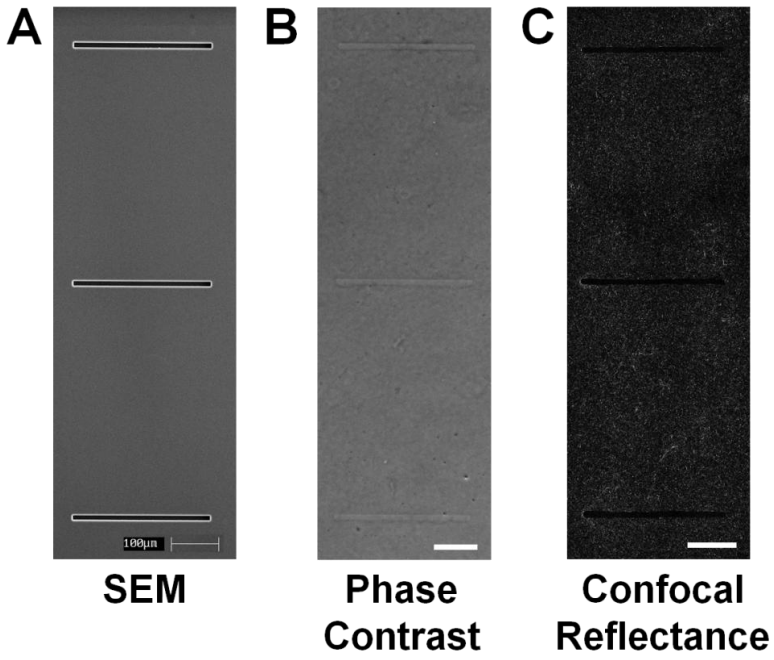

Figure 3.3. Imaging of silicon master and collagen microtracks. (A) SEM image of silicon master etched with wells measuring 300 x 10 x 25 μm (w, l, d). (B) Phase image of patterned collagen microtracks. (C) Confocal reflectance image of collagen fibrils around the tracks. Scale bars = 100 μm.

the microstructure of the patterned tracks could be directly imaged using confocal reflectance microscopy (Fig. 3.3C)(Carey et al., 2012; Kraning-Rush et al., 2012b; Kraning-Rush et al., 2011).

Patterned collagen microtracks mimic natural tracks formed by cancer cells

By subsequently capping the polymerized collagen wells with an additional thin layer of polymerized collagen, an open pathway or 'microtrack' entirely encased in collagen was successfully created in vitro (Fig. 3.4A). The dimensions of the patterned tracks were characterized by measuring their length, width, and depth over 1.5 – 5 mg/mL collagen. Concentrations lower than 1.5 mg/mL and above 5 mg/mL became more difficult to consistently replicate using this method of collagen polymerization. Lower concentrations of collagen led to poorly formed tracks, as the collagen lids appeared to sink into the track body, while higher concentrations polymerized too quickly and had observable defects. Within this range, the track length across collagen concentrations was the parameter with the highest fidelity compared to the original pattern of the silicon master, with only a slight increase in length noted in the 5 mg/mL collagen condition (Fig. 3.4B). Our analysis indicated that, while all tracks were patterned with stamps of equal width (10 μm) and depth (20 μm), the resulting width increased with collagen density (Fig. 3.4C), and the resulting depth decreased with collagen density (Fig. 3.4D). While the achieved widths were similar to the width of the pattern, the achieved depths were around half the depth of the original pattern. However, the variation within a given track was fairly low. The average deviations in the length, width, and depth within a single microtrack were 0.88 μm, 1.38 μm, and 1.47 μm (equivalent to 0.3%, 10%, and 13% difference). Notably, the deviation in width across all of the patterned microtracks (11.12 ± 1.29 μm – 15.83 ± 3.89 μm) encompasses over 90% of the range of widths created naturally by the metastatic breast cancer cells

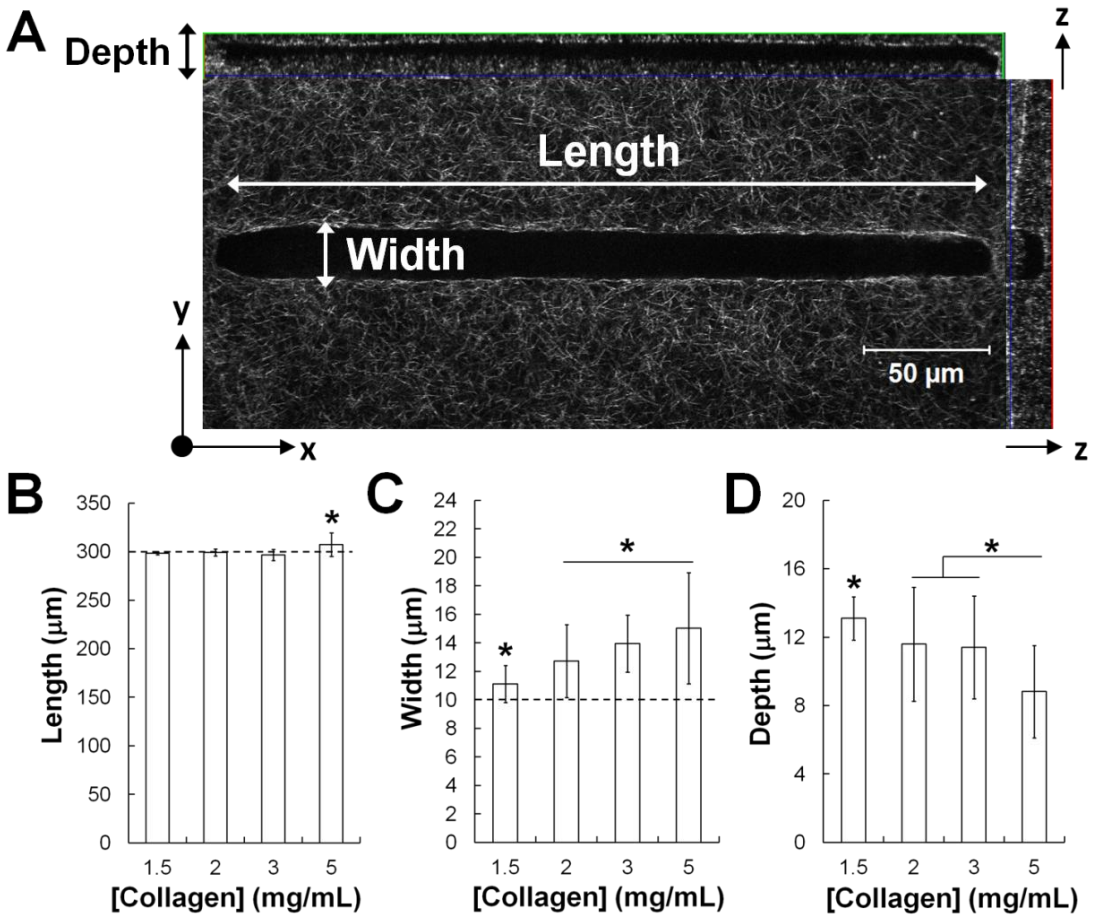

Figure 3.4. Microtracks can be reproducibly patterned with a range of collagen densities. (A) Confocal reflectance image reflecting the measured dimensions of patterned collagen tracks. Scale bar = 50 µm. Length (B), width (C), and depth (D) are quantified across tracks patterned in 1.5 – 5 mg/mL type I collagen. Mean ± SD; * indicates $p < 0.05$; $n > 45$ tracks, 2 independent experiments; dotted lines indicate length and width of original patterned silicon master.

(Fig. 3.2B). Additionally, the architecture of the native tracks was largely similar to the architecture observed in the patterned tracks (Fig. 3.5). The dimensions of the channel were not altered by the presence of cells. Importantly, the metastatic cancer cells were able to actively remodel their environment by attaching to, exerting tension on, and subsequently bundling surrounding collagen fibers (white arrows, Fig. 3.5) during a relatively short period of migration through the 3D microtrack. Notably, the cell within this microtrack is fully bounded by collagen, as indicated by the cross-section and side-view of the track. We observed that over the course of migration through the patterned microtrack, the cell would occasionally pull away slightly from one or more walls, without overt preference for either the bottom of the track or the lid, but would rarely lose contact completely with the walls. Additionally, we noted that the degree of collagen contraction dynamically changes over the course of the cell's migration, as it forms protrusions and pulls against the track walls.

Next, the cell morphology of MDAMB231 cancer cells within a 3D matrix and a patterned microtrack was compared. Our data shows that seeding cells within the patterned track did not significantly affect their spread area (Fig. 3.6A) or perimeter (Fig. 3.6B). Additionally, similar patterns of aspect ratio and circularity are observed in both 3D matrices and patterned tracks (Fig. 3.6C). Similar results were observed in MCF10A mammary epithelial cells (data not shown). There was also no observable difference in actin organization in MDAMB231 cells seeded within 3D collagen or patterned tracks. In both cases, the actin was primarily cortical, with a notable lack of stress fibers within the cell (Fig. 3.6D-E).

Collagen microtracks facilitate migration in invasive and non-invasive cell types

Because tracks can provide an uninterrupted path for cells to follow (Ilina et al., 2011),

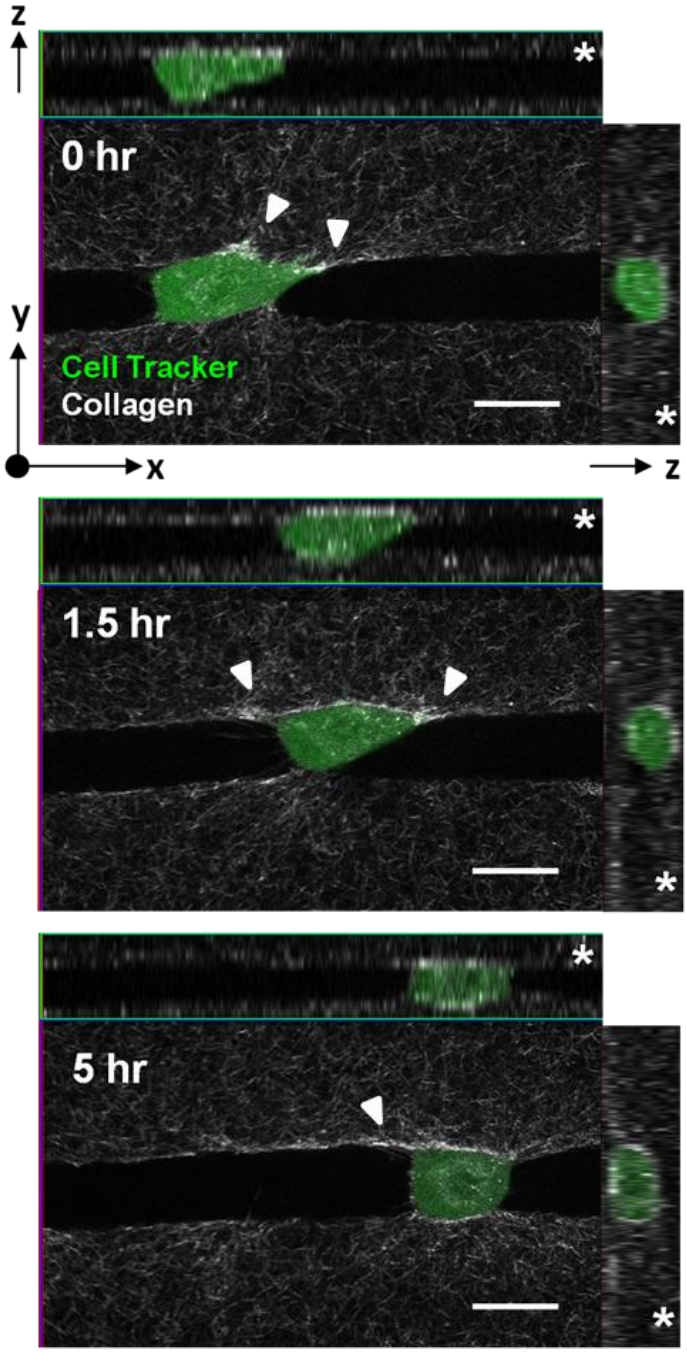

Figure 3.5. Patterned microtracks accurately reproduce tracks formed naturally by cancer cells. Cell-tracker labeled MDAMB231 cell within a patterned collagen track which has a fibrillar architecture significantly resembling that of the native proteolytic track. Cross-sectional slices indicate that cell is fully bounded by collagen (z arrow, right), and that a clear pathway is available for the cell to travel through (z arrow, top). Asterisks indicate the 'lid' side of the track. Over a period of 5 hours, the cell is able to move over 50 μm from its initial position, while remodeling the extracellular matrix by bundling collagen fibers (white arrows). Scale bars = 20 μm.

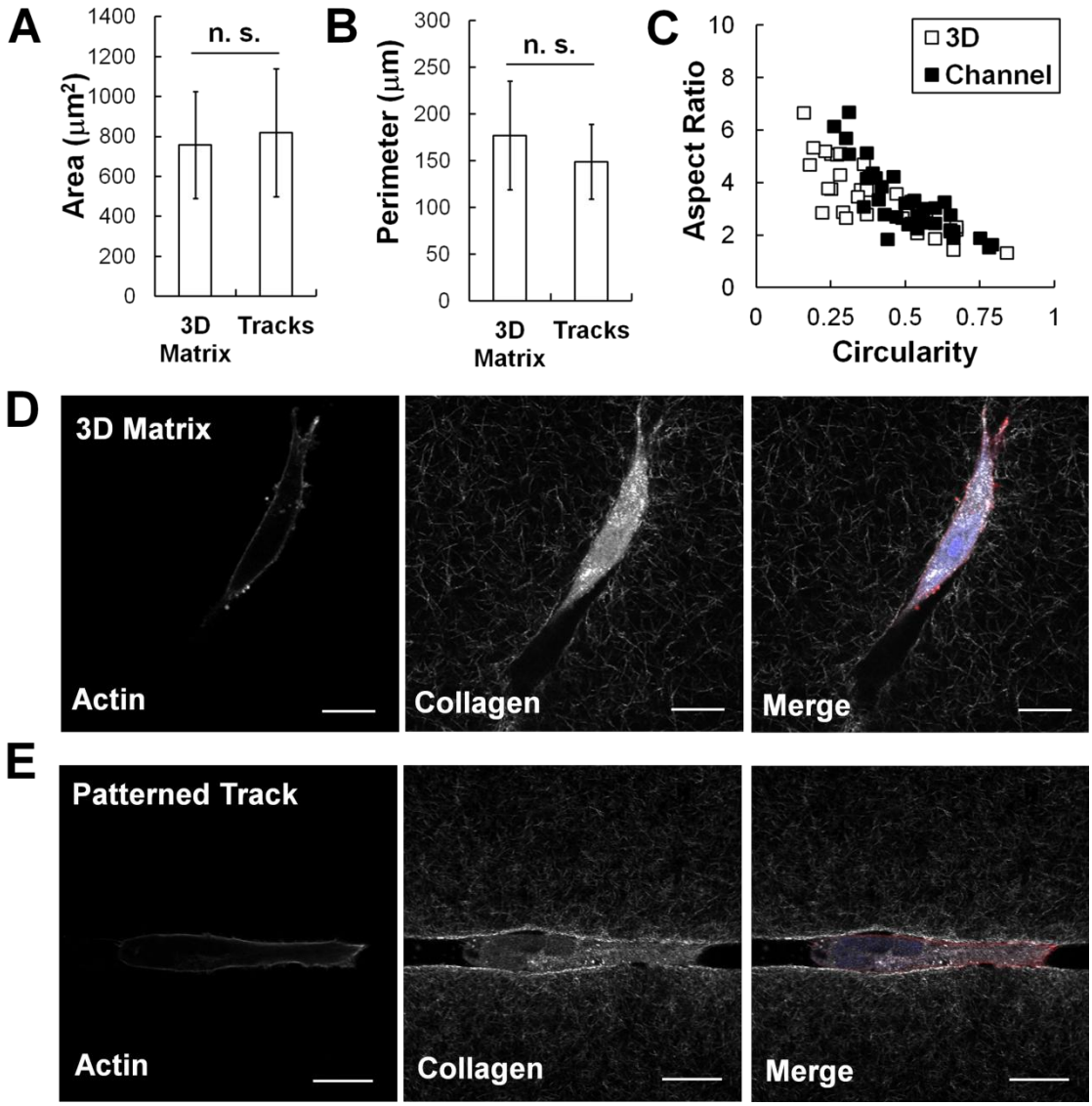

Figure 3.6. The actin cytoskeleton of cells in microtracks is similar to that in a 3D matrix. No significant difference ($p > 0.05$) is observed in MDAMB231 cell area (A) or perimeter (B) when plated within a 3D collagen matrix or microtrack environment. Mean ± SD; n > 30 cells, 2 independent experiments. Cells in 3D matrices and tracks also have similar distributions of aspect ratio and circularity (C). Actin structure of the MDAMB231 cell within a 3D matrix (D) and within a patterned collagen track (E) is largely cortical. Fluorescent staining of actin fibers (left), confocal reflectance imaging of the collagen fibers (middle), and merge image with additional DAPI staining (right). View in channel is a single slice of the x-y plane. Scale bar = 20 μm.

we first examined the effect of the nature of the collagen environment on cell migration of a non-invasive mammary epithelial cell line (MCF10A). When seeded within a 3D collagen matrix, these cells are able to spread and extend multiple protrusions into the matrix, but are largely unable to propel themselves through the matrix (Fig. 3.7A). Within 100 minutes, MCF10A cells are only able to penetrate less than 25 μm away from their initial position (Fig. 3.7B). However, when seeded within the patterned collagen microtracks, MCF10A cells are able to quickly and persistently migrate through the matrix (Fig. 3.7C). Within 100 minutes of initiating migration, these cells are able to move >150 μm away from their initial position (Fig. 3.7D), more than six times the distance they were able to achieve in a 3D matrix. As expected from these observations, the speed and invasion distance of MCF10A cells is significantly increased within the collagen tracks, compared to within 3D collagen matrices (Fig. 3.7E-F). Moreover, the percentage of motile cells in the tracks is increased by over three-fold, compared to cells in 3D collagen (Table 3.1).

The migration behavior of a cell type which is consistently found to be highly invasive in a variety of extracellular matrices (Sabeh et al., 2009; Wolf et al., 2007), the MDAMB231 metastatic breast cancer cells, was also examined. These cells were able to efficiently migrate within 3D collagen, permeating between 50 and 100 μm into a collagen matrix within 100 minutes (Fig. 3.8A). As expected, these cells were also able to migrate persistently within collagen tracks (Fig. 3.8B). Additionally, the percentage of motile cells was also increased by nearly 40% in the microtracks (Table 3.1).

Because previous studies have indicated that MDAMB231 cells require MMP activity to migrate (Sabeh et al., 2009), we treated these cells with GM6001, a commonly used

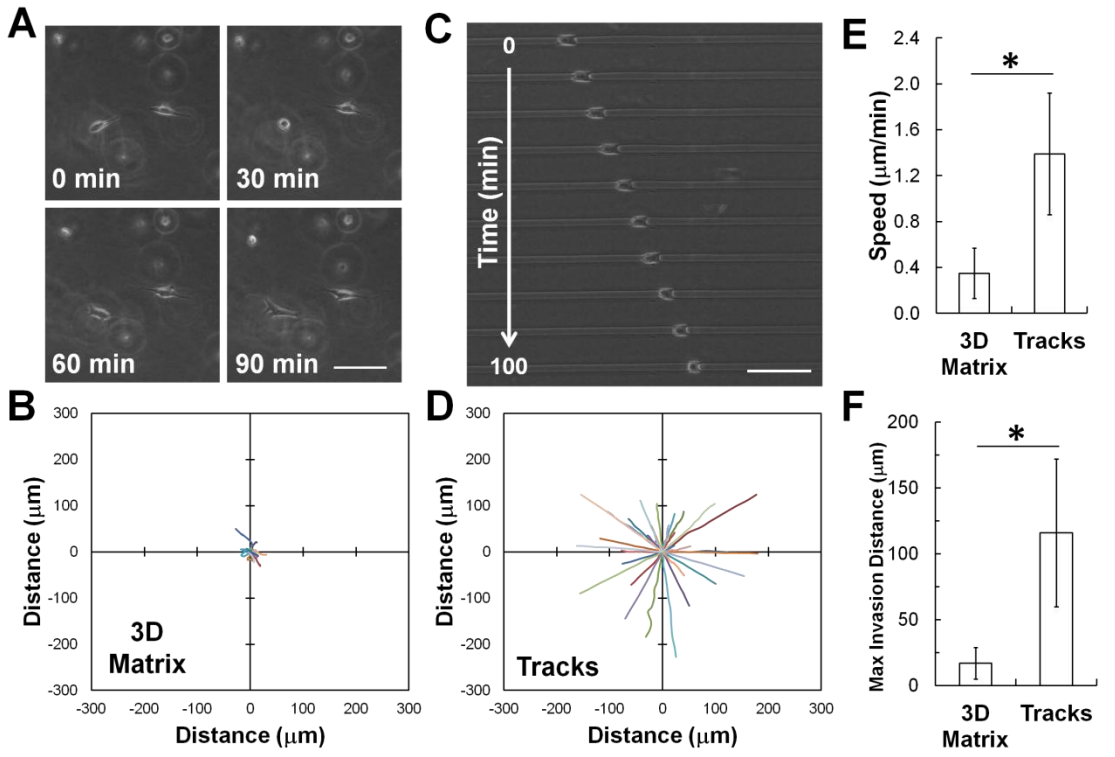

Figure 3.7. Tracks facilitate single cell migration in 3D collagen matrix in non-invasive cells. (A) Time lapse phase contrast images of MCF10A mammary epithelial cells migrating in a 3D collagen matrix show relatively little net cell displacement. (B) Rose plot shows trajectories of MCF10A cells migrating within a fully 3D type I collagen matrix over 100 minutes. (C) Time lapse phase contrast images of MCF10A cells within a patterned 3D collagen track demonstrates the ability of these cells to significantly invade the track. (D) Rose plot shows trajectories of MCF10A cells migrating within collagen tracks for 100 minutes. Note that the trajectories have been arbitrarily rotated for a more direct visual comparison. (E) Quantification of cell migration speed and (F) maximum invasion distance indicates that MCF10A cells are able to migrate more quickly and travel a greater distance within the patterned collagen microtracks than within a 3D collagen matrix. Scale bars = 100 μm. Mean ± SD; * indicates $p < 0.05$; $n > 30$ cells, 2 independent experiments.

Table 3.1. Analysis of behavior of MCF10A and MDAMB231 cells within 3D collagen matrices and patterned microtracks.

		% Cells Engaging in Behavior				
		Motile	Nonmotile	Dividing	Dead	n[a]
MCF10A	3D Matrix	24	66	10	0	124
	Tracks	81	14	3	3	73
MDAMB231	3D Matrix	56	21	21	2	92
	Tracks	77	9	9	5	64

[a] Represents total number of cells observed

broad spectrum MMP inhibitor (Sabeh et al., 2009). We found that within a 3D matrix, treatment with GM6001 appeared to slightly decrease the invasion of the MDAMB231 cells (Fig. 3.8C). Surprisingly, treating cells seeded within collagen microtracks with GM6001 significantly increased the invasive capacity of the MDAMB231 cells (Fig. 3.8D). When we quantified this data, we found that there was no statistically significant difference in cell speed with GM6001 treatment in 3D (Fig. 3.8E). On the contrary, treatment with GM6001 significantly increased the speed (Fig. 3.8E) of the MDAMB231 cells seeded within the track microenvironment while having no effect on cell migration on a rigid, 2D glass substrate (Fig. 3.8F). To further eliminate the possibility that this increase in speed is the result of off-target effects of GM6001, a functionally inactive structural analog of GM6001 (NC-GM6001) was applied to the cells in both 3D matrices and patterned tracks. Cells treated with NC-GM6001 displayed speeds that were not statistically different from the speed of control cells in either 3D collagen matrices or patterned channels (Fig. 3.8E).

To determine whether this observed increase in speed upon MMP inhibition was specific to this particular inhibitor, we treated cells with another commonly used broad spectrum MMP inhibitor which has been used clinically, BB2516 (Bramhall et al., 2001; Wolf et al., 2003; Wolf et al., 2007), as well as a commercial protease inhibitor

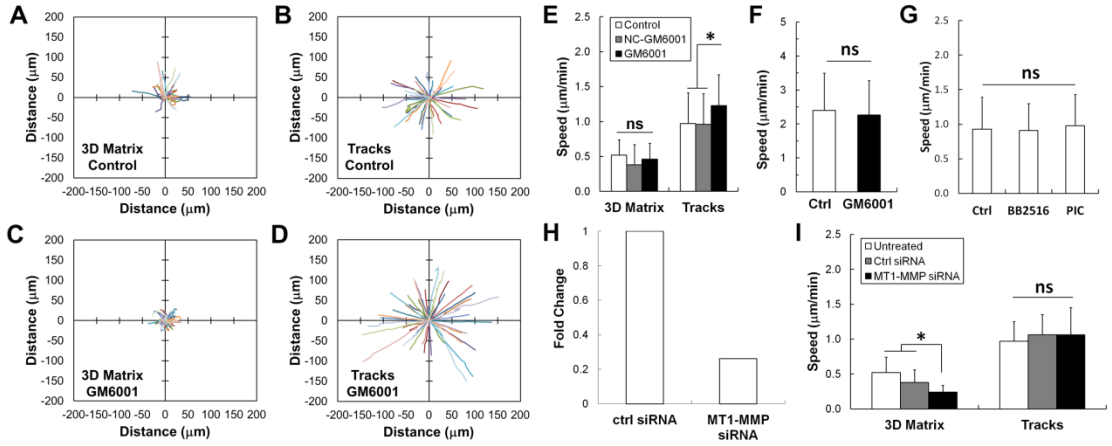

Figure 3.8. Inhibiting MMP activity increases cancer cell migration through collagen microtracks. (A) Rose plot shows trajectories of MDAMB231 metastatic breast cancer cells migrating within a fully 3D collagen matrix and (B) in collagen tracks over 100 minutes. (C) Rose plots show that treatment with GM6001, a broad spectrum MMP inhibitor, decreases invasion in 3D, but (D) increases invasion within the collagen tracks. Note that the trajectories in (B) and (D) have been arbitrarily rotated for a more direct visual comparison to (A) and (C). (E) Quantification of speed indicates that treatment with GM6001 has no effect on speed in a fully 3D matrix, but increases the speed of cells within the microtracks. Additionally, treatment with a structural analog of GM6001 (NC-GM6001) has no significant effect on speed in 3D matrices or microtracks. Mean + SD; * indicates $p < 0.05$; $n > 30$ cells, 3 independent experiments. (F) GM6001 treatment of cells migrating on 2D glass substrates has no effect on cell speed. Mean + SD; $n > 40$ cells, 1 independent experiment. (G) Treatment of cells with other broad spectrum inhibitors (BB2516 and a commercial protease inhibitor cocktail) has no effect on cell speed in the tracks. Mean + SD; $n > 60$ cells, 2 independent experiments. (H) Similarly, inhibiting MT1-MMP with siRNA significantly decreases speed in 3D matrices, but has no effect within tracks. Mean + SD; * indicates $p < 0.05$; $n > 30$ cells, 2 independent experiments.

cocktail (PIC). Interestingly, these data do not show the same trend of increasing speed with MMP inhibition observed with GM6001 (Fig. 3.8G). However, migration speed is not statistically different from control cells, indicating that treatment with these MMP inhibitors does not negatively affect cancer cell migration in the collagen microtracks.

Finally, because most exogenous MMP inhibitors act on a broad range of substrates and their effects can be difficult to interpret, we chose to specifically focus on a single MMP. MT1-MMP has been repeatedly found to be the primary driver of cancer cell invasion in 3D (Hotary et al., 2003; Sabeh et al., 2009). Therefore, we specifically examined its role in migration within our 3D microtracks. We transfected the highly metastatic MDAMB231 breast cancer cells with siRNA targeting MT1-MMP and confirmed a 75% knockdown via qRT-PCR. These cells were seeded into either 3D collagen matrices or within the patterned collagen microtracks. Our results indicate that MT1-MMP knockdown significantly decreased speed within 3D matrices, but had no effect on migration speed within the tracks (Fig. 3.8H). These results support our findings with the broad spectrum MMP inhibitors, confirming that migration within the patterned microtracks can occur independently of MMP activity.

3.5 Discussion

In this study we demonstrate the use of patterned collagen microtracks to successfully mimic the natural tracks formed by cancer cells. Our method for studying microtrack migration in single cells is easy to perform using standard laboratory micromolding techniques (Fig. 3.1C). We show that tracks can be reproducibly patterned in collagen gels (Figs. 3.3-3.4), and using confocal reflectance microscopy, we show that the structure of the microtracks is very similar to the architecture of naturally created

proteolytic tracks (Figs. 3.2, 3.5). These tracks increase both the migration speed and invasion distance of invasive MDAMB231 breast cancer cells and non-invasive MCF10A mammary epithelial cells compared to migration speed within 3D collagen matrices (Figs. 3.7, 3.8).

In this study we focus on mammary epithelial cells and breast carcinoma cells, primarily because the breast microenvironment contains many 'track-like' structures that our patterned collagen mimics (Gritsenko et al., 2012; Wolf et al., 2007). Initially, epithelial cells in the breast exist in duct structures, and tumor cells can migrate along these structures during carcinoma in situ before invasion actually occurs. Invasion begins when the basement membrane surrounding these ducts is degraded, allowing cells to penetrate beyond the duct, making first contact with the surrounding ECM fibers, and thus initiating invasion (Gritsenko et al., 2012). At this point the leading cancer cells can create new tracks into the surrounding tissue, as described previously (Friedl and Wolf, 2008). The structure of the mammary gland microenvironment is highly heterogeneous, with regions of loosely connected fibers and regions of densely bundled and aligned fibers that develop throughout neoplastic progression (Conklin et al., 2011; Gritsenko et al., 2012). Despite the increase in collagen density, there remain significant inter-fiber clefts in the peritumoral region which serve as a network of microtracks through which cancer cells have been observed to invade. Additionally, stromal carcinoma associated fibroblasts have also been shown to create proteolytic tracks that tumor cells can subsequently use to invade (Gaggioli et al., 2007).

Although we have focused our study here on the breast microenvironment, these tracks could be used to mimic other physiologically relevant microenvironments. We use fibrillar type I collagen because it is the most dominant structural protein found in

the breast and its effects on tumor cells have been extensively studied in a variety of contexts (Levental et al., 2009). However, the techniques described here could be readily adapted for use with other structural protein compositions, such as laminin or fibronectin, to mimic other regions of the body. For example, there is considerable evidence that glioma cells in the brain can invade using similar track-like structures. Interstitial migration in the brain has been shown to occur along blood vessels, myelinated fibers, and white matter tracts (Gritsenko et al., 2012). These microtracks could prove to be a useful method for studying these methods of tumor migration as well.

One of the most interesting and surprising results of this study was the effect of the broad spectrum MMP inhibitor GM6001 on the migration of metastatic MDAMB231 breast cancer cells within the confined collagen tracks. While treatment with GM6001 inhibited cell migration slightly within a 3D matrix, it had the opposite effect on cells seeded in the patterned microtracks (Fig. 3.8). We observed a significant increase in the migration speed of MDAMB231 cells treated with GM6001 within the microtracks. Because GM6001 is known to have significant off-target effects (Jacobsen et al., 2008), we treated cells with a functionally inactive structural analog (NC-GM6001) (Azuma et al., 2003). We did not observe a similar result with cells treated with this negative control, nor did treatment with GM6001 affect cell migration speed in 2D (Fig. 3.8F), suggesting that this result does not necessarily stem from an off-target effect of the drug. However, we acknowledge that the structural analog may not account for 100% of the off-target effects of GM6001. Moreover, our subsequent studies with additional broad spectrum inhibitors BB2516 and PIC, as well as our MT1-MMP siRNA knockdown studies suggest that this increased cell speed may not be a global phenomenon with respect to MMP inhibition, but may instead be specific

to this inhibitor. GM6001 acts on over 20 different targets (Levy et al., 1998), some of which are also inhibited to various extents by BB2516 and/or PIC, and therefore it is difficult to determine if one of these individual targets may be specifically responsible for this surprising result. Additionally, broad spectrum MMP inhibitors have been shown to induce activation of select MMP's under certain conditions. In particular, BB2516 and GM6001 have both been shown to lead to enhanced pro-MMP2 activation when tissue inhibitor of metalloproteinase 2 (TIMP2) is present (Ikejiri et al., 2005; Toth et al., 2000). Therefore, the complex and varied functions of these inhibitors can be difficult to interpret directly.

There are several different mechanisms that could potentially explain the increased speed observed with GM6001 treatment, if it is not the result of a simple off-target effect. It is possible that one or more of the MMP's expressed by MDAMB231 cells may expose specific cryptic binding sites (Ricard-Blum and Ballut, 2011; Rundhaug, 2005) on the collagen fibers during proteolytic degradation. These additional binding sites may lead to increased cell adhesion and subsequent decreased motility. If these cryptic sites remain unexposed when the specific MMP's responsible are inhibited under GM6001 treatment, then this could explain the resulting increase in cell speed. Importantly, we have ruled out MT1-MMP as the culprit for this behavior, as our siRNA knockdown studies did not yield a similar increase in cell speed; rather, there was no observed change in speed compared to controls.

Additionally, we speculate that the increased migration speed of cancer cells under GM6001 treatment could potentially be the result of altered receptor shedding. Receptor shedding has been a noted phenomenon for many years (Black, 1980), but is still not thoroughly understood. Receptor shedding occurs when the extracellular

region, or ectodomain, of cellular membrane proteins is cleaved by a molecule known as a 'sheddase' (Huovila et al., 2005). One key class of sheddases are the ADAM metalloproteinase disintegrins, although other MMP's have been shown to induce shedding behavior as well (Huovila et al., 2005). Interestingly, ectodomain cleavage can either activate or inactivate membrane-bound receptors, depending on the specific receptor (Blobel, 2005). It is estimated that 2-4% of proteins on the cell surface are subjected to ectodomain shedding (Arribas and Massague, 1995). Ectodomain shedding can induce paracrine signalling through the release of growth factors (Blobel, 2005). Friedl et al. have shown that MV3 melanoma cells may routinely shed $\alpha_2\beta_1$ integrins at cellular detachment sites in 3D matrices, releasing adhesions and promoting cell migration, and suggest that this behavior may be a potential prerequisite for the release of adhesive junctions (Friedl et al., 1997; Huttenlocher et al., 1995). It is possible then that GM6001 may enhance the shedding of integrins or other adhesion molecules, which would subsequently decrease the adhesion of the MDAMB231 cells to the walls of the channels and potentially lead to increased migration speed. Interestingly, BB2516 is often used to inhibit the ADAM proteinases which are responsible for many receptor shedding events (Huovila et al., 2005). Therefore, this may potentially help explain the differences observed between GM6001 and BB2516 treatment. Additionally, GM6001 could be altering the matrix deposition or matrix reorganization activities of the cell. Further experiments will be required to determine the precise mechanisms governing this phenomenon.

Regardless of the specific mechanism by which GM6001 increases cell speed in the microtracks, we observe no impairment in cell migration through the 3D microtracks under several different modes of MMP inhibition, suggesting that this behavior occurs in an MMP-independent fashion. These data lead us to speculate that perhaps one

reason that MMP inhibitors fail when administered to patients (Coussens et al., 2002) could be because cancer cells are able to continue migrating within pre-formed tracks regardless of current MMP activity. Therefore, if the cancer cells have already begun forming these structures at the time that treatment is initiated, then this could explain why the MMP inhibitor does not have a significant effect on invasion.

3.6 Conclusions

We have presented a straightforward and easily adaptable platform for studying tumor cell motility in patterned collagen microtracks which mimic the complex architecture of the native tumor microenvironment. We have shown that collagen tracks of single cell width can be reproducibly patterned over a range of collagen densities, and that these tracks qualitatively and quantitatively mimic native proteolytic collagen microtracks. Additionally, these tracks facilitate the migration of both non-invasive and invasive cell types in a 3D environment in an MMP-independent fashion, perhaps revealing novel insight into the clinical challenges currently facing MMP inhibitors.

CHAPTER 4

ACTIN CYTOSKELETON AND FOCAL ADHESIONS REGULATE MMP-INDEPENDENT CANCER CELL MIGRATION IN 3D MICROTRACKS

4.1 Abstract

While tumor cell invasion has long been believed to occur late in cancer progression, recent studies suggest that local invasion may actually occur quite early. Therefore, it is imperative to study the mechanisms which facilitate this early invasion to determine the best way to inhibit it and prevent subsequent metastasis. During invasion, tumor cells have been shown to use proteolysis to mechanically rearrange their extracellular matrix (ECM) to form tube-like "microtracks" which other secondary cancer cells can subsequently follow without having to degrade the matrix themselves. We have developed and characterized a novel *in vitro* 3D collagen microtrack model which mimics these tube-like structures. Although extensive work has characterized cancer cell migration in 2D and 3D environments, the modes of migration which cells employ to migrate within these open microtracks remain poorly understood.

In this study, we examine both the effects of the extracellular microenvironment and the intracellular structures and signaling pathways that may drive microtrack migration. Interestingly, we find that, while increased collagen density significantly inhibits migration in a 3D matrix, cancer cell speed in patterned microtracks is unaffected by high collagen density, and cells are able to maintain average speed under a β1-integrin blocking antibody. Surprisingly, we find that cancer cell migration in microtracks is not dependent on Rho-mediated contractility, but does require an

intact, polarized actin and microtubule network, as well as focal adhesion formation and turnover. These findings contrast work in rigid channel structures, and show that using a physiologically-relevant matrix is essential to informing future clinical and non-clinical studies. Additionally, our studies suggest that targeting proteolysis or cellular contractility will not inhibit migration in pre-formed tracks, while selectively targeting the cancer cytoskeleton may be a better way to specifically inhibit migration in 3D microtracks and prevent subsequent metastatic invasion through these open paths.

4.2 Introduction

Despite being responsible for over 90% of cancer fatalities annually, the mechanisms governing metastatic invasion remain poorly understood. An inherently inefficient process, during metastasis only a small fraction of cells from the primary tumor prove capable of initially escaping the tumor microenvironment; even fewer survive the subsequent migration through the body, transit through the blood stream, and extravasation into tissue to form new substantive proliferating colonies (Bissell and Hines, 2011; Hou et al., 2011; Kumar and Weaver, 2009). Because the likelihood for tumor cells to complete this process is low, metastasis has been traditionally regarded as a later event in cancer progression, one that requires a substantial amount of time to allow phenotypic pressures to surface and select for the subset of tumor cells able to successfully navigate this complex ordeal. However, recent evidence shows that this process can actually begin quite early, and progress in parallel to the growth of the primary tumor (Klein, 2009). In a mouse model of breast cancer, disseminated tumor cells are detected in the bone marrow of mice within 4-8 weeks, prior to the detection of primary tumors of measurable size (>20 weeks) in the mammary gland (Husemann et al., 2008). mRNA analysis demonstrated an upregulation of MMPs and cathepsins

in these early tumor cells, suggesting that proteolysis could be a primary factor facilitating early invasion.

The use of intravital microscopy (IVM) has also revealed more detail regarding the invasion process, as tumor cells can be observed in real time migrating away from the primary tumor *in vivo* (Beerling et al., 2011; Giampieri et al., 2010). Studies using IVM have shown that proteolytic activity during both single cell and collective cell invasion can lead to ECM remodeling and the subsequent formation of cleared matrix pathways, or 'microtracks' (Friedl and Gilmour, 2009; Giampieri et al., 2009). This process begins when tumor cells detach from the original tumor site and begin migrating into the stroma via mesenchymal migration (Friedl and Wolf, 2003). Cells generate protrusions along their leading edge which attach to the surrounding matrix through integrin binding and activation. As the pseudopod elongates, the cell generates Rho-mediated contractile forces to pull itself through the matrix. When the cell encounters a zone of physical resistance, where its nucleus is restricted by the surrounding ECM fibers, it activates a program of pericellular proteolysis to cleave these fibers and free the cell body to continue its forward migration (Friedl and Wolf, 2008). As the cell pushes forwards, it will mechanically reorient and align the surrounding collagen fibers along the direction of migration. Finally, the anterior of the cell will release its matrix adhesions and glide forward. Thus, in its wake the cell leaves behind a proteolytic microtrack, approximately the width of a single cell. As subsequent cells move into this space, they no longer encounter the initial zone of physical resistance, and therefore have no impetus to degrade the ECM further. As multiple cells enter the microtrack, the microtrack can be widened further, both with and without further degradation, eventually forming a 'macrotrack' and enabling collective cell invasion, in the form of strands or sheets, through the ECM (Friedl and

Gilmour, 2009; Friedl and Wolf, 2003; Friedl and Wolf, 2008). Interestingly, stromal cells, such as cancer-associated fibroblasts (CAFs), have also been shown to create microtracks within a 3D ECM through a combination of proteolytic activity and force-mediated matrix remodeling (Gaggioli et al., 2007; Giampieri et al., 2009).

This form of migration in the follower cells suggests that a form of protease-independent migration does exist *in vivo*, and could potentially contribute to the poor results obtained with clinical MMP inhibitors, if administered after initial invasion has begun. In point of fact, studies have shown that treatment with the synthetic MMP inhibitor batimastat initiated prior to tumor implantation and continued throughout the lifetime of the mice, led to 100% survival of those mice, with no metastases detected (Eccles et al., 1996). In contrast, mice whose treatment began after tumor implantation had only a slight reduction in number and size of metastases, and had corresponding poor survival rates. Additionally, recent *in vitro* studies have shown that treatment with a broad spectrum MMP inhibitor immediately upon seeding tumor cells within 3D collagen gels prevents migration. However, if the inhibitor is administered 24 hours later, cells have formed tracks within the collagen matrix, and can continue to migrate within those tracks under MMP inhibition (Fisher et al., 2009).

Previous work in our lab has established a novel in vitro technique for studying proteolysis-independent cancer cell migration within fully 3D collagen microtracks (Kraning-Rush et al., 2013). We demonstrated that MMP inhibition with either broad-spectrum protease inhibitors or targeted siRNA has no effect on cell migration speed within *in vitro* patterned collagen tracks (Kraning-Rush et al., 2013). Together, these studies suggest that proteolysis is undoubtedly an early requirement for invasion, but can perhaps be dispensed of once cells have completed the reorganization of matrix

fibers to form pathways through the ECM. Beyond this understanding, however, the mechanisms involved in governing this style of invasion remain unclear. Therefore, in this study we will examine the role that contractile force generation, actin filaments, microtubules, and focal adhesions play in mediating migration within patterned 3D collagen microtracks.

4.3 Materials and Methods

Cell Culture and Reagents

MDAMB231 highly metastatic breast adenocarcinoma cells (American Type Culture Collection (ATCC), Rockville, MD) were maintained in Minimum Essential Medium supplemented with 10% fetal bovine serum (Atlanta Biologicals, Lawrenceville, GA) and 1% penicillin-streptomycin (Life Technologies, Grand Island, NY). Cells were cultured at 37°C and 5% CO_2. 4B4 and FITC-4B4 were obtained from Beckman Coulter (Brea, CA). Y27632, ML7, blebbistatin, tetradecanoyl phorbol acetate (TPA), bisindolylmaleimide I (BIM), Gö6976, cytochalasin D, nocodazole, and paclitaxel were acquired from Sigma-Aldrich (St. Louis, MO). CT04 was obtained from Cytoskeleton, Inc. (Denver, CO).

RNA Interference and Western Blotting

MDAMB231 cells at 50% confluency on tissue culture plastic were transfected with 25 pM non-targeting (control) siRNA or siRNA targeting vinculin, p130Cas or zyxin using Lipofectamine 2000 (2 μg/mL, Life Technologies). The non-targeting sequence was 5'-UUCCUCUCCACGCGCAGUACAUUUA-3'. The sequence targeting vinculin (accession number NM_001191370.1) was 5'-UCCUGGAAAUCAAGCUGCUUAUGAA-3'. The sequence targeting p130Cas (accession number NM_001170715.1) was 5'-GCCUCAAGAUCUUGGUGGGCA-

UGUA-3'. The sequence targeting zyxin (accession number NM_003461.4) was 5'-CAUGACCAAGAAUGAUCCUUUCAAA-3'. All siRNA's were synthesized by Life Technologies. siRNA knockdown was confirmed with Western blotting.

MDAMB231 cells treated with siRNA in 6 well plates were rinsed once with ice-cold PBS and lysed using a solution of 25 mM Tris-HCl, pH 7.4, 0.4 M NaCl, 0.5% SDS (Sigma) for 5 minutes with mechanical scraping. Protease and phosphatase inhibitors were added to lysis buffer to prevent protein degradation (1 mM sodium fluoride, 1 mM sodium orthovanadate, and 1:100 dilution of protease inhibitor cocktail containing working concentrations of 1.04 mM 4-(2-aminoethyl)benzenesulfonyl fluoride (AEBSF), 0.8 μM aprotinin, 40 μM bestatin, 14 μM E-64, 20 μM leupeptin, 15 μM pepstatin A, all from Sigma). Cell lysate was cleared by centrifugation at 14,000 x g and the supernatant was snap frozen and stored at -80^{o}C until analysis. Lysates were separated by SDS-PAGE and transferred onto nitrocellulose (Bio-Rad, Hercules, CA). Blots were probed using antibodies against vinculin (V284, Millipore), zyxin (Z4751, Sigma), and p130cas (sc-860, Santa Cruz Biotechnology Inc., Santa Cruz, CA). Horseradish peroxidase (HRP)-conjugated secondary antibodies were obtained from Cell Signaling Technology. After incubation in SuperSignal West Pico Chemiluminescent Substrate (Thermo Scientific, Rockford, IL), blots were exposed and imaged using a FujiFilm ImageQuant LAS-4000. Protein densitometry of blots was performed with ImageJ software (v. 1.47k, National Institutes of Health, Bethesda, MD).

Flow Cytometry

Matrix binding to β_1-integrin was blocked with a mouse monoclonal antibody 4B4 (Beckman Coulter). β_1-integrin expression on the cell surface was quantified with a

4B4-FITC conjugate (Beckman Coulter) by FACS analysis using a FACS Aria high speed flow cytometer (BD Biosciences, Franklin Lakes, NJ). Separately, MDAMB231 cells transfected with a GFP-tagged LifeAct plasmid were isolated using the FACS Aria flow cytometer.

Microscopy

Phase contrast imaging was performed in a custom temperature, humidity, and CO_2-controlled stage of a Zeiss Axio Observer Z1m inverted phase contrast microscope equipped with a Hamamatsu ORCA-ER camera and operated by AxioVision software (v. 4.8.1.0). Confocal fluorescence and reflectance imaging was performed with a Zeiss LSM700 confocal microscope on a Zeiss AxioObserver Z1 inverted stand equipped with a long working distance water-immersion C-Apochromat 40x/1.1 NA Zeiss objective and operated by Zen software (v. 2010, Carl Zeiss MicroImaging GmbH, Jena, Germany). Confocal reflectance images were obtained as previously described (Carey et al., 2012; Kraning-Rush et al., 2011).

Polyacrylamide Gel Synthesis and Traction Force Microscopy

Substrates with a Young's moduli (*E*) of 5 kPa were synthesized using a ratio of 7.5% acrylamide (40% w/v solution, Bio-Rad) to 0.175% N,N'-methylene-bis-acrylamide (2% w/v solution, Bio-Rad) as described previously (Kraning-Rush et al., 2012b; Reinhart-King, 2008). Substrate surfaces were functionalized using N-6-((acryloyl)amido)hexanoic acid, synthesized in our lab (Califano and Reinhart-King, 2010a), covalently bound to 0.1 mg/mL type I rat-tail collagen (Becton Dickinson, Franklin Lakes, NJ). Traction force microscopy (TFM) was performed as previously described (Dembo and Wang, 1999; Kraning-Rush et al., 2012b; Kraning-Rush et al., 2011). Briefly, cells were seeded on polyacrylamide substrates embedded with 0.5-

μm fluorescent beads and allowed to adhere and spread for 6-8 hours before drug was applied. TFM experiments were performed ten hours after initiation of treatment. Cells were imaged in phase and bead distributions were imaged in fluorescence before and after removal of the cell with trypsin. Bead displacement within the substrate was tracked with correlation-based optical flow and converted into a strain field. These strain fields were converted into traction stresses using the LIBTRC analysis library developed by Professor Micah Dembo of Boston University, who invented the basic theory that underlies TFM (Dembo and Wang, 1999). Images were processed with LIBTRC software to determine the cellular traction vectors, T, the total magnitude of the force, |F|, and the projected cell area. |F| is an integral of the traction field over the entire area of the cell,

$$|F| = \iint \left(T_x^2(x,y) + T_y^2(x,y)\right)^{1/2} dxdy \tag{2.1}$$

where $T(x,y) = \left[T_x(x,y), T_y(x,y)\right]$ is the continuous field of local traction vectors defined at local spatial coordinates (x,y) in the projected cell area(Reinhart-King et al., 2005). 20-60 cells were analyzed per condition.

Microtrack Fabrication

Collagen microtracks with dimensions of 10 *x* 1100 *x* 20 μm (*w x l x d*) were prepared using collagen extracted from rat tail tendons (Pel-Freez Biologicals, Rogers, AR) without pepsin as previously described (Kraning-Rush et al., 2013; Nelson et al., 2008). Briefly, patterned PDMS stamps were rendered non-adhesive by incubation for 30 minutes at room temperature with 1% BSA (Sigma) in PBS before being washed twice with a neutralized collagen solution and inverted over a drop of neutralized collagen between either two thin PDMS spacers for phase-contrast imaging or onto the glass bottom of a modified petri dish (MatTek, Ashland, MA) for confocal imaging. Collagen was allowed to polymerize for 90 minutes at 37^{o}C before stamps were

removed and MDAMB231 cells were seeded into the tracks at low density to minimize cell-cell interactions. Patterned microtracks were capped with a collagen lid polymerized separately on an 18 mm diameter glass coverslip before being overlaid with 2 mL pre-warmed culture media.

Cell Migration Studies and Morphology Analysis

Cells were either seeded into 1.5-5 mg/mL type I collagen gels or into 1.5-10 mg/mL collagen microtracks at low density. Gels and microtracks were incubated for 6-8 hours prior to phase contrast time-lapse imaging. Cells were imaged every 5 minutes for 20 hours for drug treatment experiments and 10 hours for untreated experiments. Dividing cells and cells that did not move from their original location after 4 hours were excluded from analysis. ImageJ software was used to determine the area, perimeter, aspect ratio (length of long axis / length of short axis), and circularity, defined as (4πArea/Perimeter^2), where a circle has a value of 1, and a straight line has a value of 0 (Cornhill et al., 1980; Kraning-Rush et al., 2011). Cell centroid position based on cell outlines was used to calculate the mean-square displacement ($<d^2>$)(Stokes et al., 1991). For 3D migration within the collagen gel matrix, cell migration speed (S) was determined by fitting the $<d^2>$ and the time interval (t) to the persistent random walk equation:

$$\left\langle d^2 \right\rangle = 2S^2 P\left[t - P\left(1 - e^{-\left(t/P \right)} \right) \right] \tag{3.1}$$

where P is the persistence time, using nonlinear least squares regression analysis as previously described (Reinhart-King et al., 2008).

Because cells traveling in collagen microtracks do not travel in a random walk, but can only migrate in one of two directions, speed was calculated by dividing the final displacement by time, for cells migrating in one direction for a length of 100 minutes.

Maximum invasion distance was quantified by determining the displacement of the cell from its initial position at each time point up to 100 minutes. The maximum value calculated was considered the maximum invasion distance. 100 minutes was selected as the cutoff point to minimize the number of cells which migrated out of the field of view in the microtracks.

Drug Treatments

To assess the effects of various inhibitors on cell migration behavior within patterned collagen microtracks, cells were seeded as described above. Cells were allowed to adhere and spread for 6-8 hours before imaging. Drug was either applied immediately prior to imaging or after 4-5 hours of 'control' imaging. In either instance, quantification of cell speed occurred post-drug treatment.

Fluorescent Staining

Cells seeded in collagen microtracks were allowed to spread overnight and were then fixed with 3.7% (v/v) formaldehyde in PBS and permeabilized with 3:7 ratio methanol:acetone for 5 minutes at -20^{o}C. Samples were blocked overnight with PBS/0.02% (v/v) Tween (JT Baker) with 3% (w/v) BSA (Sigma) and incubated with 1:100 mouse anti-vinculin primary antibody (#V9131, Sigma) for 2 days at 37^{o}C under gentle agitation. Cells were then incubated with 1:200 Alexa Fluor 488 goat anti-mouse secondary antibody (Life Technologies) for 2 hours and washed overnight to remove excess background staining. Cells were then imaged using confocal microscopy as previously described (Carey et al., 2012; Kraning-Rush et al., 2013).

GFP-LifeAct Transfection

GFP-LifeAct plasmid was a kind gift from Jan Lammerding (Cornell University). MDAMB231 cells were seeded at 60% confluence in a 12 well plate and transfected after 24 hours. Cells were transfected by combining 3 μg DNA plasmid and 3 μL Transit-2020 transfection reagent (Mirus Bio LLC, Madison, WI) in 100 μL OptiMEM (Life Technologies) for 20 minutes before adding dropwise to cells in complete medium. Optimal transfection was achieved at 48 hours, at which time transfected cells were isolated using FACS as described above and seeded into collagen microtracks for subsequent confocal imaging.

Statistical Analysis

Data were compared using analysis of variance with a post-hoc Tukey's Honestly Significant Difference (HSD) test or Dunnett's test where appropriate using JMP software (v.10, SAS, Car, NC). Statistical significance was considered with $p < 0.05$.

4.4 Results

Microtrack migration is independent of collagen density and β1 integrin function

It has been demonstrated that cancer cells can proteolytically degrade the ECM and reorganize the cleaved ECM fibers into open pathways which other cells can traverse (Friedl and Wolf, 2008; Wolf et al., 2007). Previously, we have established a technique to mimic these tracks *in vitro* by patterning microtracks of single cell width within 3D collagen hydrogels. Cells seeded within these microtracks are bounded circumferentially by collagen fibers, but can migrate unidirectionally forward or backward through the track (Kraning-Rush et al., 2013). To investigate the relationship between collagen density and metastatic cancer cell migration, we seeded highly metastatic MDAMB231 breast cancer cells into either 3D collagen gels, wherein cells are bound on all sides by collagen (Fig. 4.1A), or within patterned 3D

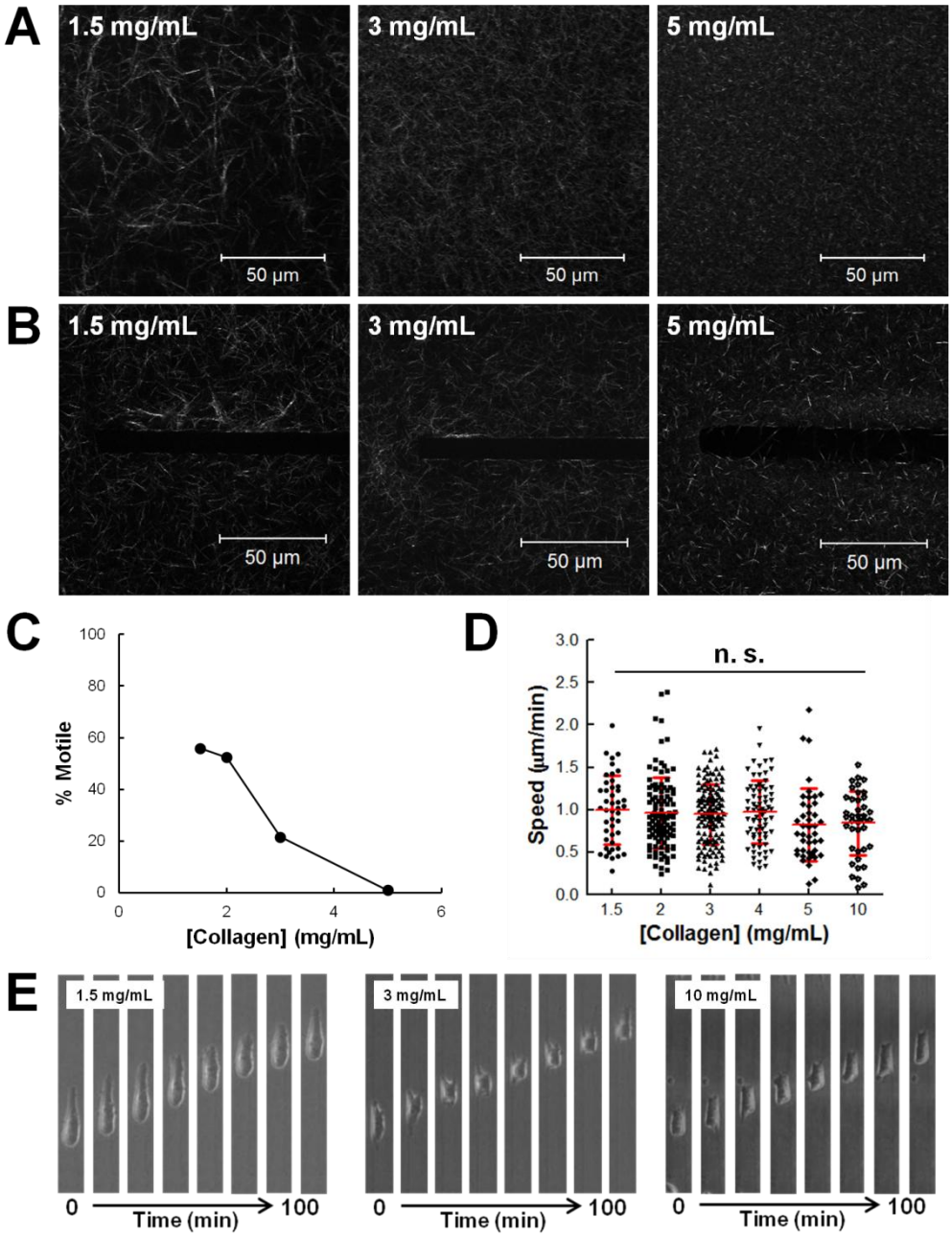

Figure 4.1. Collagen density regulates 3D matrix invasion, but not microtrack migration. A) Confocal reflectance images of a 3D type I collagen matrix at 1.5, 3 and 5 mg/mL, showing decreased fibril length and pore size with increasing density. B) Confocal reflectance images of microtracks patterned in 1.5, 3 and 5 mg/mL type I collagen. Scale bar = 50 µm. C) Motile fraction of cells significantly decreases with increased collagen density in a 3D matrix. D) Cell speed does not significantly decrease within open collagen tracks of the same collagen densities as the 3D matrices. E) Time lapse phase contrast images show no difference in MDAMB231 metastatic breast carcinoma cells migrating within patterned 3D collagen tracks of increasing density. Mean ± SD; n > 40 cells.

collagen microtracks (Fig. 4.1B) of increasing collagen density. Qualitative analysis of the collagen fibers using confocal reflectance imaging showed that within both environments, as collagen density is increased from 1.5 to 5 mg/mL, the fiber length and pore size decrease. Next, we quantified the number of cells able to move away from their initial position within 3D collagen matrices of different collagen densities. We find that as collagen density increases, the fraction of cells able to migrate within the matrix decreases dramatically, and cells are essentially unable to move within dense 5 mg/mL collagen matrices (Fig. 4.1C). In contrast, the motile fraction of cells within patterned microtracks does not change with collagen density (data not shown). The migration speed of motile cells decreases slightly, but not significantly, over a broad range of 1.5 – 10 mg/mL collagen (Fig. 4.1D). Additionally, it is important to note that cell speed can vary greatly within the collagen microtracks, ranging from ~0.5-1.5 μm/min. Time-lapse phase microscopy images of representative cells migrating in 1.5, 3, and 10 mg/mL patterned collagen tracks show similar displacements over 100 minutes (Fig. 4.1E). These data suggest that once the steric hindrance of the 3D matrix is overcome, cells become significantly less sensitive to ECM density.

To further explore the relationship between a tumor cell's adhesiveness to collagen fibers and migration within patterned collagen tracks, we used a function blocking antibody (4B4) to block the β1 integrin on cancer cells after they were seeded within the collagen tracks. First, we used a fluorescently conjugated blocking antibody to determine the threshold concentration of antibody required to achieve maximal blocking. FACS analysis showed that maximal blocking was reached at 10 μg/mL (Fig. 4.2A-B), consistent with previous reports (Zaman et al., 2006). Interestingly, as cells treated with the β1 blocking antibody travel through the collagen microtracks,

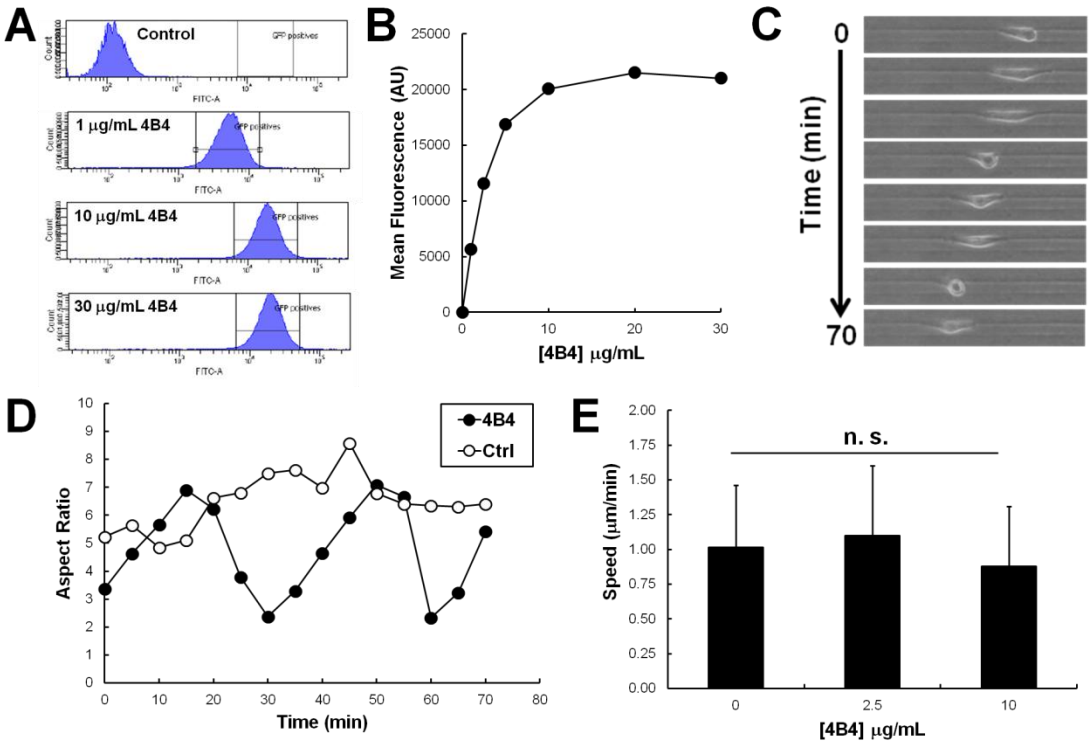

Figure 4.2. Cell migration within patterned collagen microtracks continues under β1 integrin blocking. A) Flow cytometry data shows intensity distribution of 4B4-β_1 labeled MDAMB231 cells compared to control. B) Mean fluorescence data shows that maximum blocking of β_1 integrin is reached at 10 μg/mL 4B4. C) Time lapse phase contrast images show β_1-blocked MDAMB231 cells acquire an 'inchworm' type morphology to migrate within the collagen microtrack. D) Quantification of the aspect ratio of a control and 4B4-treated cell during 70 minutes of migration demonstrates the morphology switch in the 4B4-treated cell. E) Cell migration speed within collagen microtracks is not significantly decreased when β_1 integrin is blocked. Mean + SD; n > 70 cells.

they vacillate between an elongated and mesenchymal-like state (high aspect ratio) and a more rounded, amoeboid-like state (low aspect ratio), leading to an 'inchworm' style of migration (Fig. 4.2C-D). In contrast, control cells tend to migrate in a steady, typically elongated fashion (Fig. 4.1E, 4.2D, open circles). In this manner, they are able to maintain cell migration speed similar to control cells (Fig. 4.2E), and may also yield insight into why migration speed appears to be largely unaffected by collagen density (Fig. 4.1D).

Cellular contractility is dispensable for microtrack migration

Previous research shows that migration through a 3D matrix requires a balance between cell/matrix adhesiveness and traction forces, and suggests that as adhesiveness is decreased, a correlating increase in traction force may be required to maintain normal migration speeds (Zaman et al., 2006). Therefore, we next looked at the explicit role of contractile force generation in mediating cell migration within the open pathway of the microtrack. First, we targeted several key members of the primary contractility signaling pathway with specific small molecule inhibitors: myosin light chain kinase (MLCK, inhibited with ML7), Rho-associated coiled-coil containing protein kinase (ROCK, inhibited with Y27632), and the Rho family GTPases (inhibited with CT04). We confirmed that these inhibitors decreased contractility by performing traction force microscopy (TFM) on treated MDAMB231 cells seeded on 5 kPa polyacrylamide substrates (Fig. 4.3A). Next, we treated cells seeded within the patterned collagen tracks with the same dosages of the inhibitors. Interestingly, we found no decrease in migration speed, even when 90% of the cell's traction forces were inhibited with CT04 (Fig. 4.3B). However, when we lower the affinity of myosin to actin using the nonmuscle myosin IIA inhibitor, blebbistatin, we

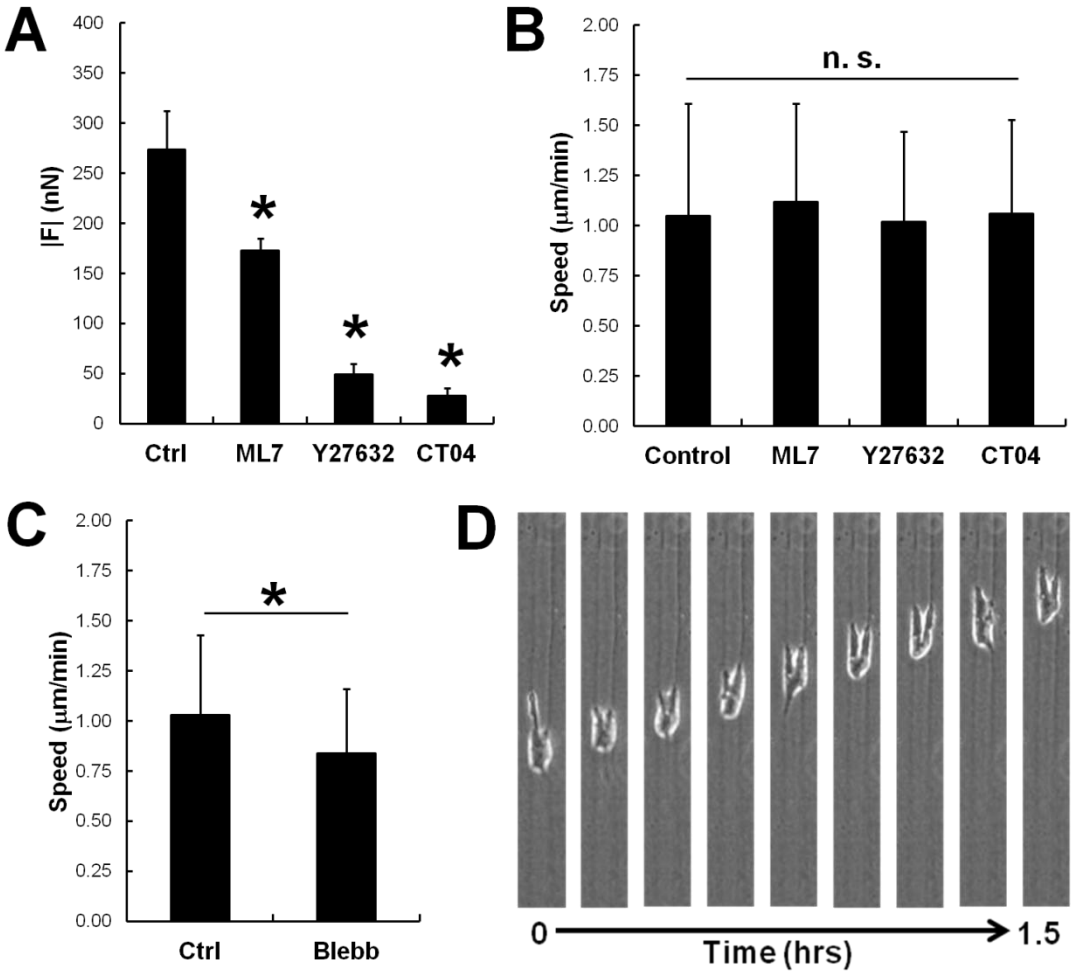

Figure 4.3. Contractility inhibition does not impair cell migration in collagen tracks. A) Traction forces of MDAMB231 cells on 5 kPa polyacrylamide gels after 10 hours of treatment with a MLCK inhibitor (ML7), ROCK inhibitor (Y27632), or Rho inhibitor (CT04). Mean + SEM; * indicates $p < 0.05$; $n > 30$ cells. B) Cell migration speed within collagen microtracks is not significantly decreased when contractility inhibitors are applied. Mean + SD; $n > 30$ cells. C) Inhibition of myosin IIa with blebbistatin significantly reduces cell speed. Mean + SD; * indicates $p < 0.05$; $n > 50$ cells. D) Time-lapse phase-contrast images show blebbistatin-treated MDAMB231 cells become elongated, with multiple protrusions, migrating within the collagen microtrack.

observe a small but significant decrease in migration speed within the patterned tracks (Fig. 4.3C). Time-lapse phase microscopy images reveal that cells moving through the collagen tracks become elongated, with multiple protrusions extending from the cell body (Fig. 4.3D).

Focal adhesions drive persistent migration

Because myosin II plays a key role in the formation and maintenance of focal complexes (Giannone et al., 2007), we next chose to analyze the consequences of directly inhibiting focal adhesion formation using siRNA. We chose to first target vinculin, a prominent, well-characterized focal adhesion protein shown to be vital to regulating cell motility and through both structural and signaling means (Goldmann et al., 2013; Mierke et al., 2010). Vinculin simultaneously binds F-actin and talin and α-actinin, the latter two of which bind integrins, thus mediating the connection of the cell cytoskeleton to the extracellular matrix and helping to transmit cellular forces (Ziegler et al., 2006). It has been shown that vinculin is required early in focal adhesion formation, with some evidence showing its presence even in nascent focal adhesions, which are highly transient (Tan et al., 2010). Additionally, vinculin knock down has been shown to correlate with smaller and fewer focal adhesions, which turn over rapidly (Saunders et al., 2006; Zent and Pozzi, 2010).

We first demonstrated that focal adhesions are present in cells within the collagen microtracks, with punctuate clustering of vinculin observed at the cell periphery (Fig. 4.4A, white arrows). Next, we knocked down vinculin expression by ~80% using targeted siRNA, confirmed with western blotting (Fig. 4.4B-C). We then seeded vinculin KD cells into patterned collagen microtracks and observed their migration behavior. While they maintained migration speed similar to cells treated with control

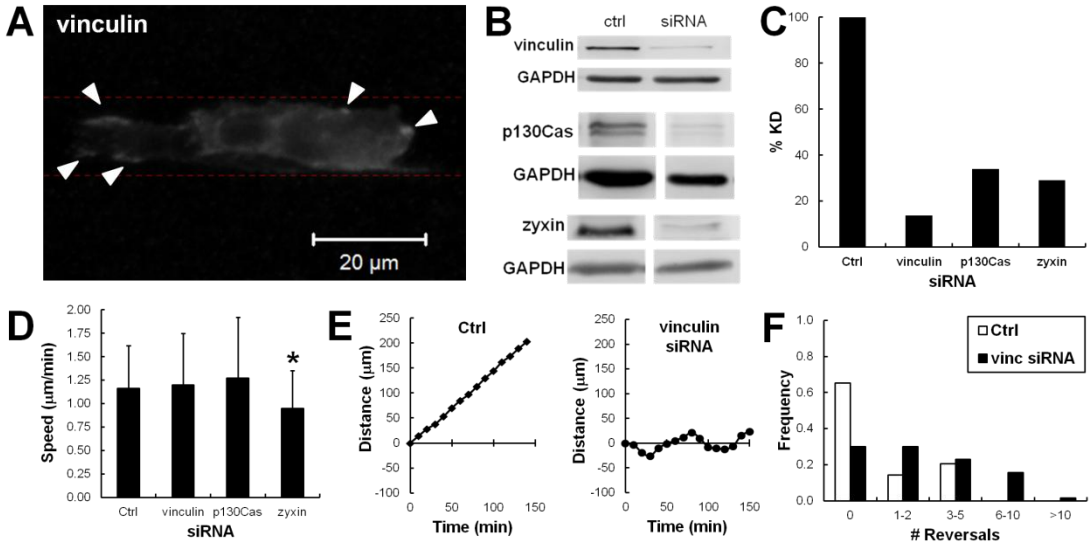

Figure 4.4. Focal adhesions are critical for maintaining directional persistence within collagen microtracks. A) Confocal fluorescence image of focal adhesions stained for vinculin (white arrowheads) within an MDAMB231 cell seeded in a collagen track. Scale bar = 20 µm. B) Western blotting confirmed knockdown of focal adhesion proteins vinculin, p130Cas, and zyxin by ~65-85% (C). D) Cells with vinculin and p130Cas proteins knocked down are able to maintain migration speed similar to control cells, while zyxin knockdown cells exhibit slightly decreased migration speed. Mean + SD; n > 100 cells. E) While control siRNA cells are able to maintain migration in a single direction for > 2 hours, vinculin siRNA treated cells travel back and forth, reversing direction several times. F) While two thirds of control cells migrate without changing direction, only 30% of vinculin siRNA cells are able to migrate persistently, while the other 70% reverse direction at least once, and often several times. n > 50 cells.

siRNA (Fig. 4.4D), we observed that, rather than migrate persistently in one direction through the microtrack, as control cells typically do, vinculin KD cells would reverse direction multiple times, sometimes in quick succession (Fig. 4.4E-F).

We next assayed two additional focal adhesion proteins which have previously been suggested to play a role in mediating migration within 3D collagen matrices – zyxin and the scaffolding protein p130Cas (Fraley et al., 2012). Previous research suggests that both of these proteins are recruited to mature focal adhesions on 2D substrates, and may be less common or absent in nascent adhesions (Beningo et al., 2001; O'Neill et al., 2000). However, it has also been demonstrated that there is little association between the roles of specific focal adhesion proteins in 2D and 3D motility (Fraley et al., 2010). Our results indicate that knockdown of p130Cas does not significantly affect cell migration speed within the collagen microtracks, while knockdown of zyxin does slightly but significantly decrease migration speed (Fig. 4.4B-D). While zyxin depletion has previously been shown to induce periodic oscillations in HT1080 fibrosarcoma cells migrating within 3D collagen matrices (Fraley et al., 2012), we did not observe this phenotype in zyxin siRNA-treated MDAMB231 cells migrating within our patterned collagen microtracks.

Next, because it has been shown in the literature that protein kinase C (PKC) activation can induce focal adhesion formation in 2D (Woods and Couchman, 1992), we stimulated MDAMB231 cells within patterned microtracks with 12-O-Tetradecanoylphorbol 13-acetate (TPA), a phorbol ester known to activate both classical and novel PKCs. Treatment with TPA leads to a statistically significant increase in cell speed in the motile population of cells (Fig. 4.5A). To confirm this

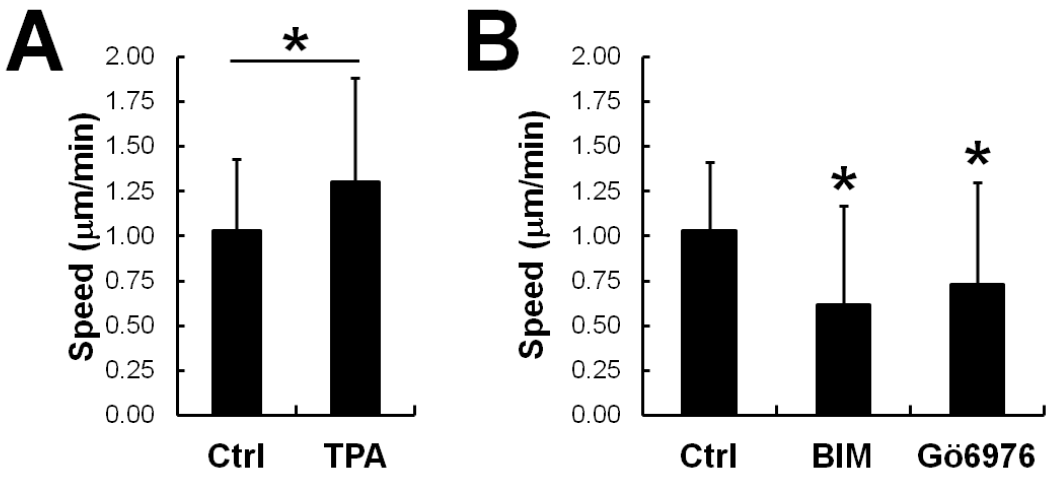

Figure 4.5. PKC activation and inhibition control cell migration speed within collagen tracks. A) Activating PKCs with tetradecanoyl phorbol acetate (TPA) significantly increases cell speed, while PKC inhibition (B) via Gö6976 or bisindolylmaleimide I (BIM) decreases cell migration speed. Mean + SD; n > 50 cells.

finding, we then treated cells within the microtracks with two commonly used inhibitors of PKCs, bisindolylmaleimide I (BIM), a general inhibitor which targets both classical and novel PKCs, and Gö6976, which is restricted to targeting classical PKCs. Both BIM and Gö6976 significantly reduced cell migration speed within the collagen microtracks, with BIM inducing a slightly greater effect than Gö6976 (Fig. 4.5B). These results support our hypothesis that focal adhesion activation and turnover could potentially be driving migration within the microtracks.

Actin filaments and microtubules are required for migration

Because focal adhesions are responsible for transmitting signals from the ECM to the actin cytoskeleton (Mierke et al., 2010), we next addressed the role of the cytoskeleton in mediating cell migration through the collagen microtracks. Immunostaining within the patterned collagen tracks (Fig. 4.6A) shows distinct actin stress fibers (top), as well as an established microtubule network (middle). The overall orientation of the actin and microtubule cytoskeleton was determined using OrientationJ analysis. OrientationJ is a free ImageJ plug-in which can be used to characterize the orientation and isotropy of an image both qualitatively (by hue) and quantitatively (by angle relative to the horizontal axis) (Brownfield et al., 2013; Fonck et al., 2009). The prevalence of blue-purple pseudo-coloring in both actin and microtubule images (Fig. 4.6B) indicates fiber orientation that is largely parallel with the horizontal axis, which lies along the length of the track (see inset). Quantification of the orientation angles of the fibers was assessed with respect to the axis of the microtrack (0^{o}), and confirms that ~70% of both actin fibers and microtubules align within 10 degrees of the track axis (Fig. 4.6C).

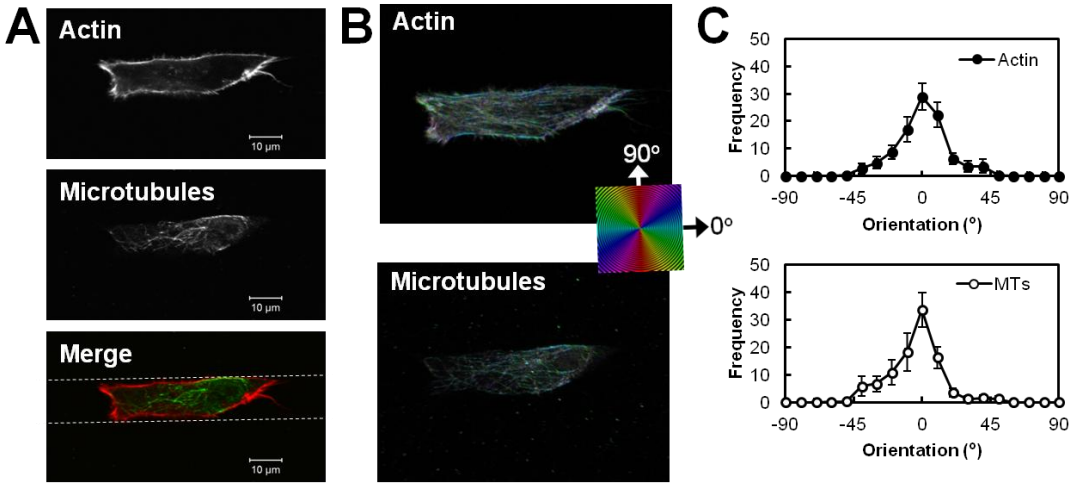

Figure 4.6. Actin filaments and microtubules align along the length of the microtrack. A) Confocal fluorescence images of stained actin filaments (red) and microtubules (green) of a MDAMB231 cell within a patterned collagen track (dotted white line). Scale bar = 10 μm. B) Orientation analysis of the actin and microtubule structure (maximum z projection) reveals a significant orientation bias towards the axis of the track (set at 0°) Inset is a legend for hue with orientation angle. C) Quantification of the orientation analysis showing ~70% of actin filaments (top) and microtubules (MTs, bottom) aligned within ±10° of microtrack axis. Mean ± SEM; n = 14 cells.

We then treated cells with inhibitors cytochalasin D (CD) and latrunculin A (LA), which depolymerize actin by binding to the growing, barbed, ends of F-actin or by binding G-actin, respectively. Both drugs abolished migration in collagen channels (Fig. 4.7A-B, black bars), even in cells that were migrating quite persistently prior to treatment (Fig. 4.7C). Because previous reports in the literature suggest that cancer cells can continue to migrate in rigid PDMS channels when actin is depolymerized (Balzer et al., 2012), we repeated these experiments in PDMS channels of equal width to the patterned collagen tracks. Interestingly, we find that a subset of cells is able to continue to migrate in the rigid channels under actin depolymerization, although their speed is slower than controls (Fig. 4.7A-B, white bars). Surprisingly, we observe that CD and LA may have some differential effects, as a larger subset of LA-treated cells are still able to migrate compared to CD-treated cells, which appear to qualitatively shift their mode of migration to a more amoeboid, less adhesive style (data not shown). Next, we transfected the MDAMB231 cells with a plasmid encoding Lifeact, a 17 amino acid peptide which stains F-actin without interfering with actin dynamics (Riedl et al., 2008). After seeding transfected cells into the patterned collagen tracks and allowing them to spread overnight, we imaged actin fibers in real time as a cell moved through the microtrack before and after treatment with CD (Fig. 4.7D). After addition of CD, we observe an overall dissociation of stress fibers into small actin bundles throughout the cell body. Qualitative OrientationJ analysis shows more disorganized fibers, no longer aligned with the microtrack axis (Fig. 4.7E).

Finally, we also interfered with microtubule dynamics by either inhibiting microtubule polymerization with nocodazole (NC), or stabilizing microtubules with paclitaxel (TX) in cells within the collagen microtracks. Under both conditions, there was a marked decrease in the number of motile cells, as well as the speed of the motile cells

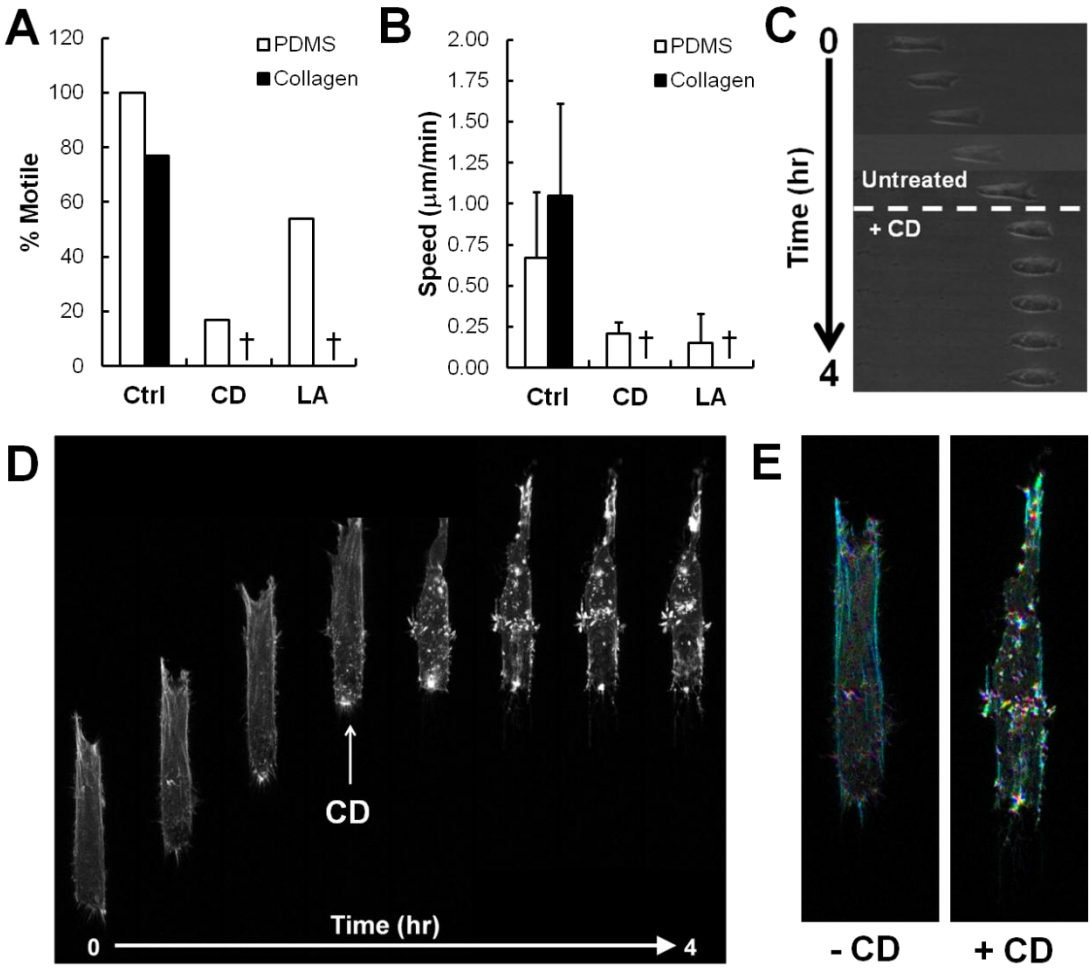

Figure 4.7. Inhibition of actin polymerization affects cell migration differentially in collagen tracks and PDMS* channels. A) Cytochalasin D (CD) and latrunculin A (LA) abolish motility within patterned collagen microtracks (black bars), while cells are still able to migrate within PDMS channels (white bars) under LA and, to a lesser extent, CD treatment. B) Migration speed of motile cells within PDMS channels does not change under CD or LA treatment. Mean + SD; n > x cells; * indicates $p < 0.05$; † indicates value of 0. C) Time lapse phase contrast images show MDAMB231 cells immediately stop moving within the collagen microtracks upon treatment with CD. D) Time lapse confocal microscopy images of GFP-LifeAct transfected cells within collagen microtracks show that upon treatment with CD, stress fibers depolymerize and actin becomes restricted to punctate bundles within the cell. E) Orientation analysis of cells under CD treatment shows a loss of polarization along the microtrack axis. *PDMS channel experiments performed in collaboration with Michael Mak and David Erickson. Collagen channel experiments performed in collaboration with Olivia Torre.

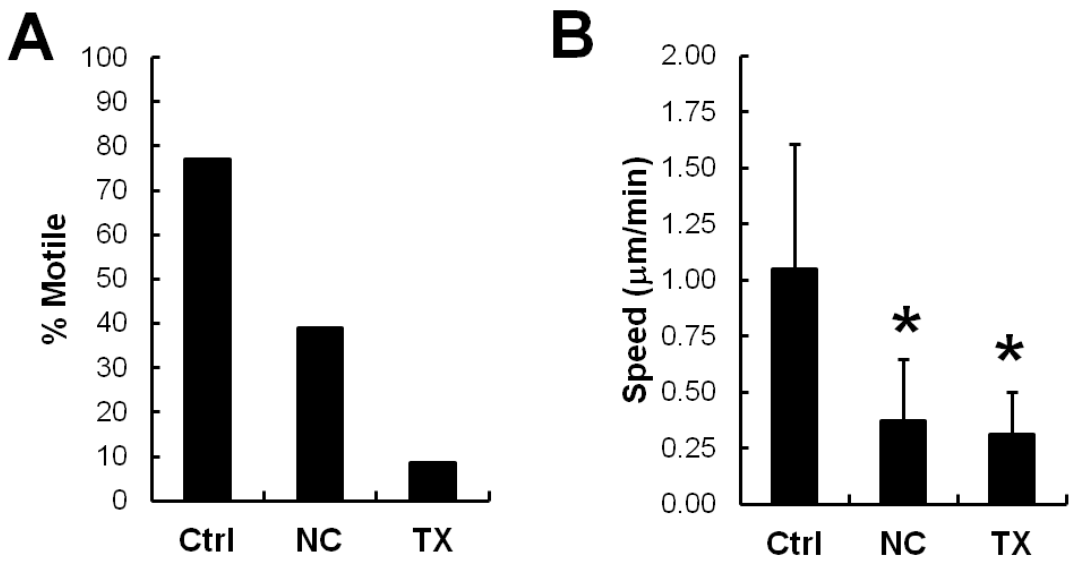

Figure 4.8. Depolymerizing or bundling microtubules impairs cell migration in collagen tracks. A) Nocodazole (NC) and Paclitaxel (TX) reduce motility within patterned collagen microtracks. B) Migration speed of motile cells within collagen tracks and PDMS channels decreases under NC and TX treatment. Mean + SD; $n > 45$ cells; * indicates $p < 0.05$. Collagen channel experiments performed in collaboration with Olivia Torre.

(Fig. 4.8A-B). This data is consistent with results observed in rigid PDMS channels (Balzer et al., 2012; Irimia and Toner, 2009; Mak et al., 2013). We speculate that this result is due to a loss of the cell's ability to polarize, a behavior which microtubules have long been considered responsible for (Kaverina et al., 2000). Additionally, it is important to note that though these two drugs are primarily used to target microtubules, they can also affect actin filament structure (Danowski, 1989; Kraning-Rush et al., 2011).

4.5 Discussion

While the sequential process of microtrack creation by leader cells and invasion by follower cells during cancer progression has been illustrated plainly over the last decade, little is known about the fundamental principles governing migration within these track structures. Using a novel collagen micropatterning technique, our previous research conclusively demonstrated that this form of migration was independent of matrix metalloproteinase (MMP) activity, once the track structures were in place (Kraning-Rush et al., 2013). Here, we investigate in more detail the role of extracellular matrix density, adhesion molecules, signaling pathways, and cytoskeletal architecture in mediating microtrack migration of breast carcinoma cells. We find that, while increased collagen density drastically reduces a cancer cell's ability to invade in a 3D matrix, it has little effect on a cell's capacity to migrate through a patterned 3D microtrack. Our results indicate that focal adhesions, PKC activation, actin filaments, and microtubules are particularly important for the maintenance of persistent migration within the tracks.

In contrast, we find that contractile force generation is dispensable for migration within the microtrack environment, as evidenced by unimpaired cancer cell migration

under inhibition of Rho, ROCK, and MLCK. This result is consistent with previous reports in the literature suggesting that Rho/ROCK activity is critical for track-generating behaviors and matrix remodeling. Provenzano et al. have demonstrated that Rho and ROCK are required for the reorganization and alignment of ECM fibers, but when tumor cells are exposed to an environment in which the ECM fibers have been pre-aligned, this contact guidance is sufficient to facilitate subsequent invasion (Provenzano et al., 2008b). Similarly, work by Brownfield et al. recently showed that during epithelial branching, contractility is required for the alignment of collagen fibers, but is not required for the cells to sense alignment (Brownfield et al., 2013). Moreover, Gaggioli et al. showed that Rho/ROCK function is required in stromal fibroblasts to generate microtracks within the matrix, but is not required in the squamous cell carcinoma cells which follow these microtracks (Gaggioli et al., 2007). It has also been shown that some cancer cell lines which maintain an elongated morphology also do not require Rho/ROCK signaling to migrate (Sahai and Marshall, 2003). Our results contribute to these findings by demonstrating that the contact guidance behavior within collagen microtracks is similarly independent of Rho-mediated contractility. Together, these findings implicate Rho/ROCK contractility in an earlier invasion step, likely during microtrack formation.

Instead, our results point towards focal adhesions and the cytoskeleton as primary regulators of cancer cell migration in collagen microtracks. When vinculin is knocked down with siRNA, we find that cancer cells are still able to move within the tracks, but cannot maintain persistent migration; instead, 70% of cells transfected with vinculin siRNA reverse direction at least once, in contrast to the 35% of control cells which reverse direction. This data is consistent with a previous study showing that inhibition of vinculin significantly inhibited persistent distance of HT1080

fibrosarcoma cells in a 3D matrix (Fraley et al., 2010), and implicate vinculin as a mediator of cell polarity (Carisey et al., 2013). Mierke et al. also demonstrated that vinculin knockout cells were significantly less invasive in a 3D matrix than wild type cells (Mierke et al., 2010). Interestingly, they also demonstrated that vinculin-expressing cells generated significantly higher traction forces, and therefore, they subsequently attribute the invasive behavior of vinculin-expressing cells to their ability to generate force and overcome the restrictive environment of a dense 3D matrix (Mierke et al., 2010). These data coupled with our results indicate that vinculin may thus play a role in both microtrack generation during initial invasion *and* in subsequent microtrack migration, perhaps through different mechanisms. Our data show that impaired traction forces do not affect persistent migration within the microtrack. Therefore, vinculin may also play a role in mediating cell polarity during migration (Carisey et al., 2013). Cells with decreased or absent vinculin are thus dually impaired – not only unable to exert force to remodel and invade a collagen matrix (Mierke et al., 2010), but also unable to persistently migrate within a permissive 3D environment.

Interestingly, while previous results have indicated that zyxin depletion leads to increased cell speed and oscillating 1D-like migration in the majority of HT-1080 fibrosarcoma cells migrating within a fully 3D matrix (Fraley et al., 2012), we do not directly observe this phenotype within patterned collagen microtracks. One important factor which may contribute to these differing observations may be the nature of the collagen environment in which these cells are moving. Fraley et al. demonstrate that zyxin-depleted cells within a 3D matrix create exceptionally narrow cell tracks compared to control cells, which lead to a more restrictive environment than the patterned tracks used in this study (Fraley et al., 2012). We speculate that the nature of

these cell tracks may potentially be indicative of the cells' altered ability to degrade the matrix, with the result being that cells may not be able to continually degrade the matrix. Instead, the cells may oscillate between a matrix-degrading phenotype and a motile phenotype, during which they probe the track they have created, leading to the observed periodic migration. Significantly more work would be required to sufficiently support this hypothesis, which is outside the current scope of this work. Alternatively, our results may be explained by the simple fact that, within the open pathway of a microtrack, cells will continue to migrate. Within our patterned channels, cells which encounter the barrier at the end of the channel typically reverse direction and subsequently migrate unidirectionally the other way, regardless of drug or siRNA treatment. Therefore, our results may actually be consistent with the previous results, depending on what the impetus is for the reversal of the leading edge in zyxin-depleted cells migrating within 3D collagen. Overall, our results suggest that the role of zyxin in mediating 3D migration behavior may be more complicated than previously believed, and may require a more in depth analysis of the matrix-degrading capabilities of zyxin-depleted cells before it can be firmly established and understood.

Additionally, previous work indicates that p130Cas knockdown cells exhibit impaired motility, with decreased cell speed, but increased persistence contributing to a unidirectional migratory phenotype in 3D (Fraley et al., 2012; Gu et al., 1999). Our data is not inconsistent with these results. Rather, our previous results demonstrate that the presence of an open microtrack induces a unidirectional migratory phenotype in cells which are otherwise unable to maintain any form of persistent migration in 3D (Kraning-Rush et al., 2013). In other words, the unidirectional phenotype is already the dominant phenotype in control cells migrating within the patterned collagen tracks.

Therefore, we would not expect that knocking down p130Cas in cells within the patterned tracks to generate an altered phenotype.

While the role of actin filaments and microtubules in mediating 2D and 3D behaviors has been fairly well-established (Danowski, 1989; Kraning-Rush et al., 2011; Stamenovic et al., 2002), studies have not yet addressed these structures in cells within a physiologically-relevant microtrack environment. However, actin and microtubule function has recently been studied within rigid PDMS channels (Balzer et al., 2012; Irimia and Toner, 2009; Mak et al., 2013). Here, we confirm the findings previously shown using actin inhibitors cytochalasin D (CD) and latrunculin A (LA). We find that a subset of cells treated with CD and LA are able to continue migration through rigid PDMS channels, while migration was completely abolished in cells under the same treatment in collagen channels of equal width. However, we find that the remaining motile population within the PDMS channels does exhibit decreased migration speed. Our PDMS experiments are consistent with a recently published computational model of dendritic cells under confinement, which demonstrates that a pressure buildup in the cell, modeled as a viscoelastic gel, caused by the confinement induced by the rigid channel walls, is sufficient to produce a forward flow of the gel (Hawkins et al., 2009). Their model also shows that migration under confinement relies on increasing friction caused by the pressure buildup, and is independent of adhesion to the channel or contractility within the cell (Hawkins et al., 2009). Our results, interpreted in the context of this model, suggest that the collagen microtrack, being an inherently compliant substrate, may not be able to induce the same pressure buildup within the cell. Therefore, the impetus which drove cell migration forward within the rigid channel environment is not present, and migration is immediately abrogated upon actin depolymerization. This difference highlights the need to

carefully consider the cellular microenvironment when designing new models and interpreting results accordingly. Interestingly, our results demonstrating that either stabilizing or depolymerizing microtubules impairs cell migration by interfering with polarization within collagen microtracks is consistent with similar experiments in rigid channels which (Balzer et al., 2012; Irimia and Toner, 2009). These results demonstrate that microtubules play an essential role in the migration of cells under confinement in a wide range of microenvironments.

These studies are the first to systematically analyze the mechanisms guiding MMP-independent cell migration within collagen microtracks. Here we use a novel *in vitro* method to pattern 3D collagen microtracks which mimic natural proteolytic microtracks. We demonstrate that Rho-mediated contractile force generation is dispensable for microtrack migration, which instead requires an intact actomyosin and microtubule cytoskeleton and focal adhesions. Collectively, our data suggests that these elements are critical to facilitating MMP-independent cancer cell migration within 3D patterned collagen microtracks.

CHAPTER 5

ADDITIONAL DATA

Portions of these data were published in *Scientific Reports* (Staunton, 2013).

Over the course of generating data for this dissertation, I have embarked on several notable side projects and collaborations which merit further discussion. In this chapter, I will provide the motivation, results, conclusions, and potential future steps for two of these studies.

5.1 MCF10A and MDAMB231 Characterization

Preface and Background

When I first began my graduate research five years ago, I chose to focus my work on breast cancer. One of the first decisions I had to make was which cell lines I wanted to begin working with. There was a vast array of cell lines available to choose from, each with unique properties and with various numbers of publications filled with previous research from which I could gather information. I ultimately chose two cell lines which had been published on frequently: the MCF10A mammary epithelial cell line, a spontaneously transformed line considered by different sources to be 'normal' or 'nonmalignant', and the highly invasive MDAMB231 highly metastatic breast adenocarcinoma cell line. Although these cells had been widely published on, there was no single source devoted to a comparison between the two cell lines. Therefore, the first goal of my work was to complete a comparison study of these two cell lines,

analyzing their migration, proliferation, spreading area, and force generation on substrates of physiological stiffness. This idea was picked up shortly thereafter by the National Cancer Institute's Physical Sciences-Oncology Centers network leadership, which began a full-fledged characterization utilizing the broad spectrum of techniques available throughout the network's labs. As part of that study, I quantified the traction forces of both cell lines on laminin-coated substrates (Staunton, 2013). Here, I present that data, and I put it in the context of the data gathered on collagen-coated substrates, presented previously in Chapter 2 (Fig. 2.3A).

Methods

Wound Healing Assay: Cells were seeded in a six-well plate at a density of 10,500 cells/cm^2 and grown to confluence. At confluence, a sterile 200 μL pipette tip was used to scratch 3 parallel lines into the monolayer. The media in each well were refreshed, and an initial time point was captured. Cells were imaged every 12 hours until wound was completely filled with cells. Open wound area was outlined and quantified in ImageJ.

2D PA Gel Migration: For single cell migration studies, cells were seeded on PA gels of varying Young's moduli (0.2 – 10 kPa) coated with 0.1 mg/mL type I collagen and glass at a density of 625 cells/cm^2. Cells were imaged every 20 minutes for 8 hours. Cell centroid position based on cell outlines was determined using ImageJ, and was used to calculate the mean-square displacement ($<d^2>$) (Stokes et al., 1991). The speed (S) and direction persistence time (P) were determined by fitting the $<d^2>$ and the time interval (t) to the persistent random walk equation (Eq. 3.1) using nonlinear least squares regression analysis as previously described (Kraning-Rush et al., 2013; Reinhart-King et al., 2008).

Cell Spreading Area: Cells were seeded at a density of 625 cells/cm^2 onto polyacrylamide (PA) hydrogels of 0.5-30 kPa coated with 0.1 mg/mL type I collagen, as well as on uncoated tissue culture plastic and were allowed to spread for 10-16 hours. Individual cells were then imaged using phase contrast microscopy. Cell spreading area was quantified by tracing the outline of each cell in ImageJ.

2D Proliferation: Cells were seeded on PA gels of varying Young's moduli (1 – 10 kPa) coated with 0.1 mg/mL type I collagen at a density of 5,210 cells/cm^2. At each time point, gels were washed with ice-cold PBS and fixed with 0.5% crystal violet in 20% methanol for 3 hours. Gels were rinsed, and crystal violet was eluted with 0.1 M sodium citrate (pH 4.2 in 50% ethanol) for 30 minutes. Absorbance was read on a BioTek μQuant Microplate Spectrophotometer at 595 nm.

3D Proliferation: Cells were seeded within 250 μL 1.5 mg/mL type I collagen gels and allowed to spread and proliferate for 0-5 days. Acellular gels were polymerized and used for a negative control. At each time point, gels were dissolved with papain for 14 hours at 60^{o}C. Samples were then analyzed using a Quant-iT PicoGreen dsDNA Reagent Kit (Invitrogen). Fluorescence was read on a BioTek μQuant Microplate Spectrophotometer at 485 nm.

Force Generation: PA gels of specific Young's moduli (5 kPa) were synthesized as previously described (Kraning-Rush et al., 2012b), and derivatized with 0.1, 10, and 50 μg/mL of laminin from Engelbreth-Holm-Swarm murine sarcoma basement membrane. Cells were seeded onto these gels at a density of 312 cells/cm^2, allowed to

spread overnight, and analyzed by traction force microscopy as previously described (Kraning-Rush et al., 2012b).

Results & Discussion

First, I analyzed the ability of the MCF10A and MDAMB231 cells to migrate on tissue culture plastic. Using a conventional wound healing assay, I found that the MDAMB231 cells were able to close the wound more quickly than MCF10A cells (Fig. 5.1A-B). I also noted that MCF10A cells appeared to migrate collectively, maintaining cell-cell connections, whereas MDAMB231 cells appeared to migrate into the wound space as single cells. Additionally, the MDAMB231 cells never formed a robust monolayer; rather, they began migrating over the top of one another. Next, I plated these cells on more 2D polyacrylamide (PA) substrates of physiologically relevant stiffness (Young's Moduli 0.2-10 kPa). The softest substrates (0.2 kPa), have been shown to be similar in stiffness to normal mammary tissue, while stiffer substrates (5-10 kPa) mimic the stiffness of tumorigenic breast tissue (Paszek et al., 2005). Interestingly, I found that MDAMB231 cells migrated most quickly on soft 2D substrates, while the speed of individual MCF10A cells tended to increase with substrate stiffness (Fig. 5.1C). Both cell lines appeared to move at similar speeds on stiff substrates (e.g. PA gels of 5-10 kPa and glass). I then analyzed the relationship between cell area and stiffness of the two cell lines, again using PA gels. I noted a biphasic relationship with stiffness, with maximal spreading area on 5 kPa substrates (Fig. 5.1D).

Next, I compared the proliferation rates of the MCF10A and MDAMB231 cells. First, I plated cells on soft (1 kPa) and stiff (10 kPa) substrates. No significant difference was observed between proliferation on soft (1 kPa) and stiff (10 kPa) substrates for

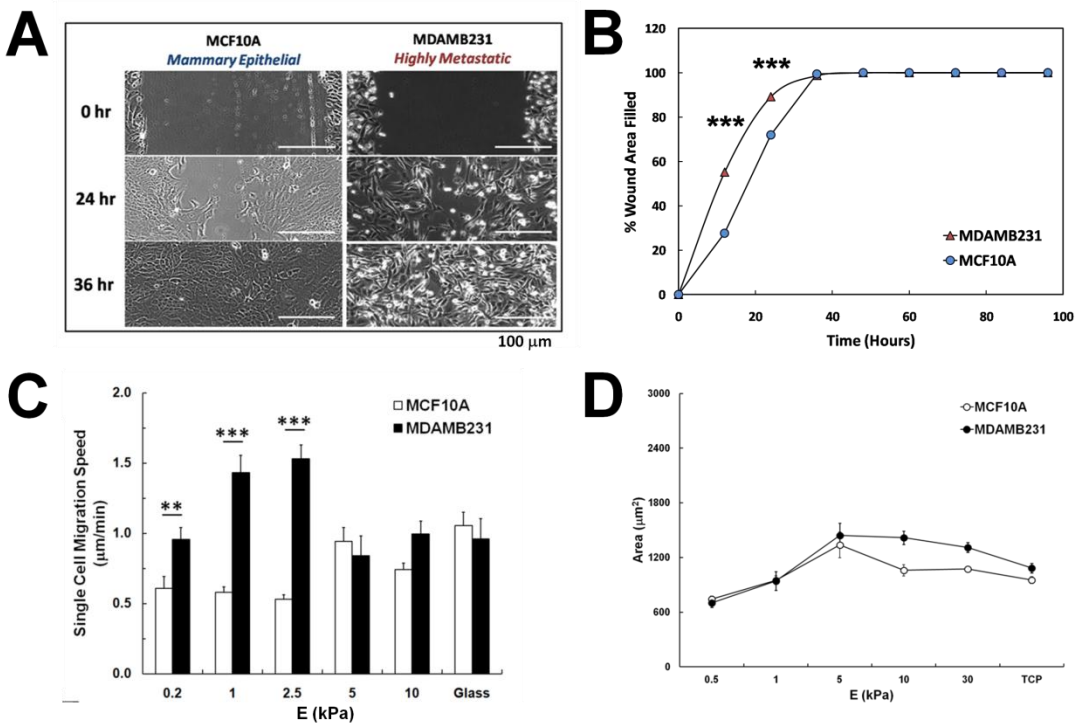

Figure 5.1. Highly metastatic MDAMB231 cells exhibit increased migration. A) Representative 10X phase images of the mammary epithelial (MCF10A) and highly metastatic (MDAMB231) cancer cells after wounding (0 hr) and throughout their migration into the scratch area (24 and 36 hrs) on tissue culture polystyrene. Scale bar = 100 μm. B) Scratch area normalized to scratch area immediately after wounding is plotted against time for mammary epithelial (MCF10A, blue circles) and highly metastatic cancer (MDAMB231, red triangles) cell lines. The highly metastatic cancer cells invade the wound site more quickly than the mammary epithelial cells, requiring only 24 hours to regain 95% confluency. C) Migration speed plotted against the Young's Modulus of the PA substrate (E = 0.2 – 10 kPa) for MCF10A and MDAMB231 cell lines. D) Cell area is plotted against the Young's Modulus of the substrate (E = 0.5 – 30 kPa). Both the MCF10A and MDAMB231 cancer cell lines exhibit a biphasic relationship between cell spread area and substrate stiffness, with a peak area at 5 kPa. Mean ± SEM; *** indicates $p < 0.001$, ** indicates $p < 0.01$.

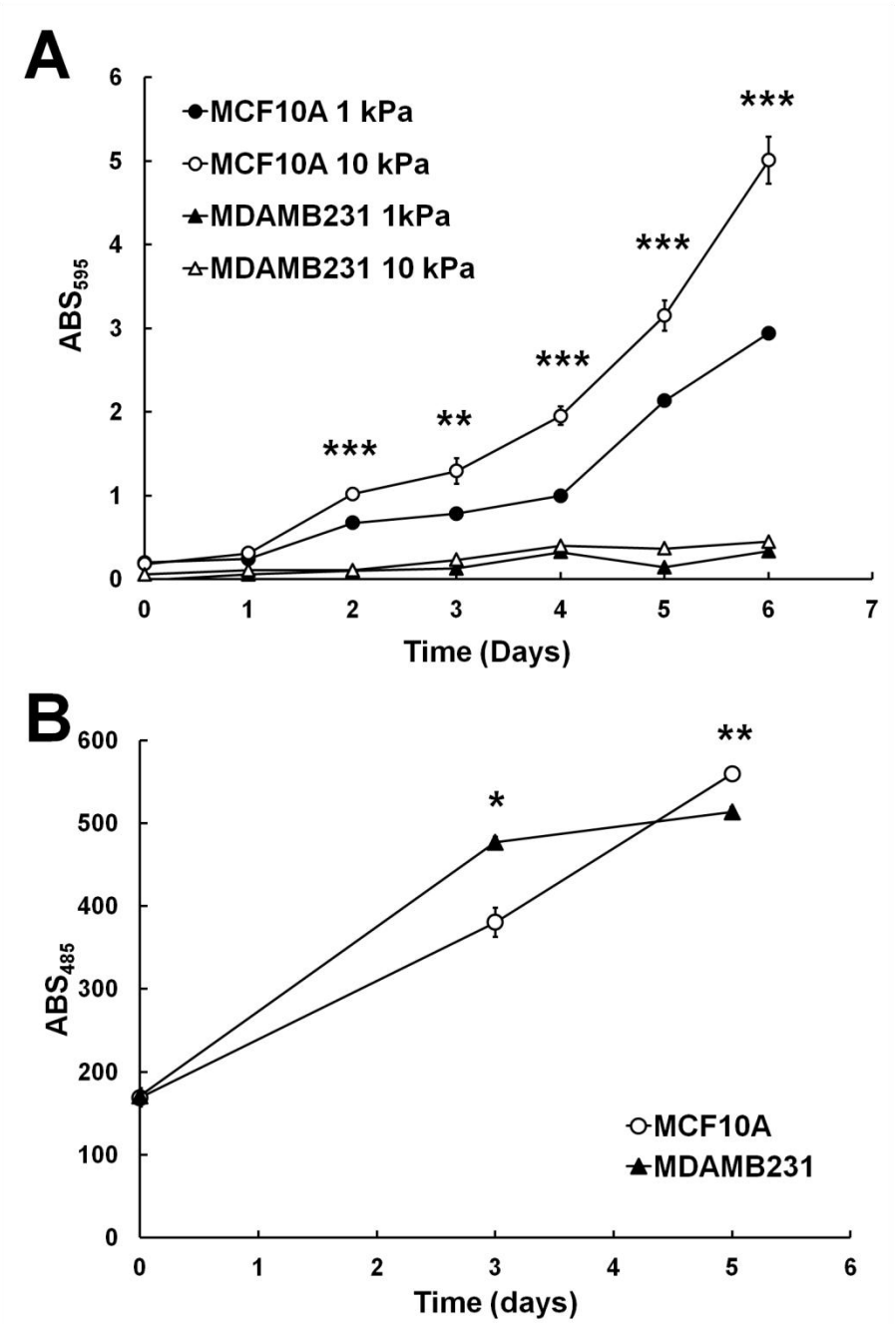

Figure 5.2. MCF10A and MDAMB231 exhibit differential proliferation on 2D and 3D substrates. A) Proliferation curves of MCF10A and MDAMB231 cells on 1 kPa and 10 kPa gels over 6 day period, quantified with a crystal violet colorimetric assay. Statistics shown comparing stiffness within cell type. B) Proliferation curves of MCF10A and MDAMB231 cells cultured in 3D collagen matrices over a 5 day period, quantified with a PicoGreen fluorimetric assay. Mean ± SEM. *** indicates $p < 0.001$, ** indicates $p < 0.01$, * indicates $p < 0.05$.

either the MCF10A or MDAMB231 cell lines (Fig. 5.2A), suggesting that in these cell types, proliferation may not be regulated by the mechanical microenvironment. Interestingly, I observed that the MCF10A non-tumorigenic cell line exhibited greater proliferation than the highly metastatic cells, a result that was later confirmed during the PS-OC's characterization study (Staunton, 2013). However, when cells are seeded in 3D collagen matrices, the differences in their proliferation behavior become less dramatic. After normalizing to the number of cells seeded at day 0, I observed that MDAMB231 cells had higher proliferation at day 3, but by day 5, MCF10A cells had proliferated slightly, but significantly, more (Fig. 5.2B).

For the PS-OC's characterization studies, I chose to characterize traction forces generated by these two cell lines on laminin-coated substrates. I had previously collected on the forces exerted by these cells on collagen-coated substrates, and set out to determine what, if any differences would be seen on laminin-coated substrates. The stiffness of all the substrates in this study was held constant at a Young's modulus of 5 kPa. My initial observations were consistent with the trend I observed on collagen-coated substrates. I found that on substrates with the highest laminin concentration used (50 μg/mL), the MDAMB231 cells exerted higher traction stresses than the MCF10A cells, and that these stresses appeared localized to the cell periphery (Fig. 5.3A). When I then looked at the net traction forces across a range of laminin concentrations (0.1 – 50 μg/mL), I found that MDAMB231 cells exerted significantly stronger forces across the entire range (Fig. 5.3B). Note that 50 μg/mL of laminin was used here in place of 100 μg/mL (maximum collagen concentration used in previous study), because at high concentrations the laminin began to noticeably aggregate and interfere with the traction measurements. Finally, I compared the net traction forces of cells on laminin with the net traction forces previously observed on collagen coated

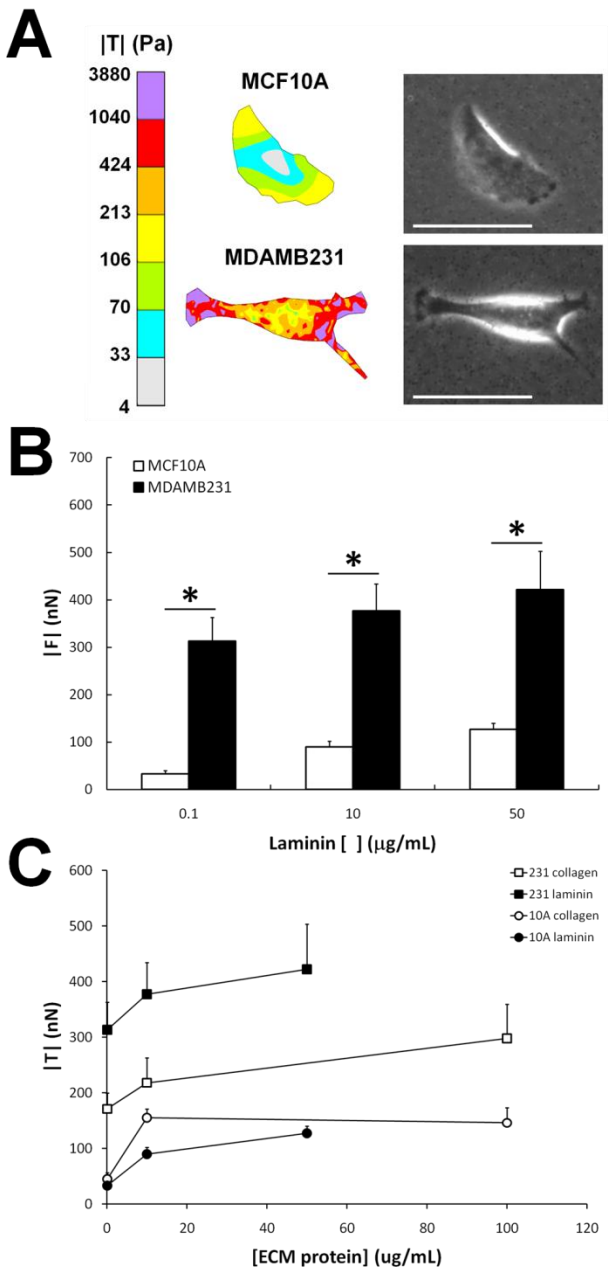

Figure 5.3. MDAMB231 cells generate high forces on laminin-coated substrates. A) Representative traction maps (left) and corresponding phase images (right) of MCF10A and MDAMB231 cells seeded on 5 kPa gels derivatized with 50 µg/mL laminin. Scale bar = 50 µm. B) MDAMB231 cells exert higher traction forces than MCF10A cells across a range of 0.1 – 50 µg/mL laminin. Mean + SEM, * indicates $p < 0.0001$. C) Forces exerted by MDAMB231 cells are increased on laminin-coated substrates, while forces exerted by MCF10A cells are decreased on laminin-coated substrates as compared to collagen-coated substrates. Note that collagen data is from Chapter 2 (Fig. 2.3A) and published in (Kraning-Rush et al., 2012a). The laminin data was separately published in (Staunton, 2013).

PA gels (data from Chapter 2) (Kraning-Rush et al., 2012b). Interestingly, I found that the laminin-coated surface led to increased forces in the MDAMB231 cells, compared to the collagen-coated surface, but had the opposite effect on the MCF10A cells (Fig. 5.3C). The MCF10A cells were found to exert weaker forces on laminin-coated substrates than on collagen-coated substrates. This result leads to interesting speculation regarding the different effects the ECM can have on cellular behavior. The differential effects of laminin are particularly interesting, given that laminin is a primary component of the basement membrane, a structure which surrounds tumors. The basement membrane represents one of the first barriers to metastatic invasion, as cells must degrade the membrane to break through it. Based on our results, I speculate that the presence of laminin may contribute to an upregulation of cellular force generation in tumor cells to facilitate their subsequent invasion through the basement membrane.

Future Work

Between the work presented here and the wider dissemination of knowledge through the publication of the results of the PS-OC's Cell Line Exercise (Staunton, 2013), the comparison between these two cell lines can be considered fairly complete. However, one key issue that arose during the undertaking of these projects is the fact that these cell lines, while excellent models for their respective cell types, have some notable limitations. The most important limitation is that the MDAMB231 and MCF10A cells are genetically distinct – they bear no relationship to one another, in terms of their original derivation. Additionally, while the MCF10A cells are often called 'normal' cells, this is a misnomer. These cells are transformed and will thus replicate indefinitely. As such, they inherently cannot behave in the same manner that a primary mammary epithelial cell would. Furthermore, like many cell lines, they have been

shown to suffer from genetic drift (Burdall et al., 2003), meaning that cells at high passage number are questionable, and highly dependent on the quality of care with which they are maintained. Future work should focus either on characterizing many more cell lines to yield a broader picture of the cancerous and normal phenotypes, or else on characterizing isogenic cell lines in more depths, such as the MCF10AT series of cells (Santner et al., 2001), which are derived from the MCF10A cells used here. Ultimately, primary cells would yield the most relevant experimental data.

5.2 Effects of Hypoxia on Force Generation in MDAMB231 Cells

Preface

This project was initiated in April 2010 at the first annual Physical Sciences – Oncology Centers (PS-OCs) Network Investigators' Meeting in National Harbor, MD. At the meeting, there was a call for submissions for a Young Investigator Trans-Network Project award. The goal of these awards was to foster collaboration between young scientists (graduate students and postdoctoral fellows) from different PS-OCs in an effort to encourage young scientists to embrace the sharing of knowledge and techniques across the network. The process was designed such that the young investigators initiated and solidified their collaborations on the first day of the conference, then wrote a two page proposal containing an identification and statement of the problem, a brief research plan with specific aims, project milestones, a description of team expertise, and an estimated budget breakdown for the $10,000 award. The proposal deadline was the afternoon of the second day of the conference, followed up with a two minute presentation to the PS-OC steering committee that evening.

The subsequent data is the result of a collaboration formed in just this manner between myself and Dr. Daniele Gilkes, from the Johns Hopkins PS-OC, a postdoctoral fellow working jointly in Dr. Gregg Semenza and Dr. Denis Wirtz's labs, studying the effects of the extracellular matrix and hypoxic conditions on tumor cell migration. This collaboration lasted for roughly a year and a half, in which time I generated interesting, but somewhat conflicting data that was not pursued further. For the purposes of this dissertation, only the results collected in the Reinhart-King lab are presented.

Background

The tumor microenvironment is a complex, heterogeneous mix of chemistry and mechanics that work together to drive cancer cell proliferation, migration, and invasion (Anderson et al., 2006; Cairns et al., 2003). Many factors influence the different stages of cancer progression, including chemical and mechanical cues, cell-cell interactions, and cell-matrix interactions. However, the effect of these independent factors on tumors does not exist in a vacuum. While these factors have been studied independently, few have been analyzed concurrently within the same system to elucidate potential synergistic effects. In this study, the synergistic effects of substrate stiffness and hypoxic growth conditions on cell force generation, cell morphology, and hypoxia-mediated protein expression levels will be assessed.

Hypoxia has been clinically linked to metastasis and poor patient prognosis, although the underlying mechanism remains unclear (Erler et al., 2006; Zhong et al., 1999). Moreover, hypoxia has been shown to exert a powerful selective pressure on cell populations *in vitro*, creating more aggressive cancer cells (Graham et al., 1999). Pioneering work by the Semenza lab has shown that the ability of cells to survive and

adapt to hypoxic conditions is dependent on hypoxia-inducible factor 1 (HIF1), which regulates many key angiogenesis, invasion, and migration genes (Krishnamachary et al., 2003; Tang et al., 2004; Wang and Semenza, 1993) and has also been shown to play a role in vascular remodeling (Rey and Semenza, 2010). Previous studies in the literature have found that exposure to hypoxic conditions can increase the invasiveness, migration, and matrix metalloproteinases (MMP) activity in MDAMB231 breast cancer cells *in vitro* (Indelicato et al., 2010). Additionally, hypoxia has also been shown to act in an epigenetic fashion, altering the expression of genes involved in stress responses and angiogenesis, with an indirect causal link to metastasis (Koong et al., 2000; Lal et al., 2001; Semenza, 2002; Semenza, 2010; Subarsky and Hill, 2003).

While much work has been done on understanding the regulators and effectors of HIF1, the effect of the tumor microenvironment on HIF1 expression and regulation has been minimal. Previous work has used poly(acrylamide) (PA) gels with tunable mechanical properties to look at the traction forces generated by cancer cells on substrates that mimic physiological stiffness (Paszek et al., 2005). Compliant substrates (1 kPa) are used to mimic normal breast tissue, while stiff substrates (10 kPa) are used to mimic the stiffness of a tumor. In the Reinhart-King lab, I have shown a marked increase in the magnitude of traction forces generated by highly metastatic breast cancer cells plated on stiffer substrates under normoxic conditions (Kraning-Rush et al., 2012a). As tumor cells naturally exist in a stiff stromal substrate, it is likely that the mechanics of the microenvironment that affect force generation could also play an important role in mediating the hypoxic response in tumor cells. Alternatively, because hypoxia is associated with more aggressive tumors, and I have shown that more aggressive tumor cells generate increased contractility, it seems

likely that hypoxic conditions can drive force generation in cancer cells.

Therefore, the objective of this project is to characterize the effects of substrate stiffness and hypoxia on tumor cell force generation, cell morphology, cell migration, and hypoxia-mediate protein expression. I hypothesize that culture under hypoxic growth conditions and stiff, tumor-like substrate will cause a synergistic increase in force generation in MDAMB231 metastatic breast cancer cells that hypoxia or stiffness alone could not create. My goal is to assess the effects of hypoxia and substrate stiffness on cancer cell behavior to elucidate cross-talk between hypoxic regulation and contractility, and more broadly, to generate a more accurate model for studying cancer progression.

Methods

MDAMB231 metastatic breast carcinoma cells were seeded onto 5 kPa polyacrylamide hydrogels conjugated with 0.1 mg/mL type I collagen, synthesized as previously described (Kraning-Rush et al., 2012b). Cells were allowed to spread for ~10 hours under normoxic conditions before exposure to experimental conditions. Control cells were kept under normoxic conditions, while other cells were transferred into an oxygen controlled incubation chamber held constant at 1% O_2, 5% CO_2, and balance N_2 at 37^{o}C. These cells were then exposed to either hypoxia or hypoxia followed by normoxia (reoxygenation). Traction forces of single cells were obtained as previously described. It should be noted that cells under hypoxic conditions were either exposed to normoxia for the duration of TFM data collection (as for Fig. 5.4A), or transferred into a stage-top incubator and kept under 1% O_2 during data collection (as for Fig. 5.4B-D).

Results and Discussion

Initial results using a large oxygen controlled chamber kept in an incubator suggested that hypoxic conditions may decrease force generation, and that reoxygenation may increase force generation compared to cells cultured under normoxic conditions (Fig. 5.4A). However, because the wide variability in these data resulted in no statistical significance, I next explored the range of heterogenous responses to hypoxia within the MDAMB231 cell population using a stage top O_2-controlled incubation system. I next quantified the forces generated by individual cells over time under different oxygenation conditions. For my control cells, I incubated MDAMB231 cells on gels for 24 hours, prior to 5 hours of TFM analysis. When I normalize the force to the initial time point, I find some fluctionation in force, but the majority of the cells do not exhibit a significant increase in force (Fig. 5.4B). In contrast, when I expose cells to 7 hours of hypoxia (Fig 5.4C, blue region), I find an initial decrease in force generation followed by a peak force generation significantly higher than the control (normoxic, green region) time point. Furthermore, under reoxygenation conditions (red region), I see a general increase in force. However, it is important to note the wide variety in force patterns of the cells, and the lack of synchronicity of a hypoxic response. These differences most likely contribute to the overall decrease in force initially observed under hypoxia (Fig. 5.4A). In a final experiment, I cultured cells either under hypoxia for 6, 12, 24, 36, and 48 hours, or under 24 hours of hypoxia followed by 6, 12, or 24 hours of normoxia (reoxygenation). The results of this experiment showed that cell forces increased under hypoxia for the first 24 hours, then appeared to decrease at 36 and 48 hours (Fig. 5.4D). Interestingly, the cells under reoxygenation conditions had significantly lower forces, suggesting that perhaps the increase in forces due to reoxygenation observed in Fig. 5.4C may be quite transient (< 2 hours). Overall, these data suggest that a subset of the cancer cell population *may* be activated under hypoxic

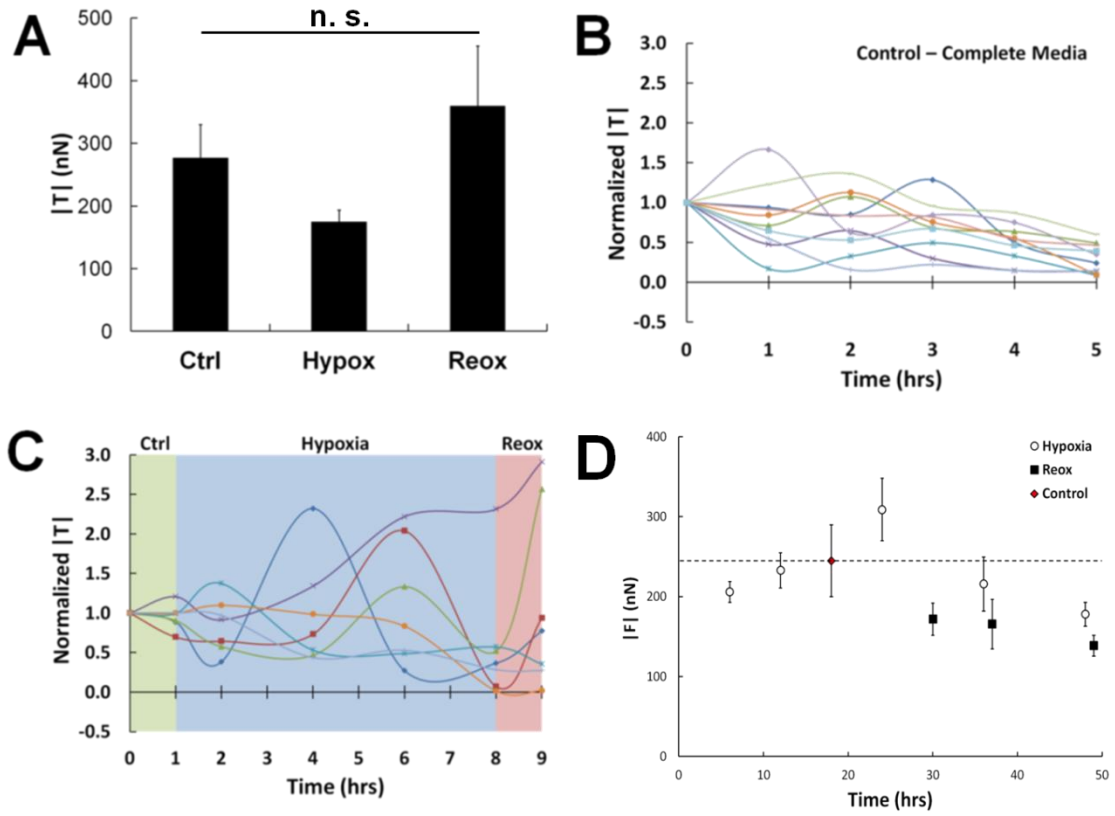

Figure 5.4. Traction forces generated under hypoxia, normoxia and reoxygenation. A) Preliminary experiments indicated that traction forces are decreased under hypoxia and increased under reoxygenation, although not significantly. B) Traction forces of individual cells cultured under normoxia indicate that cellular forces can fluctuate by as much as 50% over a period of 5 hours. Each line represents one cell. C) Traction forces of individual cells cultured first under normoxia (green), then under hypoxia for 7 hours (blue), before finally being exposed to normoxia again (red, reoxygenation), indicate that forces may first increase under hypoxia, then decrease over time before increasing again under normoxic conditions. D) Average traction forces of cells cultured under hypoxia (open circles), or under hypoxia for 24 hours followed by reoxygenation (closed squares), compared to normoxic controls (red, dotted line) suggest a transient increase in force under hypoxia, but a decrease in force under 6 hours or more of reoxygenation. Mean + SEM.

conditions to exert stronger forces, but not in a prolonged fashion. This transient increase in forces could still potentially contribute to the increase in invasion noted in the literature. Alternatively, the increased invasion could be due to any number of factors unrelated to contractility, such as increased proteolytic degradation or altered metabolism.

Future Work

This is the first study, to my knowledge, of the direct effects of oxygenation conditions on cancer cell traction forces. Because the results obtained throughout this study did not point to a strong trend of changing forces under hypoxia, it was ultimately given lower priority and I did not continue work on it after the grant funding ended. However, a great deal of future work could be done on this project to better elucidate what is happening at the molecular level with these cells under hypoxic conditions. Additionally, altering the stiffness of the polyacrylamide gels could induce a more decisive difference in cellular forces. For example, cells cultured on softer substrates could be more sensitive to reoxygenation conditions, or cells on stiffer substrates could have a synergistic increase under hypoxia and exert forces even higher than the elevated forces I have previously described on stiff substrates. Future work could also include examining the force generation of HIF-1α and HIF-2α knockdown cells under normoxia and hypoxia.

CHAPTER 6

CONCLUSIONS AND FUTURE DIRECTIONS

6.1 Conclusions

Our knowledge of the principles guiding cancer initiation and progression is continuing to expand rapidly, and each new study brings us closer to a thorough understanding of the disease, but also inevitably highlights the remaining questions that must be answered. This thesis contributes to the body of research on cancer metastasis by first identifying a potential biophysical indicator of metastatic cells, increased contractile force generation, and by then demonstrating when and how this behavior contributes to invasion. Moreover, these studies highlight the inherent adaptability and plasticity of cancer cells by showing that cellular contractility can be dispensable under certain circumstances. Using micropatterned collagen channels which mimic the natural invasion paths cells create *in vivo*, this work demonstrates that once cells have remodeled their microenvironment to sufficiently permit invasion, cancer cell migration can become reliant upon a different set of unique biophysical properties. While this work suggests some potential targets for therapy, it ultimately exemplifies the need for a more complete spatial and temporal understanding of cancer progression.

In Chapter 2, I hypothesized that increased contractile force generation could be a distinguishing characteristic of metastatic cancer cells. This hypothesis resulted from the observation that many of the behaviors which tumor cells must engage in within the body to invade appear to be dependent upon the cells' ability to generate force. Examples of these behaviors include remodeling the basement membrane to facilitate

the initial escape from the primary tumor, reorganizing the surrounding extracellular matrix fibers in the stroma, and transmigrating through the endothelial cell barrier to reach the bloodstream. Therefore, I sought to determine whether cellular force was increased in cancer cells with the ability to metastasize *in vivo*. Using polyacrylamide gels which mimic the stiffness of the breast tumor microenvironment (Young's Modulus (E) = 5 kPa) and 2D traction force microscopy, I found that human-derived metastatic cells of multiple lineages (breast, lung, and prostate) generated significantly increased traction stresses compared to their non-metastatic counterparts. Moreover, I found that both increased stiffness and increased extracellular matrix protein density induced metastatic and non-metastatic cells to exert stronger contractile forces, with the metastatic cells maintaining higher traction stresses than the non-metastatic cells under each condition tested.

While these measurements were collected on 2D substrates, previous research in our lab has demonstrated that 2D traction forces correlate well with contractility observed within 3D collagen matrices (Kraning-Rush et al., 2011). Additionally, several of the cancer cell behaviors in which we first noted force generation playing a role occur on a 2D-like surface. In particular, both the basement membrane and the endothelial cell barrier are surfaces within the body in which tumor cells will migrate and exert force in 2D. The basement membrane is a thin but mechanically strong structure (Hotary et al., 2006; Kalluri, 2003), and the tumor vasculature has been demonstrated to stiffen significantly during tumor progression (Lopez et al., 2011). Both of these environments, when interpreted in the context of my results, could directly cause increased traction forces to be generated in nearby tumor cells and could potentially enhance invasion. Interestingly, increased matrix stiffness has also been shown to induce an increase in invadopodia and matrix degradation (Parekh et al., 2011),

suggesting that matrix stiffness can directly mediate tumor metastasis both through increasing contractile forces and increasing proteolytic activity, perhaps even synergistically. Conversely, inhibiting collagen crosslinking – which leads to a decrease in both overall collagen content and in mechanical stiffness – has also been shown to reduce cell proliferation and lengthen the period of time over which a tumor remains dormant and non-invasive (Levental et al., 2009). Together, my results couple with these studies to demonstrate the importance of matrix stiffness in governing initial invasion, and suggest that increased force can contribute to this early invasive behavior.

Next, I chose to examine the role of force generation in mediating migration in a more physiologically relevant 3D system during later stages of invasion. First, I developed and perfected a micromolding technique which could be used to effectively separate and define the independent roles of contractile force and proteolytic degradation. Cancer cells migrating within a traditional 3D collagen matrix have been previously shown to require *both* behaviors to successfully degrade, remodel, and migrate through ECM fibers (Sabeh et al., 2009; Wyckoff et al., 2006). Therefore, determining the relative contribution of force generation and proteolysis, as well as the explicit functional role of each in 3D migration is quite difficult using these 3D matrices. To this end, in Chapter 3 I present a technique to pattern fully 3D channels which mimic the natural microtracks that are formed by cancer cells *in vivo* through a complex process of degrading, reorganizing and ultimately aligning the extracellular matrix surrounding a tumor. Patterned in collagen, our channels are compliant, retaining stiffness similar to physiological stromal tissue, while also maintaining the fibrous nature of the native ECM. These are critical elements of the tumor microenvironment which contribute to metastatic invasion, and which have not been captured in

previously developed PDMS and polyacrylamide models. I confirm that my *in vitro* microtracks mimic naturally formed tracks in both size and structure, and also confirm that cancer cells seeded within the microtracks are morphologically similar to cells in 3D.

Using this novel technique, I observe that patterned microtracks permit the rapid and exceptionally persistent migration of non-metastatic epithelial cells otherwise unable to invade a 3D collagen matrix. Additionally, I find that the migration speed of highly metastatic cells is also significantly higher within the microtracks, compared to migration in more restrictive 3D matrices. I validated the use of this technique for removing the element of proteolytic degradation from 3D migration studies by confirming that cell migration speed is unaffected by several commercial protease inhibitors or siRNA targeting MT1-MMP, repeatedly shown to be the dominant MMP driving proteolytic degradation and subsequent invasion into collagen matrices (Hotary et al., 2003; Sabeh et al., 2009). In this manner, I developed a technique for studying MMP-independent 3D migration. Therefore, I then returned to my initial focus on force generation, and examined the specific contribution of contractile forces to this method of 3D invasion.

In Chapter 4, I more closely examined the mechanisms governing migration of breast cancer cells within our patterned 3D collagen microtracks by analyzing the roles of Rho/ROCK contractility, focal adhesions, and the cytoskeleton. Surprisingly, I discovered that Rho/ROCK-mediated contractility is dispensable for this mode of migration, as 90% inhibition of traction forces results in no observable decrease in cell speed within the track environment. I also find that cancer cells can adapt their motility phenotype to compensate for β1-integrin blocking with no loss of speed.

Interestingly, I determine that persistent, directional migration within the microtracks is dependent on focal adhesion formation, specifically requiring the presence of the classical focal adhesion protein vinculin. Moreover, the presence of an intact and dynamic cytoskeleton is critical to microtrack migration, as interference with actin or microtubule polymerization abolishes cell migration. These studies suggest that taxane drugs routinely used in chemotherapy to target microtubules to prevent tumor cell division and proliferation could also simultaneously combat metastatic invasion in this manner. However, it is important to keep in mind that cancer cells will often develop a subpopulation which is resistant to taxane treatment. It is likely that the anti-migratory benefits of taxanes would be abolished in the taxane-resistant population.

The findings presented in this dissertation not only aid in our understanding of the role of force generation in cancer progression, but also illuminate the ways in which cancer cells are able to adapt and react to their ever-changing microenvironment. The knowledge gained through these experiments can be used to further develop appropriate therapies to successfully target and inhibit cancer invasion. Importantly, this work highlights the necessity of studying cancer cell migration in the most physiologically-relevant model available. Additionally, in the future it will be critical to develop a more thorough temporal understanding of cancer progression, and to carefully evaluate the distinct mechanisms governing tumor behavior at each stage of progression.

6.2 Future Directions

Although the work described in this dissertation contributed significantly to our knowledge of cellular forces during metastatic cancer progression, additional work is required to fully understand the principles guiding tumor invasion, particularly

regarding the adaptability and plasticity of tumor cells in response to their microenvironment. More specifically, a great deal remains to be discovered regarding metastatic invasion along proteolytic microtracks *in vivo*. There are several avenues of approach which could prove useful in progressing the field even further.

Quantifying Traction Forces of Primary Cancer Cells

While in Chapter 2 I demonstrate a trend of increasing 2D contractile force with increasing metastatic potential within several cell lines, this phenomenon should be confirmed using patient-derived cells. While cell lines are easy to work with and are generally considered to be an accurate representative of cancer cells (Masters, 2000), they have been shown to exhibit genetic and phenotypic drift, and may vary considerably from primary cells in terms of metabolic activity, growth rate, and receptor content (Burdall et al., 2003). Therefore, my studies of traction forces should be validated with primary cells, particularly through multiple comparisons of the forces generated by primary and secondary tumor cells derived from the same patient. However, there are numerous obstacles to successfully using primary tumor cells. While tumor samples themselves are not difficult to acquire, isolating individual cancer cells from the non-cancerous epithelial and stromal cells which surround them presents a significant challenge. Techniques have been developed (with differing degrees of success) which attempt to isolate cancer cells using differential centrifugation (Ponti et al., 2005) or seeding single cells into 96 well plates and subsequently growing up individual clonal populations (Marsden et al., 2009). Because traction force microscopy is a technique inherently designed to measure the forces of individual cells, it is critical that the single cells all be of tumor origin, with as little contamination as possible. Ideally, the lineage of each individual cell would be

confirmed either prior to or after the TFM measurement is acquired, perhaps utilizing a specific live cell stain.

Additionally, it would be of interest to analyze the force profiles of cells during different phases of cancer progression. My studies indicate that traction forces may be important for specific behaviors, while largely dispensable for others. Therefore, it would be interesting to observe whether the strength of these forces would vary or correlate directly with certain phases. For example, one could compare the forces generated by cells within the primary tumor, cells which have begun to breach the basement membrane and invade into the ECM, circulating tumor cells (CTCs) in the bloodstream, and cells which have established metastases and micrometastases in secondary locations. This knowledge would greatly contribute to determining how the requirement for contractile force changes during metastasis, and would aid in confirming or refuting my hypothesis that contractile force is required for specific behaviors throughout progression, primarily in the earlier stages leading to invasion and during extravasation and intravasation.

It could also be informative to compare the force profiles of cells which have metastasized to different organs, to determine whether different stromal microenvironments require different degrees of contractile force. However, there is obviously inherent difficulty in this type of study. Once a tumor is known to have metastasized, the course of treatment for the patient is typically drastically changed. While it is common to surgically excise a primary tumor, metastases are rarely operated on – rather, they are treated with chemotherapy or radiation. Additionally, even if cells from a metastatic site could be acquired, it is likely that the patient would have undergone adjuvant therapy, which can considerably alter a tumor cell's

characteristics. Instead, for this type of study, the best compromise would be to use tumors collected from mice. While the relevance of mouse-derived tumors to human cancer is still being debated (Dennis, 2006), this is the best way for a systematic study on a larger scale to be conducted. In this study, a mouse would be sacrificed and cells from each metastatic site, as well as the primary tumor, would be collected and analyzed for force generation and other biophysical properties.

Future Studies Using Collagen Microtracks

The technique and results described herein regarding patterned collagen microtracks have opened the door for a wealth of new studies and applications. The use of patterned collagen wells for studying branching morphogenesis in epithelial cells has already been extensively described (Gjorevski and Nelson, 2010; Gjorevski and Nelson, 2012; Nelson et al., 2008), but the use of this technique for studying single cell migration seems to be limited to the results presented here. Future work should further elucidate the effects of channel dimension on cancer cell migration. The resolution of micromolding features into collagen hydrogels is < 1 μm (Nelson et al., 2008; Tang et al., 2003). This size is smaller than the standard cell nucleus (Friedl et al., 2011), and studies in rigid channels have shown this to be too narrow to permit migration through the channel via nuclear deformation and squeezing (Mak et al., 2013). Therefore, the full range of dimensions applicable to cell behavior is available for testing. Moreover, different features or pathways could be patterned into the microtrack, to explore cellular decision making during invasion into physiologically relevant matrices (Mak et al., 2011; Mak et al., 2013). For example, intersecting pathways of different angles or curvatures could be utilized.

While my data indicate that contractile force generation is dispensable for migration through our collagen microtracks, future work could examine this finding more closely by integrating fluorescent bead markers into the collagen matrix to track deformations of the microtrack walls during migration. In this manner, it may be possible to calculate approximations of traction stresses being applied to the wall. It is important to keep in mind, however, that collagen matrices have complex, non-linear mechanical properties which could complicate this quantification.

Future work should also investigate the role of ECM protein deposition within the collagen microtracks. It is well-known that both normal and malignant cells can deposit various ECM proteins, including collagen, fibronectin, and laminin (Levental et al., 2009; Streuli et al., 1995; Williams et al., 2008). For example, MCF10A mammary epithelial cells seeded onto substrates coated with fibronectin begin synthesizing and depositing additional fibronectin (Williams et al., 2008). It is possible that cancer cells within the patterned microtracks may similarly be depositing matrix proteins which could affect subsequent cell migration through the track. Additionally, the microtracks could be coated with exogeneous ECM proteins prior to cell seeding to determine whether individual ECM proteins could aid in driving cell migration. Likewise, the collagen channels could potentially be filled with a second hydrogel solution containing cells to analyze the effects of an interface. This latter possibility could prove a useful *in vitro* model for studying glioma migration, which has been shown to follow white matter tracts in the brain (Beadle et al., 2008; Gritsenko et al., 2012).

In Vivo Studies of Collagen Microtracks

The greatest impact of the current work lies in the validity of my model as an accurate mimic of the native microtracks generated by tumor cells during metastatic invasion. However, to achieve maximum impact, future studies should strive towards studying microtrack invasion *in vivo*. I anticipate that this type of study could be approached in two different ways. Both approaches would require using mice which either spontaneously develop tumors or in which tumor spheroids could be implanted into the mammary fat pad. For the first approach, microtracks could be synthetically created in the stroma near the tumor using the laser ablation technique described by Ilina et al. (Ilina et al., 2011). For the second approach, one could image the tumor stroma using intravital microscopy to find natural microtracks created by the invasive cancer cells as they migrate away from the primary tumor (Beerling et al., 2011; Condeelis and Segall, 2003). Both approaches have benefits and limitations. While creating synthetic microtracks alleviates the difficulty of finding the natural microtracks, it may not accurately recapitulate them. During native microtrack formation, tumor cells must proteolytically cleave ECM fibers, exposing epitopes to which cancer cells can subsequently bind and interact. It is unclear what effect these epitopes may have on cancer cell migration, demonstrating the need to study microtrack formation in more detail. After a protocol for studying microtrack *in vivo* is developed, future work could then involve microinjecting various inhibitors into the channels to confirm that the same mechanisms that I observe *in vitro* are also at work *in vivo*.

Ultimately, future directions of this work will provide additional insights into how cancer cells utilize contractile forces to facilitate invasion, as well as potential therapies for preventing or inhibiting metastatic migration through proteolytic microtracks.

APPENDIX A

PROTOCOL FOR TRACTION FORCE MICROSCOPY AND ANALYSIS

Portions of this chapter were published in a book chapter titled "Quantifying Traction Stresses in Adherent Cells" in *Methods in Cell Biology* (Kraning-Rush et al., 2012b).

Materials:

Traction chambers

35 mm petri dish (for lids)

Polyacrylamide gels containing fluorescent beads

Kimwipes

Razor blade

Vacuum grease

T25 flask of confluent cells

Trypsin

Complete media

1X PBS

Data Collection:

1. Chamber Setup and Cell Seeding

   The following steps should be performed within a sterile biosafety cabinet.

   a. UV sterilize one traction chamber and one 35 mm petri dish for each PA gel, as well as several KimWipes (Kimberly-Clark, Neenah, WI), paper towels, and a syringe filled with vacuum grease (Dow Corning, Midland, MI) for 20 minutes.

b. Remove the coverslip containing the PA gel from PBS using a razor blade and place on paper towel. Using a KimWipe, gently dry off the excess PBS surrounding the gel surface. Be careful not to touch the gel surface with the KimWipe.
c. Invert the traction insert so that the ridged side is facing down. Apply a thin line of vacuum grease around the circular opening.
d. Invert the coverslip with the PA gel over the traction insert such that the PA gel is centered over the opening.
e. Gently press down on the coverslip until the vacuum grease has formed a tight seal around the entire opening. If the chamber leaks, it is likely that the coverslip was not properly sealed to the traction insert, and more vacuum grease is required.
f. Flip over the traction insert and add 2 mL sterile PBS to the gel to keep it hydrated during cell seeding. Repeat these steps until all PA gels are attached to their respective traction inserts. At this point, gels can be stored overnight prior to cell seeding if desired.
g. Passage the desired cell population and determine the cell count. Seed 2,000-4,000 cells onto each PA gel, depending on the size of the cells and the duration of incubation prior to imaging. Typical incubation times in our lab range from 6 to 18 hours, although this time can be extended if desired. However, note that if the cells begin to proliferate, finding isolated cells to analyze becomes more difficult.

2. Acquiring Traction Images
   a. Place traction insert containing cell-seed PA gel onto the stage of the microscope.

b. Using a 10X objective, identify isolated cells and mark their positions.
c. Using a 20X objective, acquire a phase contrast image of the cell, focusing primarily on the cell boundaries. Immediately acquire a fluorescent image of the uppermost layer of beads directly beneath the cell. It is important that these two images are taken as close in time as possible, as cells can change position (and thus change the underlying bead placement) fairly rapidly, and both images need to be consistent for quantification. Repeat for each cell. Note that for compliant gels (<2.5 kPa), it may be appropriate to use a 10X objective to acquire these images, to obtain a significant population of fluorescent beads with negligible movement.
d. Aspirate media from the well, being careful not to touch the PA gel surface with the pipette, as this will cause distortion of the bead layer and become unusable.
e. Rinse well three times with 3 mL PBS.
f. Apply 1 mL of trypsin. Let sit for 5-10 minutes depending on cell type.
g. Aspirate trypsin and wash with PBS. Check all fields of view to confirm that the cells of interest have been removed. If not, repeat PBS rinse. Once cells are removed, keep the gel hydrated with PBS.
h. Return to the location of the first cell. Open the corresponding stressed image. Align the beads in the x and y directions such that they line up at a distance far from the cell. It is generally easier to do this in a corner. Some error is acceptable in this adjustment, as the tracking software described above will ignore the most common bead displacement (Marganski et al., 2003).
i. Adjust the z direction such that the same layer of beads is in focus. Acquire an image of the unstressed bead field.
j. Repeat for each marked location.

Data Analysis:

1. Export ZVI files to TIF files.
    a. Open AxioVision software. Go to File -> Export.
    b. Select the folder with the files you want to export. Click OK.
    c. Unclick “Create project folder” and unclick “Generate merged images”.
    d. Change to export as TIFs (Tagged Image Files). Set 5% compression.
    e. Click “Batch”. Click “Add files” and select all the zvi files you want to export in the folder.
    f. Click “Run Batch”.
2. Make excel spreadsheet using template file. Write in the folders and cells for each gel. Give each cell a separate row.
3. Crop each set of 3 TIFs with the same number using Microsoft Office Picture Manager.
    a. Open the three TIFs in Picture Manager. Open p0x001 image last.
    b. Click “Edit Pictures”, then click “Crop”.
    c. Compare the n0x and s0x001 images. Look for any bright spots that disappear or beads that disappear. Look for any movement around the edges of the frame that are caused by cells pulling outside the field of view. Drag edge of frame to past the offending mark. Note the # pixels moved.
    d. Crop other 2 images the same way.
    e. Click “OK” then click “Save”. Close images.
    f. Repeat for every set of images in the folder
4. Label new folder “MMDDYY” according to date of the experiment. Create subfolders within this folder labeled “raw5rx” where 5 is the stiffness of the gel and x is #1 -> 9 then #1a -> 1z.

5. Copy the 9 sets of images into this file. Files should be labeled n01 -> n09, p01001 -> p09001, and s01001 -> s09001.
6. Change the file types from .TIF to .tif.
7. Note all file name changes and locations in the excel spread sheet.

Running Linux LIBTRC algorithm:

1. Copy folder with date title MMDDYY onto Linux computer.
2. Open first folder (raw5r1). Make a new folder called "raw5". Move all image files into this sub-folder.
3. In "scripts" folder, open "run" file. Change date to match the date of your folder. Save and close.
4. In "scripts" folder, open "run5" file. Change date (located below the parameters) and title of experiment (near top) to match the date of your folder and reflect the experiment.
5. From scripts folder, copy "opfscript" into raw5r1 folder.
6. From scripts folder, copy "fitscript", "hacscript", "lodscript", "pltscript", "run5" and "run" into raw5 folder.
7. Click File -> Open in Terminal. Type "./opfscript "raw5/n*" "raw5/s*". Will only need to do this once and then it will remember this command and you can just press the up arrow to get to it. Click enter. Script will begin running. Do not close this window.
8. Repeat for all raw5r_ folders. These will take anywhere from a few hours to overnight to run.
9. After script has finished running, a new line will appear in the terminal screen. Also, a folder will appear in the raw5r_ folder labeled "raw". It will have one file

corresponding to each set of images, labeled s0x001b.raw. Copy all of these files into the "raw5" folder.

10. Open the "raw5" folder. Click File -> Open in Terminal. Type ">xtrace –w=12 –h=12. Click enter.
11. Choose File > select phase image from directory. Press "Display Image". Phase image should appear in window.
12. Type in "p0x001cr1.raw" (where x refers to #1-9, from p0x001 label) and click "Log Points" (?). Click anywhere on the cell outline and click around the cell to outline the entire cell body. Click on the first point to save the outline.
13. If there is a second cell, change label to "p0x001cr2.raw" and repeat. Can only outline 2 cells per image.
14. Repeat for every phase image in folder.
15. Close window.
16. Double click on "run5" script in "raw5" folder. Click Run in Terminal. A new window will open, do not close it. It will run quick, < 2 minutes.
17. When it finishes, there will be a new folder labeled "tpl" in the "raw5" folder. Open this folder.
18. Each set of images now has a tpl file that corresponds to it.
19. Open the first tpl file. Change corresponding "NPIXX" and "NPIXY" to correspond to your new pixel counts in x and y. Maintain e+03 label – change only the first four numbers (e.g. if your new size is 864 x 302, NPIXX should read 0.864e+03 and NPIXY should read 0.302e+03).
20. Save file and close. Repeat for all tpl files. If there is no adjustment to the image, you don't have to change the tpl file for that image.

21. Double click on “run” script in “raw5” folder. Click Run in Terminal. Be very careful not to click the “run5” script again or it will rewrite your tpl data and you will have to re-input your sizes.
22. When this finishes running (anywhere from 20 min – 2 hours, depending on what is running concurrently), you will have a new folder, “figs” containing three folders: mag, dex, and tbs. These contain the images of the traction vectors in color contour plots (mag), the bead displacement vectors (dex), and the calculated traction vectors (tbs). Running this script will also update the “tpl” file to contain all of the traction data that I use for quantification. The data from these files will be input into a code that extracts the data to Excel.

Inputting Data into Excel:

1. Add the “TFM Template Sheet – Post Sheet” to your excel document in which you recorded the size of the new images.
2. Copy the cells from the “pre” sheet into the “post” sheet. Delete the columns corresponding to ‘Left’, ‘Right’, ‘Top’, ‘Bottom’, and ‘New Dimensions’. Move columns for “Phase”, “Folder” and “Notes” to the appropriately labeled columns on the “post” sheet.
3. Copy files from MMDDYY folder on Linux computer onto a portable drive.
4. In Windows, open two windows. In the first, open folder “tfm_extract_fixed” then “tfm_extract”. In the second, open the folders within the MMDDYY folder to get to the “raw5” folder which contains the “tpl” folder. Don’t open the “tpl” folder.
5. Drag the “tpl” folder onto the “tfm_extract.exe” folder in the other window.
6. Open the resulting .txt file (extracted_bunchofnumbers.txt). May have to set it to default open in Excel the first time.

7. Change column A to be right justified so you can see the end of the file names. Delete all rows with the ~ after the file name so that you have (at most) 9 rows, one for each image set. Can also delete column B if desired.
8. Copy cells from the extracted document into the appropriate places on the post sheet. Note that in the extracted document, frames with two cells have separate *columns* for the second cell's data, while the post sheet has separate *rows* for the second cell's data.
9. Repeat for each tpl folder until all data has been input.

Checking TFM Data:

1. Going back through and checking the data, each will be color-coded. Green is good, yellow is probably good, orange is probably bad and red is bad. Can also include notes.
2. On the excel sheet, in the "delchi" column, note any delchi number that is less than 3. These are generally the most suspect cells. Delchi is a measure of the error calculated in the stress map.
3. Open the "dex" plot and the three images (phase, null, and stressed) for each field of view and check the arrows on the dex plot against the bead movement you observe by eye. If there is a stray arrow that doesn't make sense, mark it in the notes and consider the cell questionable (orange/red). Can also check against the "tbs" plot.
4. Also check that the output |F| value is similar to what you would expect based on your observed bead movement. Note accordingly.

APPENDIX B

PROTOCOL FOR PATTERNING COLLAGEN CHANNELS

Portions of this protocol were adapted from (Nelson et al., 2008).

Materials:

Silicon wafer with pattern

Spin-coater

Sigma-cote

PDMS (monomer and initiator)

Large petri dish

Casting PDMS Stamps:

1. Wash wafer (if needed) with ethanol. Use a kimwipe to gently clean the surface.
2. Place wafer on spin-coater (1^{st} floor teaching lab) and coat with Sigma-cote ($4^{o}C$)
    a. Open the vacuum line (turn on vacuum pump outside of lab in hallway).
    b. Open the air line.
3. Remove wafer from spin-coater.
4. Mix PDMS (10:1 ratio of monomer to initiator) in a plastic container
    a. For correct stamp height (~5 mm), calculate M (total mass of PDMS needed) using the following relation: $d^2/M = 0.26388\ m^2kg^{-1}$, where d = diameter of petri dish used. Alternatively, for large petri dish, 70 g monomer, 7 g initiator is appropriate.
5. Degas PDMS mixture in vacuum chamber (repeatedly, until bubbles don't form under vacuum).

6. Place wafer in the bottom of a large petri dish and pour PDMS over the center of the wafer.
7. Gently push down on the center of the wafer (the wooden end of a cotton swab works well) to remove any PDMS underneath it.
8. Place in oven for ~2 hours at 60^{o}C (may be left overnight, but longer bake times make the cured PDMS more brittle).
9. Gently remove the PDMS from the wafer and place patterned-side up in another dish. Remove excess PDMS from wafer.

Materials:

PDMS stamps (from above)

PDMS spacers (use above protocol to cast thin layer of PDMS in petri dish)

Razor blade

100% ethanol

18 mm diameter round coverglass

1% (w/v) BSA in PBS (sterile)

10 mg/mL rat tail type I collagen stock (keep on ice)

1 N NaOH (keep on ice)

Complete media (keep on ice)

15 mL centrifuge tubes (keep on ice)

Forceps

6 well plate

Patterning Collagen Wells:

1. Carefully cut stamps in 4 x 4 sets using a razor blade.

2. In a biosafety cabinet, sterilize stamps by dipping them in 100% ethanol, wiping the back (non-feature) side with paper towel, and placing on petri dish until dry, ~ 2 min. Sterilize round 18 mm diameter coverslips for lids (set diagonally against petri dish) and spacer pieces (2/stamp).
3. Coat the feature side surface of the stamp with 120 μL of 1% (w/v) BSA in sterile 1X PBS (0.01 g in 1 mL – can prepare stock of this and store at 4^{o}C). Incubate for at least 30 minutes at room temperature or overnight at 4^{o}C. Ensure that all air bubbles are removed from the surface of the stamp before starting. Use side of pipet tip to 'roll' BSA across entire surface of the stamp.
4. Prepare a neutralized collagen solution of 3 mg/mL. A final volume of 120 - 180 μL is needed for each stamp for each step (2X washes, 1X lids, 1X channels) (prepare a little extra in each). Have separate tubes of collagen solutions for washes, lids, and channels. Use lower volume for washes and higher volume for channels.
    a. Calculate volume of collagen needed:
        i. (desired [ ])*(desired vol.) / (stock [ ]) = vol. collagen needed
    b. Calculate volume of 1 N NaOH needed:
        i. Vol. collagen needed *0.023 = vol. NaOH needed
    c. Calculate volume of media needed:
        i. Desired final vol. – vol. collagen – vol. NaOH = volume media
5. Prepare collagen 'lids' by pipetting 120 μL of neutralized collagen on the surface of an ethanol sterilized 18 mm round coverslip. Use the edge of a yellow pipette tip to 'roll' collagen across surface. Work quickly, and don't make more than four lids in one batch of collagen. Make one lid/stamp, plus an extra one or two for backup.

6. Aspirate the BSA solution from the stamps. Can touch the middle of the array to remove more. Try not to touch the features. Wash the BSA-coated surfaces 2X w/neutralized collagen (120 μL/wash/stamp).
7. Place a drop (160-180 μL) onto the bottom of a 6 well plate, between (2) 1 mm PDMS spacers. Invert collagen-washed stamp over drop. Place dishes and lids in a 37^{o}C incubator for 1.5 hours.

Materials:

T25 flask of confluent cells

Trypsin

Complete media (have both warmed and ice-cold on hand)

Protocol for Seeding Cells in Collagen Wells

1. Prepare a suspension of cells. Keep the cells on ice.
    a. Passage cells normally, then remove some suspension to second tube and spin down at normal centrifugation rate for those cells. Resuspend in ice cold media and count.
    b. Make a 3 mL suspension of 70,000 cells/mL.
2. Carefully remove the stamp from the collagen gel by pulling straight up with sterilized forceps. Avoid shearing the gel to prevent distortion of the molded wells.
3. Immediately add a drop (~120 uL) of cells to the molded surface of the collagen gels. Under a phase contrast microscope (scope in tissue culture room), monitor the sample. As soon as the wells are filled with cells (~1-2 min), check the seeding density on the scope, and if necessary, wash the sample by tipping the dish at a 45^{o} angle and gently pipetting 120 uL of **cold media** across the surface to remove excess cells. While holding at an angle, aspirate solution at bottom of well.

a. Can repeat these steps if you accidentally wash away too many cells.

4. Place the sample in the incubator for 5 minutes to allow cells to adhere to the collagen.
5. After the cells have started to adhere to the gel, gently cover the gel with a collagen lid. Allow the collagen lid to settle for 5 minutes in the incubator. Fill the dish with 2.5 mL of warmed complete media and return to incubator. Allow 6 hours minimum for cell spreading before beginning experiment.

APPENDIX C

PROTOCOL FOR IMMUNOSTAINING IN COLLAGEN CHANNELS

Materials:

43 x 50 mm coverglass

22 x 22 mm coverglass

Kim wipes

Traction chambers

Vacuum grease

35 mm petri dishes

Seeding Cells for Immunostaining:

1. Activate 43 x 50 mm coverglass, one for each channel.
2. Attach two 22 x 22 mm coverglass slips on either side of the long edge of the 43 x 50 mm glass using vacuum grease. These slips will serve as ‘spacers’. Press down gently on small converslips with q-tip to seal.
3. Prepare stamps and polymerize collagen channels as described in Appendix B.
4. When channels have completed polymerization, carefully remove small glass spacers without damaging the patterned collagen.
5. Carefully dab around edges of polymerized collagen with a Kim wipe to absorb excess collagen. If there are ‘wet’ looking areas on the vacuum grease, dab dry.
6. Invert the traction insert so that the ridged side is facing down. Apply a thin line of vacuum grease around the circular opening.
7. Invert the 43 x 50 mm coverslip with the polymerized collagen channels over the traction insert such that the channels are centered over the opening.

8. Gently press down on the coverslip until the vacuum grease has formed a tight seal around the entire opening. If the chamber leaks, it is likely that the coverslip was not properly sealed to the traction insert, and more vacuum grease is required.
9. Flip over the traction insert and continue with cell seeding protocol described in Appendix B. Use 35 mm petri dish as 'lid' to maintain sterility.
10. Incubate overnight at 37^{o}C.

Materials:

1X PBS

3.7% formaldehyde

1% Triton-X

(or ice-cold 3:7 methanol:acetone mixture)

0.5% (v/v) Tween-20 in 1X PBS

3% (w/v) BSA in 0.5% Tween-20 in 1X PBS

1% (w/v) BSA in 0.5% Tween-20 in 1X PBS

1% (w/v) BSA in 1X PBS

Primary antibody (1^{o} Ab)

Secondary antibody (2^{o} Ab)

Phalloidin

DAPI

Orbital shaker

Aluminum foil

Immunostaining:

1. Rinse the dish 2X with RT 1X PBS.
2. Fix with 2 mL of 3.7% formaldehyde for 15-30 minutes at RT.

3. Wash 3X with 1X PBS for 10 minutes each, rocking at RT.
    a. Note that samples may be stored at 4^{o}C at this step for a few days if necessary.
4. Add 2 mL of 1% Triton-X in 1X PBS for 5 minutes at RT, rocking.
    a. Alternatively, for staining of actin and focal adhesions, can fix for 5-10 minutes in 2 mL of 3:7 methanol:acetone mixture at -20^{o}C.
5. Wash 3X with 0.5% (v/v) Tween-20 in 1X PBS for 10 minutes each.
6. Block with 3% (w/v) BSA in 0.5% (v/v) Tween-20 in 1X PBS for 3 hours at RT, rocking. This step can also be done overnight at 4^{o}C, rocking.
7. For best staining, the glass coverslip on which the collagen lid was polymerized should be carefully removed using forceps prior to incubation with the 1^{o} Ab to maximize diffusion.
8. Prepare 1^{o} Ab in 1% (w/v) BSA in 1X PBS. 1:50 -1:200 is a good working range, depending on the antibody. Use 1 mL per channel.
9. Add 1^{o} Ab onto each channel. Incubate 1-2 days @ 37^{o}C on the orbital shaker, gently rocking. Use square petri dishes to guard against leaks onto the shaker.
10. Remove 1^{o} Ab and store in fridge for future use (~1-2 weeks).
11. Wash 3X with 1% BSA in 0.5% Tween-20 in 1X PBS for 10 minutes each at RT, rocking.
12. Prepare 1 mL of 2^{o} Ab for each channel in 1% BSA in 1X PBS, usually 1:200. Incubate for 2 hours at RT, rocking and covered with aluminum foil.
13. Wash 3X with 0.5% Tween-20 in 1X PBS for 10 minutes each at RT, rocking.
14. Wash 2X with 0.5% Tween-20 in 1X PBS for 1 hour each at RT, rocking.
15. Wash overnight at 4^{o}C in 1X PBS, rocking.
16. Wash 3X with 1X PBS for 5 minutes each at RT, rocking.
17. Incubate cells with 1:100 phalloidin in 1X PBS for 2 hours at RT, rocking.
18. Wash 3X with 1X PBS for 10 minutes each at RT, rocking.

19. Incubate cells with 1:100 DAPI in MilliQ water for 20 minutes at RT, rocking.
20. Wash 3X with 1X PBS for 10 minutes each at RT, rocking.
21. Image immediately.

APPENDIX D

PROTOCOL FOR TRANSFECTION OF CANCER CELLS (siRNA AND DNA PLASMIDS)

Materials for siRNA Transfection:

20 μM siRNA

Lipofectamine 2000 transfection reagent

1.7 mL centrifuge tubes

OptiMEM

Complete media without pen/strep

siRNA Transfection Protocol:

Day 0:

1. Plate cells in a 6 well plate at a density of 50,000 cells/well. Let spread and adhere overnight.

Day 1:

1. Cells should be ~40-50% confluent.
2. Dilute 5 μL Lipofectamine 2000 in 250 μL OptiMEM in a separate 1.7 mL centrifuge tube (one per well).
3. Let sit 5-15 minutes at RT.
4. Meanwhile, dilute 1.25 μL siRNA in 250 μL OptiMEM in a 1.7 mL centrifuge tube (one per well).
5. Combine mixture by pipetting gently, and incubate for 20 minutes at RT.
6. Rinse cells 1X with 1 mL of pen/strep-free media.
7. Add 2 mL of pen/strep-free media per well.

8. Add 0.5 mL of siRNA-Lipofectamine complex dropwise to each well.
9. Incubate 4 hours at 37^{o}C, then aspirate and replace with complete media.

Day 4:

1. Seed cells into desired vessel (e.g. polyacrylamide gel, 3D collagen gel, collagen channels, etc.).

Materials for DNA Plasmid Transfection:

DNA plasmid

Transit-2020 transfection reagent

1.7 mL centrifuge tubes

OptiMEM

Protocol for DNA Plasmid Transfection:

Day 0:

1. Plate cells in a 6 or 12 well plate at a density of 200,000 or 90,000 cells/well. Let spread and adhere overnight.

Day 1:

1. Cells should be ~70% confluent.
2. Add 100 μL OptiMEM (per 12 well) or 200 μL (per 6 well) to a microfuge tube (one per well).
3. Add 3 μg DNA (per 12 well) or 8 μg DNA (per 6 well) to the tube. Pipette gently to mix and let sit at RT for 5 minutes.
4. Add 3 μL Transit-2020 (per 12 well) or 7.5 μL Transit-2020 (per 6 well) to the tube. Mix gently and let sit at RT for 15-30 minutes.
5. Add dropwise to cells in well in complete media and incubate at 37^{o}C. Note that there is no need for pen/strep-free media, or to change media 4 hours later.

Day 3:

1. Seed cells into desired vessel (e.g. polyacrylamide gel, 3D collagen gel, collagen channels, etc.).

APPENDIX E

PROTOCOL FOR CULTURING CELLS UNDER HYPOXIC CONDITIONS

1. Plate cells onto desired surface.
2. Place tissue culture items into modular incubation chamber.
3. Open both inlet and outlet ports. Connect gas mixture (1% O_2, 5% CO_2, 94% N_2) to inlet port.
4. Flush gas mixture in for 4 minutes, not exceeding 2 psi.
5. Close outlet port. Remove gas line and close inlet port.
6. Place chamber into cell culture incubator.
7. Reflush after 1 hour of incubation to remove any remaining O_2. This is particularly important if chamber is over half filled with dishes.
8. Culture additional 23 hours.
9. Run experiment. Reflush as needed between removing dishes.
10. For reoxygenation experiments, remove dishes and replace media with fresh media.
11. Incubate under normal conditions for 18 hours.
12. Run experiment.

APPENDIX F

PROTOCOL FOR ANALYZING CELL MIGRATION SPEED IN 2D, 3D, AND COLLAGEN CHANNELS

Acquiring Migration Videos

1. Seed cells onto 2D, 3D, or channel substrates and allow to spread for a minimum of 6 hours.
2. Equilibrate plate on microscope with chamber set to 37oC, 5% CO2, and 40% humidity for at least 30 minutes (can be done during position marking).
    a. On main 'Live' screen, click 'Properties', go to 'Frame' and adjust binning to 2 x 2. This reduces the size of acquired files by reducing number of pixels per image (and also reduces exposure time).
3. In AxioVision software, open 'Multidimensional Acquisition' under Acquisition tab.
4. Set parameters of experiment.
    a. 'Experiment' tab: Change image name on experiment tab to ID your experiment. 'Settings for experiment' should be blank.
    b. 'C' tab: Turn voltage on microscope to 1.7V, select 'fixed' exposure time and click 'Measure' to set one exposure for all positions. Turn voltage off when done. Make sure hardware settings are **blank**.
    c. 'T' tab: For 2D and channel experiments, set images to acquire every 5 minutes (every 10 minutes is okay for 3D experiments). Set desired total time (usually 10-24 hours, depending on study). Change 'Settings before/after' to:
        i. Workgroup: TL On

ii. Workgroup: TL Off

d. ‘XY’ tab: Save positions and focus on MarkFind on XY tab. Use a different color for each well. I do not recommend changing ID labels here – it is tedious and unnecessary. Just record positions in your lab notebook and identify which well correlates to which experimental condition.

i. IMPORTANT: **Uncheck** ‘Apply setting before/after timepoint per position’. Otherwise light will turn on and off between positions.

e. Press start.

f. Watch a full run before walking away from the microscope.

g. Readjust focus after 1-2 hours.

Analyzing Cells for Random Walk Migration (e.g. 2D, 3D)

1. In AxioVision, export .zvi files to .jpeg files to facilitate analysis and data transfer (File -> Export; choose 5% compression).
2. In ImageJ, open one migration video by importing the series of .jpeg files (File -> Import -> Image Sequence).
3. Play the video to get a sense for migration movement. Identify each cell as ‘motile’, ‘non-motile’, or ‘dead/dying.’ Separately count the number of cells which divide – this number is independent from the first classification (e.g. a dividing cell can also be motile).
    a. Note: Only count each cell once, and only consider motility prior to a division event. Do not include the motility of the daughter cells in these counts.

4. In excel, record the number of cells in each category (listed as separate columns). Additionally, record notes about the cells which remain motile for at least 8 hours (e.g. 49 frames acquired at 10 minute intervals). Identify each motile cell by a descriptor of where it is within the frame (e.g. left, middle), and by the frame number at which it begins migrating.
5. In ImageJ, select measurements (Analyze -> Set Measurements) of Area, Perimeter, Centroid (*X, Y*), Fit Ellipse, and Shape Descriptors, and Display Label.
6. For each cell, trace the cell body at every other time point (e.g. every 20 minutes). As each trace is completed, click 'Measure' or 'Ctrl+M' on the keyboard. Repeat until cell has been traced 25 times.
7. Convert centroid position for trajectory from pixels to microns.
8. Input trajectory into Matlab and adjust the N_{fit} of the data (line 20, see next section) until the least squares regression closely approximates the calculated mean squared displacement. Check that line 7 indicates the appropriate time interval between images.
9. Open 'Results.xls' spreadsheet from Matlab code and copy output to new excel sheet, noting the calculated speed and persistence time.

Matlab Code for Random Walk Migration:

```
(1)   clear all
(2)   global ts MSDs
(3)   data=xlsread('Trajectory.xlsx'); %load and does not convert to
   0.645 um/pix
(4)   x=data(:,1);
(5)   y=data(:,2);
(6)   clear data;
(7)   dt=20;  %minutes between images
(8)   n=length(x);
(9)   MSD=zeros(n-2,1);
```

```
(10)
(11)  % calculate the mean squared displacement for range of time
   intervals
(12)  for i=1:n-2
(13)      MSD(i)=0;
(14)      for j=1:n-i-1
(15)        MSD(i)=MSD(i)+(x(j+i)-x(j))^2+(y(j+i)-y(j))^2;
(16)      end
(17)      MSD(i)=MSD(i)/(n-i);
(18)  end
(19)
(20)  ignore_last_x_points=12; %CHANGE FIT HERE
(21)  Nfit=length(MSD)-ignore_last_x_points;
(22)  ts=[1:Nfit]*dt;
(23)  MSDs=MSD(1:Nfit);
(24)  % perform nonlinear least squares regression of migration model
   to MSD
(25)  % data, to determine the best-fit parameters S and P. see
   Lauffenberger &
(26)  % Linderman (1993), equation 6-35a. Uses separate m-file
   "SSEcellmig.m"
(27)  c=fminsearch(@SSEcellmig,[.5;100],optimset('MaxFunEvals',
   10000,'MaxIter', 10000));
(28)  migration_speed=c(1)    %S in units of microns/min
(29)  persistence_time=c(2)   %P in units of min
(30)
(31)  % plot of cell path in x-y space
(32)  subplot(3,1,1)
(33)  plot(x,y,'r-',x,y,'bx')
(34)  xlabel('x  (\mum)')
(35)  ylabel('y  (\mum)')
(36)
(37)  % plot of MSD as a function of dt, along with best-fit model
(38)  t=[1:length(MSD)]*dt;
(39)  fit=2*c(1)^2*(c(2)*ts-c(2)^2*(1-exp(-ts/c(2))));
(40)  subplot(3,1,2)
(41)  plot(t,MSD,'b.',ts,fit,'r-')
(42)  xlabel('t  (min)')
(43)  ylabel('MSD  (\mum^2)')
(44)
(45)  % plot of MSD as a function of dt, along with best-fit model,
   cutting out
(46)  % non-fitting points
(47)  t=[1:Nfit]*dt;
(48)  fit=2*c(1)^2*(c(2)*ts-c(2)^2*(1-exp(-ts/c(2))));
(49)  subplot(3,1,3)
(50)  plot(t,MSDs,'b.',ts,fit,'r-')
(51)  xlabel('t  (min)')
```

```
(52)  ylabel('MSD  (\mum^2)')
(53)
(54)  % save results
(55)  A(:,1)=x;
(56)  A(:,2)=y;
(57)  for i=1:length(ts)
(58)      A(i,3)=ts(i);
(59)      A(i,4)=fit(i);
(60)  end
(61)  A(1,5)=c(1);
(62)  A(1,6)=c(2);
(63)  saving_results = xlswrite('results.xls',A); %RENAME WHEN DONE
```

Analyzing Cell Migration in Collagen Channels

1. In AxioVision, export .zvi files to .jpeg files to facilitate analysis and data transfer (File -> Export; choose 5% compression).
2. In ImageJ, open one migration video by importing the series of .jpeg files (File -> Import -> Image Sequence).
3. Play the video to get a sense for migration movement. Identify each cell as 'motile', 'non-motile', or 'dead/dying.' Separately count the number of cells which divide – this number is independent from the first classification (e.g. a dividing cell can also be motile).
    a. Note: Only count each cell once, and only consider motility prior to a division event. Do not include the motility of the daughter cells in these counts.
4. In excel, record the number of cells in each category (listed as separate columns). Additionally, record notes about the cells which remain motile in one direction for longer than 100 minutes (e.g. 20 frames acquired at 5 minute intervals). Identify each motile cell by a descriptor of where it is within the channel (e.g. left, middle, 2^{nd} from right), and by the frame numbers over which it migrates in a single direction (e.g. t5-t150, which would correspond to

25 minutes – 12.5 hours). This facilitates a calculation of speed during the first 100 minutes of migration, as well as speed over the maximum invasion distance.

   a. Note: Cells should only be tracked when they are isolated within the cell and not interacting with the channel end. If cells subsequently come into contact with another cell or the channel end, then the final time point should be taken as the time point just prior to this interaction.
   b. Note: A cell can be analyzed more than once, as long as each time period is at least 100 minutes (e.g. if a cell reverses direction, or comes in contact with a cell then loses contact and migrates uni-directionally again).

5. Repeat for every migration video acquired for a given experiment.
6. In ImageJ, select measurements (Analyze -> Set Measurements) of Area, Perimeter, Centroid (*X, Y*), Fit Ellipse, and Shape Descriptors, and Display Label.
7. For each cell previously identified as ‘motile’ for 100 minutes or longer, trace the cell at the first time point, the 100 minute time point, and the final time point (e.g. 3 traces per cell). As each trace is completed, click ‘Measure’ or ‘Ctrl+M’ on the keyboard.
8. For each video, find a defect in the collagen (e.g. bubble, debris, bright spot) that is located well apart from the channel and away from any moving cells. Circle the defect and collect measurements at each time point previously recorded for cells in that video. The centroid position of the defect will be used to later subtract out any bulk movement of the entire channel, to obtain a more precise distance travelled measurement.

9. After every 50 or so measurements, copy and paste the measurements from ImageJ into a temporary excel sheet. After collecting data from all of the migration videos for a given experiment, copy and paste the data into the appropriate locations in your final spreadsheet for analysis. For the collagen defects that were analyzed for each migration video, only copy and paste the centroid position for each time point (X_0, Y_0).
10. Convert centroid position from pixels to microns.
11. Calculate the migration displacement of each cell at both the 100 minute time point and the final time point:

$$Displacement = \sqrt{\left[\left(X_f - X_{f0}\right) - \left(X_i - X_{i0}\right)\right]^2 + \left[\left(Y_f - Y_{f0}\right) - \left(Y_i - Y_{i0}\right)\right]^2}$$

12. Calculate the speed of each cell over the first 100 minutes and over the entire length of analysis (e.g. initial to final time point):

$$Speed = \frac{Displacement}{t_f - t_i}$$

APPENDIX G

LIST OF PUBLICATIONS

Publications Completed at Cornell University

1. Huynh J, Bordeleau F, **Kraning-Rush C**, and Reinhart-King C. Substrate Stiffness Regulates PDGF-Induced Circular Dorsal Ruffle Formation in Vascular Smooth Muscle Cells Through Myosin Light Chain Kinase Control of Cellular Contractility. Accepted for publication, *Cellular and Molecular Bioengineering*, DOI 10.1007/s12195-013-0278-7.
2. **Kraning-Rush C**, Carey S, and Reinhart-King C. Microfabricated Collagen Tracks Facilitate Single Cell Metastatic Invasion in 3D. *Integrative Biology*, 2013:5 606-16.
3. Staunton, JR et al. (The Physical Sciences-Oncology Centers (PS-OC) Cell-Line Project Team). A Physical Sciences Network Characterization of Nonmalignant and Metastatic Cells. *Scientific Reports*, 2013:3 1449.
4. **Kraning-Rush C** and Reinhart-King C. Controlling matrix stiffness and topography for the study of tumor cell migration. *Cell Adhesion & Migration*, 2012:6(3).
5. Carey S, **Kraning-Rush C**, Williams R, and Reinhart-King C. Biophysical Control of Invasive Tumor Cell Behavior by Extracellular Matrix Microarchitecture. *Biomaterials*, 2012:33 4157-65.
6. **Kraning-Rush C**, Carey S, Califano J, and Reinhart-King C. *Methods in Cell Biology* (Chapter: Quantifying Traction Stresses in Adherent Cells) Elsevier, New York, 2012:110 139-78.

7. **Kraning-Rush C**, Califano J, and Reinhart-King C. Cellular Traction Stresses Increase with Increasing Metastatic Potential. *PLoS One*, 2012:7(2) e32572.
8. **Kraning-Rush C**, Carey S, Califano J, Smith B, and Reinhart-King C. The Role of the Cytoskeleton in Cellular Force Generation in 2D and 3D Environments. *Physical Biology*, 2011:8 015009.

Previous Publications

9. Ainslie K, **Kraning C**, and Desai T. Microfabrication of an Asymmetric, Multi-layered Microdevice for Controlled Release of Orally Delivered Therapeutics. *Lab on a Chip*, 2008:8 1042-1047.
10. **Kraning C**, Benz T, Bloome K, Campanello G, Fahrenbach V, Mistry S, Hedge C, Clevenger K, Gligorich K, Hopkins T, Hoops G, Mendes S, Chang H-C, and Su M-C. Determination of Surface Coverage and Orientation of Reduced Cytochrome c on a Silica Surface with Polarized ATR Spectroscopy. *Journal of Physical Chemistry C*, 2007:111(35) 13062-13067.

REFERENCES

Airaksinen, K. E., Salmela, P. I., Linnaluoto, M. K., Ikaheimo, M. J., Ahola, K., Ryhanen, L. J., 1993. Diminished arterial elasticity in diabetes: association with fluorescent advanced glycosylation end products in collagen. Cardiovasc Res. 27**,** 942-5.

Alcaraz, J., Mori, H., Ghajar, C. M., Brownfield, D., Galgoczy, R., Bissell, M. J., 2011. Collective epithelial cell invasion overcomes mechanical barriers of collagenous extracellular matrix by a narrow tube-like geometry and MMP14-dependent local softening. Integr Biol (Camb). 3**,** 1153-66.

Alexander, N. R., Branch, K. M., Parekh, A., Clark, E. S., Iwueke, I. C., Guelcher, S. A., Weaver, A. M., 2008. Extracellular matrix rigidity promotes invadopodia activity. Curr Biol. 18**,** 1295-9.

Amano, M., Nakayama, M., Kaibuchi, K., 2010. Rho-kinase/ROCK: A key regulator of the cytoskeleton and cell polarity. Cytoskeleton (Hoboken). 67**,** 545-54.

Anderson, A. R., Weaver, A. M., Cummings, P. T., Quaranta, V., 2006. Tumor morphology and phenotypic evolution driven by selective pressure from the microenvironment. Cell. 127**,** 905-15.

Arribas, J., Massague, J., 1995. Transforming growth factor-alpha and beta-amyloid precursor protein share a secretory mechanism. J Cell Biol. 128**,** 433-41.

Azuma, H., Inamoto, T., Sakamoto, T., Kiyama, S., Ubai, T., Shinohara, Y., Maemura, K., Tsuji, M., Segawa, N., Masuda, H., Takahara, K., Katsuoka, Y., Watanabe, M., 2003. Gamma-aminobutyric acid as a promoting factor of cancer metastasis; induction of matrix metalloproteinase production is potentially its underlying mechanism. Cancer Res. 63**,** 8090-6.

Baker, A. M., Bird, D., Lang, G., Cox, T. R., Erler, J. T., 2012. Lysyl oxidase enzymatic function increases stiffness to drive colorectal cancer progression through FAK. Oncogene.

Baker, E. L., Bonnecaze, R. T., Zaman, M. H., 2009. Extracellular matrix stiffness and architecture govern intracellular rheology in cancer. Biophys J. 97**,** 1013-21.

Baker, E. L., Lu, J., Yu, D., Bonnecaze, R. T., Zaman, M. H., 2010. Cancer cell stiffness: integrated roles of three-dimensional matrix stiffness and transforming potential. Biophys J. 99**,** 2048-57.

Balzer, E. M., Tong, Z., Paul, C. D., Hung, W. C., Stroka, K. M., Boggs, A. E., Martin, S. S., Konstantopoulos, K., 2012. Physical confinement alters tumor cell adhesion and migration phenotypes. FASEB J.

Beadle, C., Assanah, M. C., Monzo, P., Vallee, R., Rosenfeld, S. S., Canoll, P., 2008. The role of myosin II in glioma invasion of the brain. Mol Biol Cell. 19**,** 3357-68.

Beerling, E., Ritsma, L., Vrisekoop, N., Derksen, P. W., van Rheenen, J., 2011. Intravital microscopy: new insights into metastasis of tumors. J Cell Sci. 124**,** 299-310.

Beningo, K. A., Dembo, M., Kaverina, I., Small, J. V., Wang, Y. L., 2001. Nascent focal adhesions are responsible for the generation of strong propulsive forces in migrating fibroblasts. J Cell Biol. 153**,** 881-8.

Bettinger, C. J., Langer, R., Borenstein, J. T., 2009. Engineering substrate topography at the micro- and nanoscale to control cell function. Angew Chem Int Ed Engl. 48**,** 5406-15.

Biela, S. A., Su, Y., Spatz, J. P., Kemkemer, R., 2009. Different sensitivity of human endothelial cells, smooth muscle cells and fibroblasts to topography in the nano-micro range. Acta Biomater. 5**,** 2460-6.

Bissell, M. J., Hines, W. C., 2011. Why don't we get more cancer? A proposed role of the microenvironment in restraining cancer progression. Nat Med. 17**,** 320-9.

Black, P. H., 1980. Shedding from normal and cancer-cell surfaces. N Engl J Med. 303**,** 1415-6.

Blobel, C. P., 2005. ADAMs: key components in EGFR signalling and development. Nat Rev Mol Cell Biol. 6**,** 32-43.

Bloom, R. J., George, J. P., Celedon, A., Sun, S. X., Wirtz, D., 2008. Mapping local matrix remodeling induced by a migrating tumor cell using three-dimensional multiple-particle tracking. Biophys J. 95**,** 4077-88.

Bramhall, S. R., Rosemurgy, A., Brown, P. D., Bowry, C., Buckels, J. A., 2001. Marimastat as first-line therapy for patients with unresectable pancreatic cancer: a randomized trial. J Clin Oncol. 19**,** 3447-55.

Brandley, B. K., Weisz, O. A., Schnaar, R. L., 1987. Cell attachment and long-term growth on derivatizable polyacrylamide surfaces. J Biol Chem. 262**,** 6431-7.

Brown, X. Q., Bartolak-Suki, E., Williams, C., Walker, M. L., Weaver, V. M., Wong, J. Y., 2010. Effect of substrate stiffness and PDGF on the behavior of vascular smooth muscle cells: implications for atherosclerosis. J Cell Physiol. 225**,** 115-22.

Brownfield, D. G., Venugopalan, G., Lo, A., Mori, H., Tanner, K., Fletcher, D. A., Bissell, M. J., 2013. Patterned collagen fibers orient branching mammary epithelium through distinct signaling modules. Curr Biol. 23**,** 1-7.

Burdall, S. E., Hanby, A. M., Lansdown, M. R., Speirs, V., 2003. Breast cancer cell lines: friend or foe? Breast Cancer Res. 5**,** 89-95.

Burton, K., Taylor, D. L., 1997. Traction forces of cytokinesis measured with optically modified elastic substrata. Nature. 385**,** 450-4.

Butler, J. P., Tolic-Norrelykke, I. M., Fabry, B., Fredberg, J. J., 2002. Traction fields, moments, and strain energy that cells exert on their surroundings. Am J Physiol Cell Physiol. 282**,** C595-605.

Cairns, R. A., Khokha, R., Hill, R. P., 2003. Molecular mechanisms of tumor invasion and metastasis: an integrated view. Curr Mol Med. 3**,** 659-71.

Califano, J. P., Reinhart-King, C. A., 2008. A balance of substrate mechanics and matrix chemistry regulates endothelial cell network assembly. Cell Mol Bioeng. 1**,** 122-132.

Califano, J. P., Reinhart-King, C. A., 2010a. Substrate Stiffness and Cell Area Predict Cellular Traction Stresses in Single Cells and Cells in Contact. Cellular and Molecular Bioengineering. 3**,** 68-75.

Califano, J. P., Reinhart-King, C. A., 2010b. Substrate stiffness and cell area predict cellular traction stresses in single cells and cells in contact. Cell Mol Bioeng. 3**,** 68-75.
Carey, S. P., Kraning-Rush, C. M., Williams, R. M., Reinhart-King, C. A., 2012. Biophysical control of invasive tumor cell behavior by extracellular matrix microarchitecture. Biomaterials.
Carisey, A., Tsang, R., Greiner, A. M., Nijenhuis, N., Heath, N., Nazgiewicz, A., Kemkemer, R., Derby, B., Spatz, J. P., Ballestrem, C., 2013. Vinculin regulates the recruitment and release of core focal adhesion proteins in a force-dependent manner. Curr Biol. 23**,** 271-281.
Charest, J. M., Califano, J. P., Carey, S. P., Reinhart-King, C. A., 2012. Fabrication of substrates with defined mechanical properties and topographical features for the study of cell migration. Macromol Biosci. 12**,** 12-20.
Christofori, G., 2006. New signals from the invasive front. Nature. 441**,** 444-50.
Condeelis, J., Segall, J. E., 2003. Intravital imaging of cell movement in tumours. Nat Rev Cancer. 3**,** 921-30.
Conklin, M. W., Eickhoff, J. C., Riching, K. M., Pehlke, C. A., Eliceiri, K. W., Provenzano, P. P., Friedl, A., Keely, P. J., 2011. Aligned collagen is a prognostic signature for survival in human breast carcinoma. Am J Pathol. 178**,** 1221-32.
Corey, J. M., Feldman, E. L., 2003. Substrate patterning: an emerging technology for the study of neuronal behavior. Exp Neurol. 184 Suppl 1**,** S89-96.
Cornhill, J. F., Levesque, M. J., Herderick, E. E., Nerem, R. M., Kilman, J. W., Vasko, J. S., 1980. Quantitative study of the rabbit aortic endothelium using vascular casts. Atherosclerosis. 35**,** 321-37.
Coussens, L. M., Fingleton, B., Matrisian, L. M., 2002. Matrix metalloproteinase inhibitors and cancer: trials and tribulations. Science. 295**,** 2387-92.
Cross, S. E., Jin, Y. S., Rao, J., Gimzewski, J. K., 2007. Nanomechanical analysis of cells from cancer patients. Nat Nanotechnol. 2**,** 780-3.
Curtis, A., Wilkinson, C., 1999. New depths in cell behaviour: reactions of cells to nanotopography. Biochem Soc Symp. 65**,** 15-26.
Danowski, B. A., 1989. Fibroblast contractility and actin organization are stimulated by microtubule inhibitors. J Cell Sci. 93 (Pt 2)**,** 255-66.
Darling, E. M., Zauscher, S., Block, J. A., Guilak, F., 2007. A thin-layer model for viscoelastic, stress-relaxation testing of cells using atomic force microscopy: do cell properties reflect metastatic potential? Biophys J. 92**,** 1784-91.
Debnath, J., Muthuswamy, S. K., Brugge, J. S., 2003. Morphogenesis and oncogenesis of MCF-10A mammary epithelial acini grown in three-dimensional basement membrane cultures. Methods. 30**,** 256-68.
Delanoe-Ayari, H., Iwaya, S., Maeda, Y. T., Inose, J., Riviere, C., Sano, M., Rieu, J. P., 2008. Changes in the magnitude and distribution of forces at different Dictyostelium developmental stages. Cell Motil Cytoskeleton. 65**,** 314-31.
Dembo, M., Oliver, T., Ishihara, A., Jacobson, K., 1996. Imaging the traction stresses exerted by locomoting cells with the elastic substratum method. Biophys J. 70**,** 2008-22.

Dembo, M., Wang, Y. L., 1999. Stresses at the cell-to-substrate interface during locomotion of fibroblasts. Biophys J. 76**,** 2307-16.
Dennis, C., 2006. Cancer: off by a whisker. Nature. 442**,** 739-41.
Dikovsky, D., Bianco-Peled, H., Seliktar, D., 2008. Defining the role of matrix compliance and proteolysis in three-dimensional cell spreading and remodeling. Biophys J. 94**,** 2914-25.
Discher, D. E., Janmey, P., Wang, Y. L., 2005. Tissue cells feel and respond to the stiffness of their substrate. Science. 310**,** 1139-43.
Doyle, A. D., Wang, F. W., Matsumoto, K., Yamada, K. M., 2009. One-dimensional topography underlies three-dimensional fibrillar cell migration. J Cell Biol. 184**,** 481-90.
du Roure, O., Saez, A., Buguin, A., Austin, R. H., Chavrier, P., Silberzan, P., Ladoux, B., 2005. Force mapping in epithelial cell migration. Proc Natl Acad Sci U S A. 102**,** 2390-5.
Duffy, M. J., 1996. Proteases as prognostic markers in cancer. Clin Cancer Res. 2**,** 613-8.
Eccles, S. A., Box, G. M., Court, W. J., Bone, E. A., Thomas, W., Brown, P. D., 1996. Control of lymphatic and hematogenous metastasis of a rat mammary carcinoma by the matrix metalloproteinase inhibitor batimastat (BB-94). Cancer Res. 56**,** 2815-22.
Ehrbar, M., Sala, A., Lienemann, P., Ranga, A., Mosiewicz, K., Bittermann, A., Rizzi, S. C., Weber, F. E., Lutolf, M. P., 2011. Elucidating the role of matrix stiffness in 3D cell migration and remodeling. Biophys J. 100**,** 284-93.
Engler, A., Bacakova, L., Newman, C., Hategan, A., Griffin, M., Discher, D., 2004. Substrate compliance versus ligand density in cell on gel responses. Biophys J. 86**,** 617-28.
Engler, A. J., Sen, S., Sweeney, H. L., Discher, D. E., 2006. Matrix elasticity directs stem cell lineage specification. Cell. 126**,** 677-89.
Enomoto, D. N., Mekkes, J. R., Bossuyt, P. M., Hoekzema, R., Bos, J. D., 1996. Quantification of cutaneous sclerosis with a skin elasticity meter in patients with generalized scleroderma. J Am Acad Dermatol. 35**,** 381-7.
Erler, J. T., Bennewith, K. L., Nicolau, M., Dornhofer, N., Kong, C., Le, Q. T., Chi, J. T., Jeffrey, S. S., Giaccia, A. J., 2006. Lysyl oxidase is essential for hypoxia-induced metastasis. Nature. 440**,** 1222-6.
Fisher, K. E., Sacharidou, A., Stratman, A. N., Mayo, A. M., Fisher, S. B., Mahan, R. D., Davis, M. J., Davis, G. E., 2009. MT1-MMP- and Cdc42-dependent signaling co-regulate cell invasion and tunnel formation in 3D collagen matrices. J Cell Sci. 122**,** 4558-69.
Fonck, E., Feigl, G. G., Fasel, J., Sage, D., Unser, M., Rufenacht, D. A., Stergiopulos, N., 2009. Effect of aging on elastin functionality in human cerebral arteries. Stroke. 40**,** 2552-6.
Fraley, S. I., Feng, Y., Giri, A., Longmore, G. D., Wirtz, D., 2012. Dimensional and temporal controls of three-dimensional cell migration by zyxin and binding partners. Nat Commun. 3**,** 719.

Fraley, S. I., Feng, Y., Krishnamurthy, R., Kim, D. H., Celedon, A., Longmore, G. D., Wirtz, D., 2010. A distinctive role for focal adhesion proteins in three-dimensional cell motility. Nat Cell Biol. 12**,** 598-604.

Freed, L. E., Langer, R., Martin, I., Pellis, N. R., Vunjak-Novakovic, G., 1997. Tissue engineering of cartilage in space. Proc Natl Acad Sci U S A. 94**,** 13885-90.

Friedl, P., Gilmour, D., 2009. Collective cell migration in morphogenesis, regeneration and cancer. Nat Rev Mol Cell Biol. 10**,** 445-57.

Friedl, P., Maaser, K., Klein, C. E., Niggemann, B., Krohne, G., Zanker, K. S., 1997. Migration of highly aggressive MV3 melanoma cells in 3-dimensional collagen lattices results in local matrix reorganization and shedding of alpha2 and beta1 integrins and CD44. Cancer Res. 57**,** 2061-70.

Friedl, P., Wolf, K., 2003. Tumour-cell invasion and migration: diversity and escape mechanisms. Nat Rev Cancer. 3**,** 362-74.

Friedl, P., Wolf, K., 2008. Tube travel: the role of proteases in individual and collective cancer cell invasion. Cancer Res. 68**,** 7247-9.

Friedl, P., Wolf, K., 2010. Plasticity of cell migration: a multiscale tuning model. J Cell Biol. 188**,** 11-9.

Friedl, P., Wolf, K., Lammerding, J., 2011. Nuclear mechanics during cell migration. Curr Opin Cell Biol. 23**,** 55-64.

Fu, J., Wang, Y. K., Yang, M. T., Desai, R. A., Yu, X., Liu, Z., Chen, C. S., 2010. Mechanical regulation of cell function with geometrically modulated elastomeric substrates. Nat Methods. 7**,** 733-6.

Gaggioli, C., Hooper, S., Hidalgo-Carcedo, C., Grosse, R., Marshall, J. F., Harrington, K., Sahai, E., 2007. Fibroblast-led collective invasion of carcinoma cells with differing roles for RhoGTPases in leading and following cells. Nat Cell Biol. 9**,** 1392-400.

Galbraith, C. G., Sheetz, M. P., 1997. A micromachined device provides a new bend on fibroblast traction forces. Proc Natl Acad Sci U S A. 94**,** 9114-8.

Gaudet, C., Marganski, W. A., Kim, S., Brown, C. T., Gunderia, V., Dembo, M., Wong, J. Y., 2003. Influence of type I collagen surface density on fibroblast spreading, motility, and contractility. Biophys J. 85**,** 3329-35.

Geiger, B., Spatz, J. P., Bershadsky, A. D., 2009. Environmental sensing through focal adhesions. Nat Rev Mol Cell Biol. 10**,** 21-33.

Gerlinger, M., Rowan, A. J., Horswell, S., Larkin, J., Endesfelder, D., Gronroos, E., Martinez, P., Matthews, N., Stewart, A., Tarpey, P., Varela, I., Phillimore, B., Begum, S., McDonald, N. Q., Butler, A., Jones, D., Raine, K., Latimer, C., Santos, C. R., Nohadani, M., Eklund, A. C., Spencer-Dene, B., Clark, G., Pickering, L., Stamp, G., Gore, M., Szallasi, Z., Downward, J., Futreal, P. A., Swanton, C., 2012. Intratumor heterogeneity and branched evolution revealed by multiregion sequencing. N Engl J Med. 366**,** 883-92.

Giampieri, S., Manning, C., Hooper, S., Jones, L., Hill, C. S., Sahai, E., 2009. Localized and reversible TGFbeta signalling switches breast cancer cells from cohesive to single cell motility. Nat Cell Biol. 11**,** 1287-96.

Giampieri, S., Pinner, S., Sahai, E., 2010. Intravital imaging illuminates transforming growth factor beta signaling switches during metastasis. Cancer Res. 70**,** 3435-9.
Giannone, G., Dubin-Thaler, B. J., Rossier, O., Cai, Y., Chaga, O., Jiang, G., Beaver, W., Dobereiner, H. G., Freund, Y., Borisy, G., Sheetz, M. P., 2007. Lamellipodial actin mechanically links myosin activity with adhesion-site formation. Cell. 128**,** 561-75.
Gjorevski, N., Nelson, C. M., 2010. Endogenous patterns of mechanical stress are required for branching morphogenesis. Integr Biol (Camb). 2**,** 424-34.
Gjorevski, N., Nelson, C. M., 2012. Mapping of mechanical strains and stresses around quiescent engineered three-dimensional epithelial tissues. Biophys J. 103**,** 152-62.
Goldmann, W. H., Auernheimer, V., Thievessen, I., Fabry, B., 2013. Vinculin, cell mechanics and tumour cell invasion. Cell Biol Int. 37**,** 397-405.
Graham, C. H., Forsdike, J., Fitzgerald, C. J., S., M.-G., 1999. Hypoxia-mediated stimulation of carcinoma cell invasiveness via upregulation of urokinase receptor expression. International Journal of Cancer. 80**,** 617-623.
Gritsenko, P. G., Ilina, O., Friedl, P., 2012. Interstitial guidance of cancer invasion. J Pathol. 226**,** 185-99.
Gu, J., Tamura, M., Pankov, R., Danen, E. H., Takino, T., Matsumoto, K., Yamada, K. M., 1999. Shc and FAK differentially regulate cell motility and directionality modulated by PTEN. J Cell Biol. 146**,** 389-403.
Guck, J., Schinkinger, S., Lincoln, B., Wottawah, F., Ebert, S., Romeyke, M., Lenz, D., Erickson, H. M., Ananthakrishnan, R., Mitchell, D., Kas, J., Ulvick, S., Bilby, C., 2005. Optical deformability as an inherent cell marker for testing malignant transformation and metastatic competence. Biophys J. 88**,** 3689-98.
Hanahan, D., Weinberg, R. A., 2000. The hallmarks of cancer. Cell. 100**,** 57-70.
Hanahan, D., Weinberg, R. A., 2011. Hallmarks of cancer: the next generation. Cell. 144**,** 646-74.
Harris, A. K., Stopak, D., Wild, P., 1981. Fibroblast traction as a mechanism for collagen morphogenesis. Nature. 290**,** 249-51.
Harris, A. K., Wild, P., Stopak, D., 1980. Silicone rubber substrata: a new wrinkle in the study of cell locomotion. Science. 208**,** 177-9.
Harris, A. L., 2002. Hypoxia--a key regulatory factor in tumour growth. Nat Rev Cancer. 2**,** 38-47.
Hawkins, R. J., Piel, M., Faure-Andre, G., Lennon-Dumenil, A. M., Joanny, J. F., Prost, J., Voituriez, R., 2009. Pushing off the walls: a mechanism of cell motility in confinement. Phys Rev Lett. 102**,** 058103.
Hotary, K., Li, X. Y., Allen, E., Stevens, S. L., Weiss, S. J., 2006. A cancer cell metalloprotease triad regulates the basement membrane transmigration program. Genes Dev. 20**,** 2673-86.
Hotary, K. B., Allen, E. D., Brooks, P. C., Datta, N. S., Long, M. W., Weiss, S. J., 2003. Membrane type I matrix metalloproteinase usurps tumor growth control imposed by the three-dimensional extracellular matrix. Cell. 114**,** 33-45.

Hou, J. M., Krebs, M., Ward, T., Sloane, R., Priest, L., Hughes, A., Clack, G., Ranson, M., Blackhall, F., Dive, C., 2011. Circulating tumor cells as a window on metastasis biology in lung cancer. Am J Pathol. 178**,** 989-96.

Hua, H., Li, M., Luo, T., Yin, Y., Jiang, Y., 2011. Matrix metalloproteinases in tumorigenesis: an evolving paradigm. Cell Mol Life Sci. 68**,** 3853-68.

Huovila, A. P., Turner, A. J., Pelto-Huikko, M., Karkkainen, I., Ortiz, R. M., 2005. Shedding light on ADAM metalloproteinases. Trends Biochem Sci. 30**,** 413-22.

Husemann, Y., Geigl, J. B., Schubert, F., Musiani, P., Meyer, M., Burghart, E., Forni, G., Eils, R., Fehm, T., Riethmuller, G., Klein, C. A., 2008. Systemic spread is an early step in breast cancer. Cancer Cell. 13**,** 58-68.

Huttenlocher, A., Sandborg, R. R., Horwitz, A. F., 1995. Adhesion in cell migration. Curr Opin Cell Biol. 7**,** 697-706.

Huynh, J., Nishimura, N., Rana, K., Peloquin, J. M., Califano, J. P., Montague, C. R., King, M. R., Schaffer, C. B., Reinhart-King, C. A., 2011. Age-related intimal stiffening enhances endothelial permeability and leukocyte transmigration. Sci Transl Med. 3**,** 112ra122.

Hynes, R. O., 2002. Integrins: bidirectional, allosteric signaling machines. Cell. 110**,** 673-87.

Ikejiri, M., Bernardo, M. M., Bonfil, R. D., Toth, M., Chang, M., Fridman, R., Mobashery, S., 2005. Potent mechanism-based inhibitors for matrix metalloproteinases. J Biol Chem. 280**,** 33992-4002.

Ilina, O., Bakker, G. J., Vasaturo, A., Hofmann, R. M., Friedl, P., 2011. Two-photon laser-generated microtracks in 3D collagen lattices: principles of MMP-dependent and -independent collective cancer cell invasion. Phys Biol. 8**,** 015010.

Indelicato, M., Pucci, B., Schito, L., Reali, V., Aventaggiato, M., Mazzarino, M. C., Stivala, F., Fini, M., Russo, M. A., Tafani, M., 2010. Role of hypoxia and autophagy in MDA-MB-231 invasiveness. J Cell Physiol. 223**,** 359-68.

Indra, I., Undyala, V., Kandow, C., Thirumurthi, U., Dembo, M., Beningo, K. A., 2011. An in vitro correlation of mechanical forces and metastatic capacity. Phys Biol. 8**,** 015015.

Ioachim, E., Charchanti, A., Briasoulis, E., Karavasilis, V., Tsanou, H., Arvanitis, D. L., Agnantis, N. J., Pavlidis, N., 2002. Immunohistochemical expression of extracellular matrix components tenascin, fibronectin, collagen type IV and laminin in breast cancer: their prognostic value and role in tumour invasion and progression. Eur J Cancer. 38**,** 2362-70.

Irimia, D., Toner, M., 2009. Spontaneous migration of cancer cells under conditions of mechanical confinement. Integr Biol (Camb). 1**,** 506-12.

Isenberg, B. C., Dimilla, P. A., Walker, M., Kim, S., Wong, J. Y., 2009. Vascular smooth muscle cell durotaxis depends on substrate stiffness gradient strength. Biophys J. 97**,** 1313-22.

Jacobsen, F. E., Buczynski, M. W., Dennis, E. A., Cohen, S. M., 2008. A macrophage cell model for selective metalloproteinase inhibitor design. Chembiochem. 9**,** 2087-95.

Jannat, R. A., Robbins, G. P., Ricart, B. G., Dembo, M., Hammer, D. A., 2010. Neutrophil adhesion and chemotaxis depend on substrate mechanics. J Phys Condens Matter. 22**,** 194117.

Kalluri, R., 2003. Basement membranes: structure, assembly and role in tumour angiogenesis. Nat Rev Cancer. 3**,** 422-33.

Kang, Y., Siegel, P. M., Shu, W., Drobnjak, M., Kakonen, S. M., Cordon-Cardo, C., Guise, T. A., Massague, J., 2003. A multigenic program mediating breast cancer metastasis to bone. Cancer Cell. 3**,** 537-49.

Kaverina, I., Krylyshkina, O., Gimona, M., Beningo, K., Wang, Y. L., Small, J. V., 2000. Enforced polarisation and locomotion of fibroblasts lacking microtubules. Curr Biol. 10**,** 739-42.

Kim, A., Lakshman, N., Petroll, W. M., 2006. Quantitative assessment of local collagen matrix remodeling in 3-D culture: the role of Rho kinase. Exp Cell Res. 312**,** 3683-92.

Kim, J. H., Asthagiri, A. R., 2011. Matrix stiffening sensitizes epithelial cells to EGF and enables the loss of contact inhibition of proliferation. J Cell Sci. 124**,** 1280-7.

Kim, S. H., Miller, F. R., Tait, L., Zheng, J., Novak, R. F., 2009. Proteomic and phosphoproteomic alterations in benign, premalignant and tumor human breast epithelial cells and xenograft lesions: biomarkers of progression. Int J Cancer. 124**,** 2813-28.

Klein, C. A., 2009. Parallel progression of primary tumours and metastases. Nat Rev Cancer. 9**,** 302-12.

Klein, E. A., Yin, L., Kothapalli, D., Castagnino, P., Byfield, F. J., Xu, T., Levental, I., Hawthorne, E., Janmey, P. A., Assoian, R. K., 2009. Cell-cycle control by physiological matrix elasticity and in vivo tissue stiffening. Curr Biol. 19**,** 1511-8.

Kononov, S., Brewer, K., Sakai, H., Cavalcante, F. S., Sabayanagam, C. R., Ingenito, E. P., Suki, B., 2001. Roles of mechanical forces and collagen failure in the development of elastase-induced emphysema. Am J Respir Crit Care Med. 164**,** 1920-6.

Koong, A. C., Denko, N. C., Hudson, K. M., Schindler, C., Swiersz, L., Koch, C., Evans, S., Ibrahim, H., Le, Q. T., Terris, D. J., Giaccia, A. J., 2000. Candidate genes for the hypoxic tumor phenotype. Cancer Res. 60**,** 883-7.

Kraning-Rush, C. M., Califano, J. P., Reinhart-King, C. A., 2012a. Cellular traction stresses increase with increasing metastatic potential. PLoS One. 7**,** e32572.

Kraning-Rush, C. M., Carey, S. P., Califano, J. P., Reinhart-King, C. A., 2012b. Quantifying traction stresses in adherent cells. Methods Cell Biol. 110**,** 139-78.

Kraning-Rush, C. M., Carey, S. P., Califano, J. P., Smith, B. N., Reinhart-King, C. A., 2011. The role of the cytoskeleton in cellular force generation in 2D and 3D environments. Phys Biol. 8**,** 015009.

Kraning-Rush, C. M., Carey, S. P., Lampi, M. C., Reinhart-King, C. A., 2013. Microfabricated collagen tracks facilitate single cell metastatic invasion in 3D. Integr Biol (Camb). 5**,** 606-16.

Kraning-Rush, C. M., Reinhart-King, C. A., 2012. Controlling matrix stiffness and topography for the study of tumor cell migration. Cell Adh Migr. 6**,** 274-9.
Krishnamachary, B., Berg-Dixon, S., Kelly, B., Agani, F., Feldser, D., Ferreira, G., Iyer, N., LaRusch, J., Pak, B., Taghavi, P., Semenza, G. L., 2003. Regulation of colon carcinoma cell invasion by hypoxia-inducible factor 1. Cancer Res. 63**,** 1138-43.
Krishnan, R., Klumpers, D. D., Park, C. Y., Rajendran, K., Trepat, X., van Bezu, J., van Hinsbergh, V. W., Carman, C. V., Brain, J. D., Fredberg, J. J., Butler, J. P., van Nieuw Amerongen, G. P., 2011. Substrate stiffening promotes endothelial monolayer disruption through enhanced physical forces. Am J Physiol Cell Physiol. 300**,** C146-54.
Kulangara, K., Leong, K. W., 2009. Substrate topography shapes cell function. Soft Matter. 5**,** 4072-4076.
Kumar, S., Maxwell, I. Z., Heisterkamp, A., Polte, T. R., Lele, T. P., Salanga, M., Mazur, E., Ingber, D. E., 2006. Viscoelastic retraction of single living stress fibers and its impact on cell shape, cytoskeletal organization, and extracellular matrix mechanics. Biophys J. 90**,** 3762-73.
Kumar, S., Weaver, V. M., 2009. Mechanics, malignancy, and metastasis: the force journey of a tumor cell. Cancer Metastasis Rev. 28**,** 113-27.
Lal, A., Peters, H., St Croix, B., Haroon, Z. A., Dewhirst, M. W., Strausberg, R. L., Kaanders, J. H., van der Kogel, A. J., Riggins, G. J., 2001. Transcriptional response to hypoxia in human tumors. J Natl Cancer Inst. 93**,** 1337-43.
Landau, L. D., Lifshitz, E. M., Kosevich, A. M., PitaevskiÄ-, L. P., 1986. Theory of elasticity. Butterworth-Heinemann.
Lauffenburger, D. A., Horwitz, A. F., 1996. Cell migration: a physically integrated molecular process. Cell. 84**,** 359-69.
Lee, J., 2007. The use of gelatin substrates for traction force microscopy in rapidly moving cells. Methods Cell Biol. 83**,** 297-312.
Lee, J., Leonard, M., Oliver, T., Ishihara, A., Jacobson, K., 1994. Traction forces generated by locomoting keratocytes. J Cell Biol. 127**,** 1957-64.
Legant, W. R., Miller, J. S., Blakely, B. L., Cohen, D. M., Genin, G. M., Chen, C. S., 2010. Measurement of mechanical tractions exerted by cells in three-dimensional matrices. Nat Methods.
Lemmon, C. A., Chen, C. S., Romer, L. H., 2009. Cell traction forces direct fibronectin matrix assembly. Biophys J. 96**,** 729-38.
Levental, K. R., Yu, H., Kass, L., Lakins, J. N., Egeblad, M., Erler, J. T., Fong, S. F., Csiszar, K., Giaccia, A., Weninger, W., Yamauchi, M., Gasser, D. L., Weaver, V. M., 2009. Matrix crosslinking forces tumor progression by enhancing integrin signaling. Cell. 139**,** 891-906.
Levy, D. E., Lapierre, F., Liang, W., Ye, W., Lange, C. W., Li, X., Grobelny, D., Casabonne, M., Tyrrell, D., Holme, K., Nadzan, A., Galardy, R. E., 1998. Matrix metalloproteinase inhibitors: a structure-activity study. J Med Chem. 41**,** 199-223.

Liu, L., Sun, B., Pedersen, J. N., Aw Yong, K. M., Getzenberg, R. H., Stone, H. A., Austin, R. H., 2011. Probing the invasiveness of prostate cancer cells in a 3D microfabricated landscape. Proc Natl Acad Sci U S A. 108**,** 6853-6.

Liu, Z., Tan, J. L., Cohen, D. M., Yang, M. T., Sniadecki, N. J., Ruiz, S. A., Nelson, C. M., Chen, C. S., 2010. Mechanical tugging force regulates the size of cell-cell junctions. Proc Natl Acad Sci U S A. 107**,** 9944-9.

Lo, C. M., Wang, H. B., Dembo, M., Wang, Y. L., 2000. Cell movement is guided by the rigidity of the substrate. Biophys J. 79**,** 144-52.

Lombardi, M. L., Knecht, D. A., Dembo, M., Lee, J., 2007. Traction force microscopy in Dictyostelium reveals distinct roles for myosin II motor and actin-crosslinking activity in polarized cell movement. J Cell Sci. 120**,** 1624-34.

Lopez, J. I., Kang, I., You, W. K., McDonald, D. M., Weaver, V. M., 2011. In situ force mapping of mammary gland transformation. Integr Biol (Camb). 3**,** 910-21.

Mak, M., Reinhart-King, C. A., Erickson, D., 2011. Microfabricated physical spatial gradients for investigating cell migration and invasion dynamics. PLoS One. 6**,** e20825.

Mak, M., Reinhart-King, C. A., Erickson, D., 2013. Elucidating mechanical transition effects of invading cancer cells with a subnucleus-scaled microfluidic serial dimensional modulation device. Lab Chip. 13**,** 340-8.

Marganski, W. A., Dembo, M., Wang, Y. L., 2003. Measurements of cell-generated deformations on flexible substrata using correlation-based optical flow. Methods Enzymol. 361**,** 197-211.

Marsden, C. G., Wright, M. J., Pochampally, R., Rowan, B. G., 2009. Breast tumor-initiating cells isolated from patient core biopsies for study of hormone action. Methods Mol Biol. 590**,** 363-75.

Martin, L. J., Boyd, N. F., 2008. Mammographic density. Potential mechanisms of breast cancer risk associated with mammographic density: hypotheses based on epidemiological evidence. Breast Cancer Res. 10**,** 201.

Masters, J. R., 2000. Human cancer cell lines: fact and fantasy. Nat Rev Mol Cell Biol. 1**,** 233-6.

Mehta, K., Fok, J., Miller, F. R., Koul, D., Sahin, A. A., 2004. Prognostic significance of tissue transglutaminase in drug resistant and metastatic breast cancer. Clin Cancer Res. 10**,** 8068-76.

Mierke, C. T., Kollmannsberger, P., Zitterbart, D. P., Diez, G., Koch, T. M., Marg, S., Ziegler, W. H., Goldmann, W. H., Fabry, B., 2010. Vinculin facilitates cell invasion into three-dimensional collagen matrices. J Biol Chem. 285**,** 13121-30.

Mierke, C. T., Rosel, D., Fabry, B., Brabek, J., 2008a. Contractile forces in tumor cell migration. Eur J Cell Biol. 87**,** 669-76.

Mierke, C. T., Zitterbart, D. P., Kollmannsberger, P., Raupach, C., Schlotzer-Schrehardt, U., Goecke, T. W., Behrens, J., Fabry, B., 2008b. Breakdown of the endothelial barrier function in tumor cell transmigration. Biophys J. 94**,** 2832-46.

Miller, K., Chinzei, K., Orssengo, G., Bednarz, P., 2000. Mechanical properties of brain tissue in-vivo: experiment and computer simulation. J Biomech. 33**,** 1369-76.

Munevar, S., Wang, Y. L., Dembo, M., 2001. Distinct roles of frontal and rear cell-substrate adhesions in fibroblast migration. Mol Biol Cell. 12**,** 3947-54.

Munter, S., Sabass, B., Selhuber-Unkel, C., Kudryashev, M., Hegge, S., Engel, U., Spatz, J. P., Matuschewski, K., Schwarz, U. S., Frischknecht, F., 2009. Plasmodium sporozoite motility is modulated by the turnover of discrete adhesion sites. Cell Host Microbe. 6**,** 551-62.

Nelson, C. M., Inman, J. L., Bissell, M. J., 2008. Three-dimensional lithographically defined organotypic tissue arrays for quantitative analysis of morphogenesis and neoplastic progression. Nat Protoc. 3**,** 674-8.

O'Neill, G. M., Fashena, S. J., Golemis, E. A., 2000. Integrin signalling: a new Cas(t) of characters enters the stage. Trends Cell Biol. 10**,** 111-9.

Ochsner, M., Dusseiller, M. R., Grandin, H. M., Luna-Morris, S., Textor, M., Vogel, V., Smith, M. L., 2007. Micro-well arrays for 3D shape control and high resolution analysis of single cells. Lab Chip. 7**,** 1074-7.

Oliver, T., Dembo, M., Jacobson, K., 1995. Traction forces in locomoting cells. Cell Motil Cytoskeleton. 31**,** 225-40.

Ozanne, B. W., McGarry, L., Spence, H. J., Johnston, I., Winnie, J., Meagher, L., Stapleton, G., 2000. Transcriptional regulation of cell invasion: AP-1 regulation of a multigenic invasion programme. Eur J Cancer. 36**,** 1640-8.

Parekh, A., Ruppender, N. S., Branch, K. M., Sewell-Loftin, M. K., Lin, J., Boyer, P. D., Candiello, J. E., Merryman, W. D., Guelcher, S. A., Weaver, A. M., 2011. Sensing and modulation of invadopodia across a wide range of rigidities. Biophys J. 100**,** 573-82.

Parsons, J. T., Horwitz, A. R., Schwartz, M. A., 2010. Cell adhesion: integrating cytoskeletal dynamics and cellular tension. Nat Rev Mol Cell Biol. 11**,** 633-43.

Paszek, M. J., Zahir, N., Johnson, K. R., Lakins, J. N., Rozenberg, G. I., Gefen, A., Reinhart-King, C. A., Margulies, S. S., Dembo, M., Boettiger, D., Hammer, D. A., Weaver, V. M., 2005. Tensional homeostasis and the malignant phenotype. Cancer Cell. 8**,** 241-54.

Pathak, A., Kumar, S., 2012. Independent regulation of tumor cell migration by matrix stiffness and confinement. Proc Natl Acad Sci U S A. 109**,** 10334-9.

Pelham, R. J., Jr., Wang, Y., 1997. Cell locomotion and focal adhesions are regulated by substrate flexibility. Proc Natl Acad Sci U S A. 94**,** 13661-5.

Pelham, R. J., Jr., Wang, Y., 1999. High resolution detection of mechanical forces exerted by locomoting fibroblasts on the substrate. Mol Biol Cell. 10**,** 935-45.

Peyton, S. R., Putnam, A. J., 2005. Extracellular matrix rigidity governs smooth muscle cell motility in a biphasic fashion. J Cell Physiol. 204**,** 198-209.

Pickle, L. W., Hao, Y., Jemal, A., Zou, Z., Tiwari, R. C., Ward, E., Hachey, M., Howe, H. L., Feuer, E. J., 2007. A new method of estimating United States and state-level cancer incidence counts for the current calendar year. CA Cancer J Clin. 57**,** 30-42.

Pink, D. B., Schulte, W., Parseghian, M. H., Zijlstra, A., Lewis, J. D., 2012. Real-time visualization and quantitation of vascular permeability in vivo: implications for drug delivery. PLoS One. 7**,** e33760.

Ponti, D., Costa, A., Zaffaroni, N., Pratesi, G., Petrangolini, G., Coradini, D., Pilotti, S., Pierotti, M. A., Daidone, M. G., 2005. Isolation and in vitro propagation of tumorigenic breast cancer cells with stem/progenitor cell properties. Cancer Res. 65**,** 5506-11.

Provenzano, P. P., Eliceiri, K. W., Campbell, J. M., Inman, D. R., White, J. G., Keely, P. J., 2006. Collagen reorganization at the tumor-stromal interface facilitates local invasion. BMC Med. 4**,** 38.

Provenzano, P. P., Inman, D. R., Eliceiri, K. W., Knittel, J. G., Yan, L., Rueden, C. T., White, J. G., Keely, P. J., 2008a. Collagen density promotes mammary tumor initiation and progression. BMC Med. 6**,** 11.

Provenzano, P. P., Inman, D. R., Eliceiri, K. W., Trier, S. M., Keely, P. J., 2008b. Contact guidance mediated three-dimensional cell migration is regulated by Rho/ROCK-dependent matrix reorganization. Biophys J. 95**,** 5374-84.

Ramaswamy, S., Ross, K. N., Lander, E. S., Golub, T. R., 2003. A molecular signature of metastasis in primary solid tumors. Nat Genet. 33**,** 49-54.

Ravdin, P. M., Siminoff, L. A., Davis, G. J., Mercer, M. B., Hewlett, J., Gerson, N., Parker, H. L., 2001. Computer program to assist in making decisions about adjuvant therapy for women with early breast cancer. J Clin Oncol. 19**,** 980-91.

Reinhart-King, C. A., 2008. Endothelial cell adhesion and migration. Methods Enzymol. 443**,** 45-64.

Reinhart-King, C. A., Dembo, M., Hammer, D. A., 2003. Endothelial cell traction forces on RGD-derivatized polyacrylamide substrata. Langmuir. 19**,** 1573-1579.

Reinhart-King, C. A., Dembo, M., Hammer, D. A., 2005. The dynamics and mechanics of endothelial cell spreading. Biophys J. 89**,** 676-89.

Reinhart-King, C. A., Dembo, M., Hammer, D. A., 2008. Cell-cell mechanical communication through compliant substrates. Biophys J. 95**,** 6044-51.

Rey, S., Semenza, G. L., 2010. Hypoxia-inducible factor-1-dependent mechanisms of vascularization and vascular remodelling. Cardiovasc Res. 86**,** 236-42.

Ricard-Blum, S., Ballut, L., 2011. Matricryptins derived from collagens and proteoglycans. Front Biosci. 16**,** 674-97.

Rolli, C. G., Seufferlein, T., Kemkemer, R., Spatz, J. P., 2010. Impact of tumor cell cytoskeleton organization on invasiveness and migration: a microchannel-based approach. PLoS One. 5**,** e8726.

Rosel, D., Brabek, J., Tolde, O., Mierke, C. T., Zitterbart, D. P., Raupach, C., Bicanova, K., Kollmannsberger, P., Pankova, D., Vesely, P., Folk, P., Fabry, B., 2008. Up-regulation of Rho/ROCK signaling in sarcoma cells drives invasion and increased generation of protrusive forces. Mol Cancer Res. 6**,** 1410-20.

Rundhaug, J. E., 2005. Matrix metalloproteinases and angiogenesis. J Cell Mol Med. 9**,** 267-85.

Sabeh, F., Ota, I., Holmbeck, K., Birkedal-Hansen, H., Soloway, P., Balbin, M., Lopez-Otin, C., Shapiro, S., Inada, M., Krane, S., Allen, E., Chung, D., Weiss, S. J., 2004. Tumor cell traffic through the extracellular matrix is controlled by the membrane-anchored collagenase MT1-MMP. J Cell Biol. 167**,** 769-81.

Sabeh, F., Shimizu-Hirota, R., Weiss, S. J., 2009. Protease-dependent versus -independent cancer cell invasion programs: three-dimensional amoeboid movement revisited. J Cell Biol. 185**,** 11-9.

Sahai, E., Marshall, C. J., 2003. Differing modes of tumour cell invasion have distinct requirements for Rho/ROCK signalling and extracellular proteolysis. Nat Cell Biol. 5**,** 711-9.

Samuel, M. S., Lopez, J. I., McGhee, E. J., Croft, D. R., Strachan, D., Timpson, P., Munro, J., Schroder, E., Zhou, J., Brunton, V. G., Barker, N., Clevers, H., Sansom, O. J., Anderson, K. I., Weaver, V. M., Olson, M. F., 2011. Actomyosin-mediated cellular tension drives increased tissue stiffness and beta-catenin activation to induce epidermal hyperplasia and tumor growth. Cancer Cell. 19**,** 776-91.

Santner, S. J., Dawson, P. J., Tait, L., Soule, H. D., Eliason, J., Mohamed, A. N., Wolman, S. R., Heppner, G. H., Miller, F. R., 2001. Malignant MCF10CA1 cell lines derived from premalignant human breast epithelial MCF10AT cells. Breast Cancer Res Treat. 65**,** 101-10.

Sanz-Moreno, V., Gadea, G., Ahn, J., Paterson, H., Marra, P., Pinner, S., Sahai, E., Marshall, C. J., 2008. Rac activation and inactivation control plasticity of tumor cell movement. Cell. 135**,** 510-23.

Saunders, R. M., Holt, M. R., Jennings, L., Sutton, D. H., Barsukov, I. L., Bobkov, A., Liddington, R. C., Adamson, E. A., Dunn, G. A., Critchley, D. R., 2006. Role of vinculin in regulating focal adhesion turnover. Eur J Cell Biol. 85**,** 487-500.

Scherber, C., Aranyosi, A. J., Kulemann, B., Thayer, S. P., Toner, M., Iliopoulos, O., Irimia, D., 2012. Epithelial cell guidance by self-generated EGF gradients. Integr Biol (Camb). 4**,** 259-69.

Semenza, G. L., 2002. Signal transduction to hypoxia-inducible factor 1. Biochemical Pharmacology. 64**,** 993-998.

Semenza, G. L., 2010. Defining the role of hypoxia-inducible factor 1 in cancer biology and therapeutics. Oncogene. 29**,** 625-634.

Shih, W., Yamada, S., 2010. Myosin IIA dependent retrograde flow drives 3D cell migration. Biophys J. 98**,** L29-31.

Sidransky, D., 2002. Emerging molecular markers of cancer. Nat Rev Cancer. 2**,** 210-9.

Smith, L. A., Aranda-Espinoza, H., Haun, J. B., Dembo, M., Hammer, D. A., 2007. Neutrophil traction stresses are concentrated in the uropod during migration. Biophys J. 92**,** L58-60.

Sniadecki, N. J., Chen, C. S., 2007. Microfabricated silicone elastomeric post arrays for measuring traction forces of adherent cells. Methods Cell Biol. 83**,** 313-28.

Sotiriou, C., Neo, S. Y., McShane, L. M., Korn, E. L., Long, P. M., Jazaeri, A., Martiat, P., Fox, S. B., Harris, A. L., Liu, E. T., 2003. Breast cancer

classification and prognosis based on gene expression profiles from a population-based study. Proc Natl Acad Sci U S A. 100**,** 10393-8.
Stacker, S. A., Caesar, C., Baldwin, M. E., Thornton, G. E., Williams, R. A., Prevo, R., Jackson, D. G., Nishikawa, S., Kubo, H., Achen, M. G., 2001. VEGF-D promotes the metastatic spread of tumor cells via the lymphatics. Nat Med. 7**,** 186-91.
Stamenovic, D., Mijailovich, S. M., Tolic-Norrelykke, I. M., Chen, J., Wang, N., 2002. Cell prestress. II. Contribution of microtubules. Am J Physiol Cell Physiol. 282**,** C617-24.
Staunton, J. R. e. a., 2013. A physical sciences network characterization of non-tumorigenic and metastatic cells. Scientific Reports. 3**,** 1449.
Steeg, P. S., 2006. Tumor metastasis: mechanistic insights and clinical challenges. Nat Med. 12**,** 895-904.
Stokes, C. L., Lauffenburger, D. A., Williams, S. K., 1991. Migration of individual microvessel endothelial cells: stochastic model and parameter measurement. J Cell Sci. 99 (Pt 2)**,** 419-30.
Streuli, C. H., Schmidhauser, C., Bailey, N., Yurchenco, P., Skubitz, A. P., Roskelley, C., Bissell, M. J., 1995. Laminin mediates tissue-specific gene expression in mammary epithelia. J Cell Biol. 129**,** 591-603.
Subarsky, P., Hill, R. P., 2003. The hypoxic tumour microenvironment and metastatic progression. Clin Exp Metastasis. 20**,** 237-50.
Tan, J. L., Tien, J., Pirone, D. M., Gray, D. S., Bhadriraju, K., Chen, C. S., 2003. Cells lying on a bed of microneedles: an approach to isolate mechanical force. Proc Natl Acad Sci U S A. 100**,** 1484-9.
Tan, L., Meyer, T., Pfau, B., Hofmann, T., Tan, T. W., Jones, D., 2010. Rapid vinculin exchange dynamics at focal adhesions in primary osteoblasts following shear flow stimulation. J Musculoskelet Neuronal Interact. 10**,** 92-9.
Tang, M. D., Golden, A. P., Tien, J., 2003. Molding of three-dimensional microstructures of gels. J Am Chem Soc. 125**,** 12988-9.
Tang, N., Wang, L., Esko, J., Giordano, F. J., Huang, Y., Gerber, H. P., Ferrara, N., Johnson, R. S., 2004. Loss of HIF-1alpha in endothelial cells disrupts a hypoxia-driven VEGF autocrine loop necessary for tumorigenesis. Cancer Cell. 6**,** 485-95.
Tang, X., Kuhlenschmidt, T. B., Zhou, J., Bell, P., Wang, F., Kuhlenschmidt, M. S., Saif, T. A., 2010. Mechanical force affects expression of an in vitro metastasis-like phenotype in HCT-8 cells. Biophys J. 99**,** 2460-9.
Teixeira, A. I., Abrams, G. A., Bertics, P. J., Murphy, C. J., Nealey, P. F., 2003. Epithelial contact guidance on well-defined micro- and nanostructured substrates. J Cell Sci. 116**,** 1881-92.
Tilghman, R. W., Cowan, C. R., Mih, J. D., Koryakina, Y., Gioeli, D., Slack-Davis, J. K., Blackman, B. R., Tschumperlin, D. J., Parsons, J. T., Matrix rigidity regulates cancer cell growth and cellular phenotype. PLoS One. 5**,** e12905.
Tong, Z., Balzer, E. M., Dallas, M. R., Hung, W. C., Stebe, K. J., Konstantopoulos, K., 2012. Chemotaxis of cell populations through confined spaces at single-cell resolution. PLoS One. 7**,** e29211.

Toth, M., Bernardo, M. M., Gervasi, D. C., Soloway, P. D., Wang, Z., Bigg, H. F., Overall, C. M., DeClerck, Y. A., Tschesche, H., Cher, M. L., Brown, S., Mobashery, S., Fridman, R., 2000. Tissue inhibitor of metalloproteinase (TIMP)-2 acts synergistically with synthetic matrix metalloproteinase (MMP) inhibitors but not with TIMP-4 to enhance the (Membrane type 1)-MMP-dependent activation of pro-MMP-2. J Biol Chem. 275**,** 41415-23.

Trappmann, B., Gautrot, J. E., Connelly, J. T., Strange, D. G., Li, Y., Oyen, M. L., Cohen Stuart, M. A., Boehm, H., Li, B., Vogel, V., Spatz, J. P., Watt, F. M., Huck, W. T., 2012. Extracellular-matrix tethering regulates stem-cell fate. Nat Mater.

Tse, J. M., Cheng, G., Tyrrell, J. A., Wilcox-Adelman, S. A., Boucher, Y., Jain, R. K., Munn, L. L., 2011. Mechanical compression drives cancer cells toward invasive phenotype. Proc Natl Acad Sci U S A.

Tseng, Q., Wang, I., Duchemin-Pelletier, E., Azioune, A., Carpi, N., Gao, J., Filhol, O., Piel, M., Thery, M., Balland, M., 2011. A new micropatterning method of soft substrates reveals that different tumorigenic signals can promote or reduce cell contraction levels. Lab Chip. 11**,** 2231-40.

Ulrich, T. A., de Juan Pardo, E. M., Kumar, S., 2009. The mechanical rigidity of the extracellular matrix regulates the structure, motility, and proliferation of glioma cells. Cancer Res. 69**,** 4167-74.

Wang, G. L., Semenza, G. L., 1993. General involvement of hypoxia-inducible factor 1 in transcriptional response to hypoxia. Proc Natl Acad Sci U S A. 90**,** 4304-8.

Wang, N., Butler, J. P., Ingber, D. E., 1993. Mechanotransduction across the cell surface and through the cytoskeleton. Science. 260**,** 1124-7.

Wang, N., Naruse, K., Stamenovic, D., Fredberg, J. J., Mijailovich, S. M., Tolic-Norrelykke, I. M., Polte, T., Mannix, R., Ingber, D. E., 2001. Mechanical behavior in living cells consistent with the tensegrity model. Proc Natl Acad Sci U S A. 98**,** 7765-70.

Wang, W., Wyckoff, J. B., Frohlich, V. C., Oleynikov, Y., Huttelmaier, S., Zavadil, J., Cermak, L., Bottinger, E. P., Singer, R. H., White, J. G., Segall, J. E., Condeelis, J. S., 2002. Single cell behavior in metastatic primary mammary tumors correlated with gene expression patterns revealed by molecular profiling. Cancer Res. 62**,** 6278-88.

Wang, Y. L., Pelham, R. J., Jr., 1998. Preparation of a flexible, porous polyacrylamide substrate for mechanical studies of cultured cells. Methods Enzymol. 298**,** 489-96.

Wellman, P., Howe, R., Dalton, E., Kern, K. A., 1999. Breast tissue stiffness in compression is correlated to histological diagnosis. Tech. Rep. (Harvard BioRobotics Laboratory).

Wells, R. G., 2008. The role of matrix stiffness in regulating cell behavior. Hepatology. 47**,** 1394-400.

Willcox, P. J., Reinhart-King, C. A., Lahr, S. J., DeGrado, W. F., Hammer, D. A., 2005. Dynamic heterodimer-functionalized surfaces for endothelial cell adhesion. Biomaterials. 26**,** 4757-66.

Williams, C. M., Engler, A. J., Slone, R. D., Galante, L. L., Schwarzbauer, J. E., 2008. Fibronectin expression modulates mammary epithelial cell proliferation during acinar differentiation. Cancer Res. 68**,** 3185-92.

Wojciak-Stothard, B., Curtis, A., Monaghan, W., MacDonald, K., Wilkinson, C., 1996. Guidance and activation of murine macrophages by nanometric scale topography. Exp Cell Res. 223**,** 426-35.

Wolf, K., Mazo, I., Leung, H., Engelke, K., von Andrian, U. H., Deryugina, E. I., Strongin, A. Y., Brocker, E. B., Friedl, P., 2003. Compensation mechanism in tumor cell migration: mesenchymal-amoeboid transition after blocking of pericellular proteolysis. J Cell Biol. 160**,** 267-77.

Wolf, K., Wu, Y. I., Liu, Y., Geiger, J., Tam, E., Overall, C., Stack, M. S., Friedl, P., 2007. Multi-step pericellular proteolysis controls the transition from individual to collective cancer cell invasion. Nat Cell Biol. 9**,** 893-904.

Woods, A., Couchman, J. R., 1992. Protein kinase C involvement in focal adhesion formation. J Cell Sci. 101 (Pt 2)**,** 277-90.

Wozniak, M. A., Modzelewska, K., Kwong, L., Keely, P. J., 2004. Focal adhesion regulation of cell behavior. Biochim Biophys Acta. 1692**,** 103-19.

Wyckoff, J. B., Pinner, S. E., Gschmeissner, S., Condeelis, J. S., Sahai, E., 2006. ROCK- and myosin-dependent matrix deformation enables protease-independent tumor-cell invasion in vivo. Curr Biol. 16**,** 1515-23.

Yang, M. T., Fu, J., Wang, Y. K., Desai, R. A., Chen, C. S., 2011. Assaying stem cell mechanobiology on microfabricated elastomeric substrates with geometrically modulated rigidity. Nat Protoc. 6**,** 187-213.

Yang, M. T., Sniadecki, N. J., Chen, C. S., 2007. Geometric considerations of micro- to nanoscale elastomeric post arrays to study cellular traction forces. Advanced Materials. 19**,** 3119-3123.

Yeung, T., Georges, P. C., Flanagan, L. A., Marg, B., Ortiz, M., Funaki, M., Zahir, N., Ming, W., Weaver, V., Janmey, P. A., 2005. Effects of substrate stiffness on cell morphology, cytoskeletal structure, and adhesion. Cell Motil Cytoskeleton. 60**,** 24-34.

Zaman, M. H., Trapani, L. M., Sieminski, A. L., Mackellar, D., Gong, H., Kamm, R. D., Wells, A., Lauffenburger, D. A., Matsudaira, P., 2006. Migration of tumor cells in 3D matrices is governed by matrix stiffness along with cell-matrix adhesion and proteolysis. Proc Natl Acad Sci U S A. 103**,** 10889-94.

Zent, R., Pozzi, A., 2010. Cell-extracellular matrix interactions in cancer. Springer, New York.

Zhong, H., De Marzo, A. M., Laughner, E., Lim, M., Hilton, D. A., Zagzag, D., Buechler, P., Isaacs, W. B., Semenza, G. L., Simons, J. W., 1999. Overexpression of hypoxia-inducible factor 1alpha in common human cancers and their metastases. Cancer Res. 59**,** 5830-5.

Ziegler, W. H., Liddington, R. C., Critchley, D. R., 2006. The structure and regulation of vinculin. Trends Cell Biol. 16**,** 453-60.

Zysset, P. K., Guo, X. E., Hoffler, C. E., Moore, K. E., Goldstein, S. A., 1999. Elastic modulus and hardness of cortical and trabecular bone lamellae measured by nanoindentation in the human femur. J Biomech. 32**,** 1005-12.